THE NOVEL USE OF PHASE CHANGE MATERIALS IN REFRIGERATED DISPLAY CABINETS FOR ENERGY CONSERVATION

A thesis submitted for the degree of
Doctor of Philosophy

By

Falah Alzuwaid, M.Sc.

Department of Mechanical, Aerospace and Civil Engineering
College of Engineering, Design and Physical Sciences
Brunel University London

JULY 2016

ABSTRACT

Each day the world's attention increases on how to minimize the energy consumption in order to reduce energy cost and carbon emissions as well as conserve the energy resources we have. Open-type vertical refrigerated display cabinets take the largest refrigeration load in a supermarket refrigeration system. One technique that has been used to improve the efficiency of such refrigeration equipment is to employ thermal energy storage inside. This approach will lead to improve the overall efficiency and also reduce the required cooling of the equipment due to the reduction of food temperature variation. This research project details the effect of phase change materials (PCMs) integration on the thermal performance of an open type multi-deck display cabinet in terms of energy savings, food product temperature improvements, cabinet air temperature and comparisons with conventional units. This work is divided into two parts of experiment and theoretical analysis.

The experimental part included a series of tests that were carried out to determine that effect of incorporation of PCM through two types of display cabinets depending on their availability with nearly same design. Two integration procedures of PCM-HEs with different PCM types were employed for each cabinet depending on its design. The test results showed that the energy saving of the cabinets with PCM significantly improved at climate class 3. In terms of product and cabinet air temperatures, the results also showed considerable benefit from reducing the maximum value of air temperature. Moreover, the defrost period was found to be the most affected parameter for the Norpe cabinet with PCM. It was approximately 5 min longer than the basic cabinet, which represented 70% of the original defrost time resulting in energy savings. It is worth noting that savings are a function of the ambient temperature, relative humidity, operational settings of the cabinet and PCM freezing point.

The theoretical study involves a 2D CFD model established for the Norpe display cabinet. The model is used to investigate the effect of adding PCM-HE on the energy consumption of display cabinet, thermal performance and cabinet air temperatures in similar method and same test conditions. Validation was carried out by comparing experimental results. Calculations are carried out for this cabinet first without PCM integration, then with a container filled with pure water as a PCM. It has been shown that an enhancement of thermal system performance and reduction in the cabinet air and product temperatures when the cabinet is off and increasing defrost, on and off periods. It is also found that with PCM, the energy saving potential of the cabinet is significantly improved. In addition, in the CDF results, the defrost and compressor off intervals are the most affected factors for the modified cabinet. They are increased by approximately 98% and 50%, respectively, compared to those with the basic cabinet. Furthermore, a significant decrease (27%) in the number of starts/stops of the compressor is observed for the modified cabinet. Also optimum PCM container width was found to be 16 mm such that the required air flow pattern is still achieved. The effect of different conditions; ambient air and fan pressure jump, on the PCM effectiveness is also considered in this study.

Dedication

To

My parents

Abdulhassan Jasim and Alia Naser

My wife

Mithal Hatem

And my three beautiful children

Zahraa, Fatimah, and Muhammad

PUBLICATIONS

.

Alzuwaid, F., Ge, Y.T., Tassou, S. & Sun, J. 2016, "The novel use of phase change materials in an open type refrigerated display cabinet: A theoretical investigation", Applied Energy, vol. 180, pp. 76-85.

Alzuwaid F, Ge Y, Tassou S, Raeisi A, Gowreesunker L. The novel use of phase change materials in a refrigerated display cabinet: An experimental investigation. *Appl. Therm. Eng*. 2015; 75:770-8.

F. Alzuwaid., Y.T. Ge., S.A. Tassou. Jining Sun, 2015. Simulation of a Refrigerated Display Cabinet Integrated with Phase Change Materials. 3rd Sustainable Thermal Energy Management International Conference, Newcastle University (susTEM2015), Newcastle upon Tyne, UK**.**

F. Alzuwaid., Y.T. Ge., S.A. Tassou. A. Raeisi, B. Gowreesunker., 2014. THE NOVEL USE OF PHASE CHANGE MATERIALS IN A REFRIGERATED DISPLAY CABINET: AN EXPERIMENTAL INVESTIGATION. *3rd IIR International Cold Chain Conference,* London.

ACKNOWLEDGEMENTS

I would like to express my special appreciation and gratitude to Dr. Yunting Ge for his guidance and enthusiastic support throughout the research. His advice and encouragement have strongly inspired me to complete the project successfully and this thesis. I would also like to thank my second supervisor, Prof. Savvas Tassou, for his assistance.

I would like to express my equally deep thanks to Dr. Jining Sun. His constant support and being there for me when the going got tough could not be more appreciated. And for that I am truly in debt.

Many thanks go to the refrigeration laboratory technical team and all my colleagues in the Mechanical Engineering Dept.; Konstantinos, Amir, Dewa and Lesh for all their support and encouragement, their friendship, and support during those four tough years made all the difference. Thanks a million.

Work presented in this research was carried out with financial support from the Department of Environment, Food and Rural Affairs (Defra: AFM280). I would like to acknowledge the support of Defra and the input from the collaborating partners.

Finally, I would like to express my very special gratitude to my wife, Mithal Hatem, and my daughters, Zahraa and Fatimah, for their patience and fortitude during the most arduous time. I also express my gratitude to my parents and relatives for their support and encouragement.

CONTENTS

LIST OF FIGURES

LIST OF TABLES

LIST OF ABBREVIATIONS

GHG	Green House Gases
ASHRAE	American Society of Heating Refrigerating and Air-conditioning Engineers
CFD	Computational Fluid Dynamic
CCC	Committee on Climate Change
CO_2	Carbon dioxide
DEFRA	Department for Environment, Food & Rural Affairs
ETSAP	ENERGY TECHNOLOGY SYSTEMS ANALYSIS PROGRAMME
HEs	Heat Exchangers
HFCs	Hydro-fluorocarbons
IEA	International Energy Agency
IRENA	International Renewable Energy Agency
LHS	Latent Heat Storage
ORDCs	Open-type refrigerated display cabinets
PCM	Phase Change Material
TES	Thermal energy storage

NOMENCLATURE

E_t	Total Energy Consumption (kWh)
E_n	Instant Energy Consumption (kW)
t	Time (h)
n	Experimental time step number
N_{max}	Total number of experimental time step
$PCML_t$	Total latent heat of PCM (kJ)
M_{PCM}	PCM total mass (kg)
Δh_{PCM}	Total specific enthalpy of PCM (kJ/kg)
$PCML_a$	Actual amount of PCM latent heat (kJ)
ΔT_a	Actual PCM temperature difference (°C)
ΔT_t	Total PCM temperature difference (°C)
Q_s	Sensible cooling capacity of evaporator (kW)
m_a	Air mass flow rate (kg/s)
Cp_a	Air specific heat (kJ/kg.K)
t_{on}	Air temperature inlet to evaporator (°C)
t_{off}	Air temperature outlet from evaporator (°C)
E_r	Energy required from PCM (kJ)
DEF_{eff}	Effective defrost duration (s)
U, u	Momentary velocity in x direction (m/s)
V, v	Momentary velocity in y direction (m/s)
x	Coordinate in x direction (m)
y	Coordinate in y direction (m)
z	Coordinate in z direction (m)

T	Temperature (K)
P	Pressure (Pa)
q	specific heat source (W/m^3)
R	Gas constant (J/(gk))
S	Source term (W/m^3)
k	Turbulent kinetic energy (m^2/ s^2)
V	Volume (m^3)
Q_{source}	UDF heat source (kW)
H, h	Enthalpy (kJ/kg)
L	Latent heat (kJ/kg)

Subscripts

evap	evaporator
l	liquid
ref	reference
S	solid
W,w	with PCM
Wo,wo	without PCM
a	air
k	turbulent kinetic energy (m^2/ s^2)

Greek symbols

ε	dissipation rate of turbulent kinetic energy
	effectiveness (m^2/s^3)
Δ	difference

β	liquid fraction
Γ_k	diffusion coefficient of k (m^2/s)
$\Gamma\varepsilon$	diffusion coefficient of ε (m^2/s)
α	Thermal diffusivity (m^2/s)
ρ	Density (Kg/m^3)

CHAPTER 1

INTRODUCTION

1.1 Energy consumption and environmental impacts

World energy demand has been increasing along with the growth of world population and economy. That increases greenhouse gas (GHG) emissions which contribute to the retrogradation of ambient air quality and environmental impacts. According to (IEA 2010), global energy demand related to GHG emissions in the year 2030 will be 40% higher than 2007. Consequently, European Union countries have been developing an aspirant energy policy to tackle climate changes and harmful emissions. In the UK, the goals are a 60% and 80% reduction in GHG emissions by 2030 and 2050, respectively, compared to 1990 levels (CCC 2010). In contrast, a tendency of increasing food products consumption, which in them has an impact on GHG emissions, is still there. It is estimated that (20-30)% of GHG emissions is caused by the food industry in Western Europe (Tassou and Suamir, 2010).

Energy use by manufacturing processes, food distribution and retail is considered one of the main sources of emissions. Approximately 7% of total emissions has resulted from food distribution and retail as reported by (DEFRA 2005). Refrigeration technology, which is progressively important in the food processing and preservation, is actually responsible for the major footprint on the environment. Suamir (2012) described that refrigeration is responsible for 15% of global electricity consumption. Therefore,

decreasing the energy demand of refrigeration unit in food sector has become one of the priorities in the reduction of GHG emissions.

In the UK, annual CO2 emissions due to the energy consumption of major retail food outlets amount to 4 metric tons of indirect emissions (Raeisi et al. 2013; Tassou et al. 2011).. Therefore, the world is progressively focussing its attention on how to minimize energy consumption in order to reduce energy costs and carbon emissions, as well as conserving the energy resources we already have.

Supermarkets are viewed as one of the largest consumers of electric energy, of which 50% relates to refrigeration systems and equipment (Tahir and Bansal 2005). In the UK, around 40%-50% of the total energy consumption of a typical store is used for refrigeration purposes, and around 70% of this refrigeration energy is required for open type display cabinets; thus the energy cost for such appliances is more expensive (Faramarzi 1999). UK food retailer consumes substantial amounts of energy with superstores accounting for between 3% and 5% of total electricity consumption (Tassou et al. 2007). Air conditioning and refrigeration systems contain potent GHG known as hydrofluorocarbons (HFCs), and the recent researches show global emissions of HFC have increased by more than 50% from 2007 to 2012 (Lunt et al. 2015). Also, Suamir (2012) stated that superstores are the principal source of (HFCs) emissions with their air conditioning and refrigeration equipment being responsible for 2 $MtCO_2e$ emissions. All those risks are driving the demand for the development of sustainable refrigeration technologies in supermarkets.

1.2 Open-type refrigerated display cabinets

Since the popularity of chilled food products progressively increased, techniques were developed to display the products in an attractive and accessible manner while still keeping their trophic characteristics (A. Hadawey 2006). Devices of food display first appeared in the 1930's and involved air circulating around food stored in spaces which were then considered as display cabinets. Chilled display cabinets with different styles have started to appear and the temperature and airflow around the products, in the display area, were given a little attention. Open-type vertical multideck cabinets were

the most common types of display cabinets for chilled food applications. Nowadays, these cabinets are extensively used in retail stores in the United Kingdom and around the world to store and display dairy and food products in recommended allowable temperatures. Such a cabinet is common and preferred in order to save floor space, easy access to the products and maintain a sizeable retailing surface.

Supermarkets are mainly dependent on refrigeration fixtures in order to maintain many types of perishable food in safe conditions. The mainstay of the refrigerated products passageways is horizontal and vertical display cabinets, both open and closed. The total length of medium temperature, open-type, vertical, multideck, display cabinets may reach up to 100m in a typical superstore, altogether contributing considerably to the overall energy consumption. Therefore, finding new techniques to cut down the operating cost of such equipment will achieve higher profitability to the retailers (A. Al-Sahhaf 2011).

Although the close-type cabinets have higher efficiency, open-type display cabinets are still common and preferred as they are more attractive to the customers because the products are easy to reach and totally visible (Alzuwaid et al. 2015). However, due to the wide display area and the absence of doors in such cabinets create more difficulties in the reduction of energy consumption and the control of allowable food product temperatures. The research studies of total efficiency of those cabinets over the past years were good to achieve some improvements, but the need to manufacture and design such cabinets, with more energy efficient system which allows displaying food products at a lower cost of running, was rising due to increasing fuel prices. Many academic and industrial researchers are now following more efficient designs for open display cabinets. In such a ferociously competitive manufacturing, the food retailing sector, accomplishing even small developments will enhance the retailers' profit, let alone longer shelf life and better products quality which will be achieved by preserving homogeneous and more stable products temperature. One of the improvements to the current designs that could be accomplished by install thermal energy storage (TES) inside the cabinet to reduce the energy consumption and that will be the goal of this project.

1.3 Thermal energy storage (TES)

TES is a technique that stocks the extra thermal energy by using many different technologies that can accommodate a varied range of requirements allowing stored energy to be used in future. As examples; energy needs can be balanced between day and night times, solar energy in summer can be collected for use in winter and cold winter air can be given for air conditioning systems in summer time (E. Oró, de Gracia, et al. 2012). Mediums of storage could include; small and huge ice tanks, deep bedrocks of earth, deep aquifers, and phase change materials. TES sources can include; heat collected during off-peak times (lower electricity cost), heat from combined heat-power plants, extra heat gathered by renewable power plants, and industrial waste heat. Heat storage is considered a vital means for inexpensively balancing great shares of variable renewable energy production and integration of heating and electricity sectors in energy systems partially or totally fed by a renewable source.

Figure 1.1 PCM effect

TES scheme is used mainly in buildings and industrial processes in which thermal energy forms about 50% of the energy consumed (IRENA and ETSAP 2013). The

demand for such energy may differ from time to time. Thus, TES system helps balance energy supply and demand see Figure 1.1. Also, it can decrease energy consumption, peak demand, harmful emissions and cost. TES becomes important for electrical power storage in combination with solar power plants where solar energy can be stored for electricity production at no-sunlight times.

TES systems are divided into three schemes; sensible, latent and chemical storages. The sensible TES stores energy by heating or cooling the storage mediums which could be water, rocks or sand. This type of TES is rather cheap and is applicable to central heating, domestic systems and industrial necessities, but needs big volumes due to its energy density is low (Demirbas 2006). On the other hand, the latent TES uses PCMs which allows greater storage abilities at nearly isothermal conditions with a limited temperature range and small unit size (El-Dessouky, 1997). Finally, chemical TES, such as adsorption, has high energy density and can be used to store cold and heat, and control humidity. A number of researchers in some European countries are working to develop new techniques and materials that include TES integration into building walls and transfer of thermal energy between two places. Choosing the appropriate TES scheme is significant and needs accurate inspection. Among these options PCMs gets a great consideration.

1.4 Phase change materials (PCMs)

PCM is a material with a high heat of fusion which is capable of storing and releasing large amounts of energy during melting and solidifying processes that happen at a certain (transition) temperature. Energy is released or absorbed when the material changes its phase from liquid to solid and vice versa; hence, PCM is classified as latent heat storage (LHS) as shown in Figure1.2. PCM-LHS can be done through solid–liquid (melting), liquid-solid (freezing), liquid–gas (vaporization) and solid–gas (sublimation) phase changes. However, the freezing/melting changes are the only phase changes used for PCMs. Although that vaporization phase changes do have a higher heat of transformation than freezing/melting transitions, they are not practical for use as (TES) due to the high pressures or large volumes required to store the materials in the gas

phase. Sublimation phase changes are normally slow and have the low heat of transformation.

Figure1.2 Principles of PCMs

The liquid-solid transformation starts when the temperature decreases as PCM releases heat. When PCM reaches the temperature at which it changes phase (its freezing temperature) it releases large amounts of heat at a nearly constant temperature. The PCM continues to release heat without an important drop in temperature until all the material is transformed to the solid phase. When the ambient temperature around the solid material rises, the PCM starts to melt, absorbing large amounts of latent heat from ambient. A large number of PCMs are available in any required temperature range from −5 up to 190 °C (Kenisarin and Mahkamov 2007). In the human comfort range (20–30) °C, some PCMs are very operative. They can store 5 to 14 times more heat per unit volume than conventional storage materials such as rock, masonry or water (Sharma et al. 2009).

TES based PCM schemes can be categorized by the types of PCMs used; they are divided into organic or inorganic mixtures. Organic PCMs, such as fatty acids and paraffin, have self-nucleating properties but a lower thermal conductivity and higher

cost (Bruno 2005). Inorganic materials such as salt hydrates have good availability at a lower cost but exhibit difficulties in phase separation and their abilities to melt incongruently. It is, therefore, important to select the optimal PCM in any particular application to satisfy terms of operation and cost (Alzuwaid et al. 2015). It is common that using TES based on PCMs has played a key role in wide range of applications in the electronic, construction, biomedical and automotive industries (Pielichowska and Pielichowski 2014). Furthermore, using PCMs as a TES has played an effective role in the refrigeration systems by integrating them into the equipment, such as display cabinets, directly for energy savings and better controls.

1.5 Water and Ice as a PCM

Using water and ice as a TES in cool storages was available and known since more than a few thousands of years when the ice was stored underground during the winter and then used in the hot summer for cooling purposes. Furthermore, ice was transported until the mid-19th century for foodstuff preservation applications. In modern developed Countries, the best and first TES utilized to stock cooling capacity in refrigeration/air conditioning equipment was water and ice due its availability and stable characteristics (Demirbas 2006). Sensible heat systems based pure water improves the refrigeration performance by increasing evaporation temperatures; but, this requires large storage volume as the storage capacity is low. Unlike, the sensible ice-bank system has a substantially larger capacity of storage; however, it requires lower operation temperature causing higher energy consumption.

Using the water as a solid/liquid PCM was more attractive and has wide applications due to high storage density (334kJ/kg) that can be released and absorbed during the phase changing processes. Moreover, any PCM should have high latent heat, suitable transition temperature, melt and freeze correspondingly, minimum sub-cooling, chemically stable, low cost, noncorrosive and nontoxic (Farid et al. 2004). In the experimental part of this project, we have used the water as a PCM with some additives to improve and modify its characteristics to fit the current application. The PCM in the simulation part is pure water as we can control its properties.

1.6 PCM applications in refrigeration/ air conditioning

Since the 1980s, PCMs have been found significant applications in big refrigeration and air conditioning schemes (WANG 2003). They were mainly employed to introduce capacity inside building energy systems to allow them to consider of variations in the daily cooling load. Low rate of heat transfer is the major drawback of PCM applications in refrigeration and air conditioning systems. The reasons for that are; moving the mushy zone away from the heat transfer surface causes an increase in the thermal resistance of the growing layer thickness of the molten/solidified medium. In the case of solidification, conduction is the only transport mechanism, and in most cases it is very poor. In the case of melting, natural convection can occur in the molten layer and this generally increases a bit the heat transfer rate compared to the solidification process (if the layer is thick enough to allow natural convection to occur), as well as low thermal conductivity of the PCMs used in such applications (Cabeza et al. 2002). Advanced techniques, to enhance the heat transfer, are presently employed to increase performance such as; greater heat transfer surfaces, direct contact systems and higher thermal conductivity, however, just partial progress is made which are not enough comparing to the cost. New approaches to PCM applications in refrigeration systems are being studied.

1.7 Approach towards sustainability

Different technologies related to energy storage have been established in recent times; LHS materials are one of them as they exhibit a higher density of heat comparing with SHS. Latent heat TES can provide significant development in the overall energy efficiency of the conventional display cabinet's energy approach. This technique can also make substantial contribution to reduce the environmental impacts of supermarkets. This study aims to decrease further the energy consumption and CO_2 emission savings potential of display cabinets through its integration with PCMs-TES systems. The research programme consists of two parts; experimental and simulation.

The experimental part is based on two types of display cabinets (Bond and Norpe); each one incorporates with different TES module; PCM-heat exchanger module and PCM containers module. The approach employed is to use the available space of back duct to

install the TES units. The heat transfer between the TES units and the cabinet is achieved by the circulated air which will be in direct contact with all cabinet's parts and products.

The simulation part of the research programme is based on computational fluid dynamic (CFD) for Norpe cabinet and consisted of two parts.). The first part includes what we have done in the laboratory for the basic cabinet to compare the both results for validation and to give us the flexibility to explore the effect of more parameters. The second part involves adding the PCM at the suggested place and optimizing its thickness.

1.8 Aims and objectives

This research project aims to design, develop and investigate an open chilled display cabinet with integrated PCMs for latent thermal energy storage (TES). Thermal performance and energy consumption were considered in order to understand, identify, and consequently optimize various design parameters experimentally and numerically. The project included a number of sub-objectives as follows:

1. To carry out comprehensive experimental tests on two types of conventional open multideck refrigerated display cabinets (Bond and Norpe cabinets) in order to investigate the performance of the cabinets over a range of operating conditions, and find the ideal conditions which are appropriate for our application.

2. To modify the Bond refrigerated display cabinet by adding two different types of PCM heat exchangers after the evaporator in the airway and repeat the previous experiments at the same conditions to find what the difference in the results compared with the conventional case.
3. To develop a proposed PCM (for Norpe cabinet) after some experimental trials for different ratios of different materials to be appropriate with the desired transition temperature.

4. To modify the Norpe refrigerated display cabinet by adding two PCM containers after the evaporator in the rear duct and run the tests again to examine the performance comparing to the corresponding basic cabinet.
5. To develop and validate a 2D CFD model for the (Norpe) ordinary cabinet at the experimental operating conditions.
6. To adjust the 2D CFD model by adding the PCM model to the display cabinet in order to predict the PCM effect on the cabinet efficiency, the temperature distributions and the air flow patterns inside the cabinet under specific operating conditions.
7. To use the simulation models to explore and analyse the cabinet performance at various operating and design conditions.

1.9 Structure of the thesis

This thesis consists of seven chapters. Following the introduction of the work in this chapter, **Chapter 2** presents an overview of previous work done on PCM integration on refrigeration equipment and describes the concept of energy saving and most findings affecting the performance of open display cabinets. The chapter also outlines and covers the advanced methods, recent applications and development used for the study of adding the PCM to such systems for food preservation in supermarkets over the past few years.

Test standards, experimental facilities used, which include the two vertical display cabinets, test chamber and measurement tools, and the primary experimental outcomes are illustrated in **Chapter 3.**

Modifying Bond and Norpe cabinets by incorporating with PCM-HEs and PCM containers respectively are treated in **Chapter 4**. The chapter also describes and analyses the new experimental results for the same conditions to highlight the differences comparing with the conventional systems.

The basic CFD theory and the philosophy behind choosing different numerical algorithms as well as validation of Norpe cabinet model are presented in **Chapter 5**. The various issues considered for pre-processing, solving, and post-processing the data

are addressed. Boundary conditions together with turbulence, species, and radiation models used during the setup of the models are presented.

Chapter 6 considers the validation and simulation results for Norpe cabinet with PCM incorporation and compares these results with the simulation results of the conventional model. The Chapter also presents the effect of some parameters on the PCM behaviour in the modified cabinet model.

Finally, **Chapter 7** highlights the areas of contribution, summarizes the main conclusions reached and proposes further development and investigations required to improve system performance and optimisation.

CHAPTER 2

BACKGROUND AND LITERATURE REVIEW

This chapter provides a comprehensive literature review for the most significant works carried out using wide international databases. In the beginning, the use of PCMs as a TES in refrigeration systems is addressed. Then, heat transfer enhancement approaches and new techniques to overcome the PCM problems are discussed. Some important studies about PCM-HEs with emphasis on their different configurations through cabinets are then presented. Finally a background and some attractive research regarding different aspects of display cabinets related to their design and operations are considered.

2.1 TES in Refrigeration systems

Refrigeration systems play a vital role in food conservation, as low temperatures assist to avoid or delay physiological, microbial and chemical changes in foodstuff (Martínez, 2003). Preserving perishable frozen food at unchanging temperature (under -18 C) in the storage is important requirement such as ice cream and meat. Frozen foods have to be preserved at this temperature. However, during storage or transportation stages, frozen products may experience some fluctuations in temperature as heating loads executed on the system.

2.1.1 Freezer

The effect of PCM on temperature storage conditions has been studied for different types of freezers. A study into the effect of low temperature PCM (-15.4 °C) sheets, positioned beside the internal walls of domestic freezer during daily power outage over two weeks period, was conducted (Gin and Farid 2010). After comparison the freezer with and without PCM, it was found that the air and product fluctuations temperature in the freezer with PCM was lower than that without PCM. Products analysis was also implemented in this study to find out that the crystallization size in the ice cream and drip loss in meat were found to be lower in the modified freezer.

Another investigation conducted on the freezer was by the same previous researcher (B. Gin, 2010). The same test rig was used, but this time the effectiveness of PCM in maintaining temperatures in the presence of heat loads such as defrosting, door openings, and power failure was considered. During these conditions it was noticed that the PCM integrated has considerably lowered the increase rate of products temperature, and the energy consumption measured was slightly lower compared to without PCM.

Moreover, E. Oró et al. (2012) inserted PCM (Climsel-18) stainless steel panels into different positions of a commercial freezer to augment its performance under interrupting conditions; door openings and power loss. During 3 hours power supply absence, the freezer temperature was maintained at 4-6 ºC lower and for much longer time in which the products temperature were within standard limits. For the period of frequent door openings, it was found that the benefit of PCM is evident when the cabinet temperature was near the PCM melting temperature. Some frozen products spent long time outside the freezers, such as serving ice cream in restaurants, causing a decrease in quality. That what (Oró, De Gracia, and Cabeza 2013) tried to deal with when they designed and examined a commercial ice cream container combined with PCM package to enhance the storage conditions. A validated mathematical model, parametrical study and experimental investigation were implemented to prove the PCM advantage to keep the frozen foodstuff quality while it is out the freezer.

Integration a suitable quantity and quality of PCM in a freezer could achieve a significant reduction in energy consumption. This was considered by (A. Raeisi, IN.

Suamir 2013) when they attach PCM layers between the evaporator coils on the four internal sides of a 300 litre chest type freezer. The results showed that the energy saving of the cabinet with integrated PCM was found to be 12.8% at climate class 3 conditions, resulting from increasing the defrost period by maintaining freezer temperature below the defrost termination temperature for longer time. These savings are a function of the ambient temperature and thermostat control settings of the cabinet, narrower product temperature range can be achieved compared to conventional freezer cabinet.

2.1.2 Refrigerators

Refrigerators with PCM integrated also were studied by some researchers as this appliance is considered an essential part in every house. A domestic refrigerator with cold storage integration has been simulated (Cerri 2003). This model was employed to find suitable operating conditions in which minimum energy consumption could be achieved. Although a low amount of PCM was used in this research, the outcome was 12% improvement in the coefficient of performance that was achieved by extending the of time period.

Furthermore, the effect of adding PCM slab on the external side of the evaporator in a refrigerator was studied and a dynamic mathematical model of the refrigeration cycle with the attendance of PCM was presented and experimentally validated (Azzouz et al. 2005) and (Azzouz, Leducq, and Gobin 2008). During the off cycle, the PCM extended the lower temperature time without power supply. It was concluded that the addition of thermal inertia globally enhances heat transfer from the evaporator and allows a higher evaporating temperature, which increases the energy efficiency of the system. Experimental tests for the same household refrigerator was presented later by same researcher (Azzouz, 2009). In this study, the PCM was positioned behind the evaporator to increase its efficiency and offer a storage capacity maintaining the temperature within accepted levels for longer time in the absence of power supply. Two types of PCM were used; water and eutectic aqueous solution and different operating conditions were experienced which were ambient temperature, PCM thickness and thermal load. An important improvement in thermal performance was observed in the results compared to the ordinary system.

Another different study regarding PCM incorporation into a refrigerator was conducted by (Cheng et al. 2011). In this work, storage condensers were constructed with kind of shape-stabilized (PCM) and equipped in a novel household refrigerator. A comparison study was done between the novel and the conventional refrigerators, charge and discharge processes in the PCM were noticed during the on and off times respectively. Therefore, unlike to ordinary setup, the heat dissipation was continuous even through the off times of the novel refrigerator. Hence, significant improvement in the condensers' thermal efficiency was detected, that resulted in a higher evaporation temperature, a lower condensation temperature and a more sub-cooling degree at the condenser outlet. These results were agreed with a corresponding dynamic model, with shape-stabilized PCM for the same refrigerator, was carried out by (Cheng and Yuan 2013). The simulation results indicated 12% energy saving and 19% increase in COP by a continuous heat transfer through the condenser due to energy stored in the PCM. This study also provides a theoretical optimization design by taking in account the influence of three parameters; freezer temperature, PCM transition temperature and ambient temperature.

Marques et al. (2013) proposed a CFD model to describe the distribution of temperature and airflow in a natural convection TES refrigerator. Different types (water or eutectics) and patterns (vertical or horizontal) of PCMs were incorporated, investigated and compared in terms of temperature stability. After validation the model, the results showed a lower refrigerator temperature when horizontal PCM configurations were used compared to vertical, and a eutectic at a transition temperature under 0 ºC must be added to keep the refrigerator within acceptable temperature limits. A second study for (Marques et al. 2014) in which he suggested a new design, for a TES refrigerator, by analysing the compressor performance at range of operation conditions for the refrigerator. The results stated that the efficiency of bigger compressors is better, and 19.5% energy reduction could be achieved when larger compressors (doubled displacement) were used instead of the conventional size. But using that size of compressor will increase the number of its stops/starts, and to overcome such drawback, the researchers suggested collecting the cooling capacity output of high performance

compressors in a PCM slab to extend the cooling effect of the refrigerator without power supply.

The latest interesting study about PCM combination with refrigerators was done by (Yuan and Cheng 2014). He combined an optimization method called Genetic algorithm and refrigerator dynamic model to produce a multi-purpose optimization method in order to enhance the household refrigerator performance. A novel refrigerator with TES condenser and a conventional one are compared in terms of energy consumption and total cost, and daily basis optimized. The outcome revealed that total performance was increased for both cases, but it was better for the novel refrigerator.

2.1.3 Refrigerated trailer trucks

Food transport refrigeration is considered one of the important stages in food chain in terms of keeping the transported food temperature, energy consumption and CO2 emissions. According to (Defra 2005), the food sectors, comprising agriculture, transport and retailing are responsible for 22% of the UK's GHG emissions. One third of this caused by distribution and retailing, and about 1.8% of total emissions produced by food transport. Tassou et al. (2009) stated that air cycle refrigeration and hybrid systems in which ordinary refrigeration technology is combined with TES are encouraging technologies that can lead to a decline in CO2 emissions. However, additional development and research work is required for these systems to be effective competitor with diesel driven refrigeration systems, and to decrease their weight and increase their efficiency.

The perishable food is transferred by refrigerated truck trailers which have refrigeration units run by vapour compression cycle. The heat transfer reduction insulation was developed by inserting paraffin based PCM in the ordinary trailer walls. A total reduction of 29.1% in highest rate of heat transfer was recorded from all compartment walls, and 16.3% overall daily heat reductions into the refrigerated space were indicated. These findings can be translated into energy savings, GHG emissions regression, smaller refrigeration equipment and longer equipment life. This investigation was proposed by (Ahmed, Meade, and Medina 2010).

Enough quantity of proposed selective and fully charged PCM could play the role of vapour compression cycle for specific durations according to (Liu, Saman, and Bruno 2012). They suggested a new refrigeration scheme integrating PCM to preserve refrigerated trucks at the required temperature. In this system, it does not have to put the conventional refrigeration unit on-board the vehicle as this unit will be situated off the vehicle and used to charge the PCM system when stationary and discharge when in service, providing the required cooling. The benefits are maintaining low temperatures, lower energy consumption and much lower GHG emissions. Furthermore, a new low cost PCM was proposed to maintain the temperature at -18 ºC inside the refrigerated truck. The experimental results of a built prototype system demonstrated that the recommended refrigeration system is practicable for mobile transport.

Eduard Oró et al.(2012) simulated food transportation in not refrigerated trucks by adding low solidus temperature PCM and then assessing their thermal characteristics during a refrigeration system failure. Two types of PCM (C-18 and E-21) with different melting temperatures were experimented. It was found that the products and air temperatures continued at lower values for longer time when the refrigeration was absent.

2.1.4 Refrigeration cycles

TES techniques have been established and combined into compression cycles of the refrigeration and air conditioning systems directly for saving energy, balancing the loads and for better control. A study proposed by (Ure 2001) who suggested a refrigeration unit including PCM-HEs in contact with the liquid and suction lines. Putting the PCM-HE in the liquid line was to allow the refrigeration plant to profit from night low temperature providing an extra load on the condenser, keeping the night cold energy to be released during daytime. While the advantage of the suction line PCM-HE is providing thermal capacitance by limiting the superheat. Results stated that 10% and 15% enhancement in peak unit efficiency could be achieved by increasing the sub-cooling a 15 K and by reducing the superheat a 5 K respectively.

The most common study about the novel use of PCMs in refrigeration plant was done into three parts; experimental investigation (Wang et al. 2007a), theoretical

investigation (Wang et al. 2007b) and control and energy savings (Wang et al. 2007c) for the combined system. In the first part, a prototype has been established and experienced by integrating a PCM-HE as a pre-condensing unit in a refrigeration plant. The result of study proved that about 8% energy savings and 6% COP improvement can be reached in the UK weather by pulling down the sub-cooling temperature of the refrigerant. This was done by putting PCM-HE between the condenser and compressor such that lower condensing pressure and higher sub-cooling were achieved, where PCM acted as an extra condenser. The second part included a coupling of PCM-HE and the refrigeration system has been mathematically established. The model validation showed good agreement with the experimental results and the PCM-HE was considered as a one dimensional model. The simulation results of the mathematical dynamic model predicted the refrigerant states and dynamic COP in the system in respect of time.

The last part presented a novel control purpose of employing PCM-HE in the refrigeration system. The novel applications of PCM at different locations through the refrigeration system circuit with a shell-tube structure have been explored comprehensively by the dynamic model described in part 2. The outcome shows that for PCM-HEs at different positions give higher COP that reaches to 8% by decreasing the sub-cooling level. PCM also improves the system COPs up to 7% and 4% for the orifice systems and the thermostatic expansion valve, respectively, by lowering the superheat as well as system stabilization.

2.1.5 TES in display cabinets

Display cabinets utilise convective mode of heat transfer for cooling the products, and they usually show non-uniform distribution and noticeable increase in products temperature during defrost durations. There is no studies about PCM integration within refrigerated display cabinets except the one proposed by (Lu et al. 2010). In this research, an improved novel shelf design for display cabinet was suggested. Heat pipes of new structure and suitable PCM was selected and filled inside the shelf. Experimental tests of cabinets with heat pipe only, with both heat pipe and PCM and conventional case have been accompanied and compared. The experimental results for the shelf with only heat pipe reduced the products temperature by about (3.0 - 5.5) ºC

comparing to basic cabinet. While the shelf with both heat pipe and PCM decreased 1.5 ºC of products temperature rise during defrost time and enhanced the uniformity of products temperature distribution while the power consumption was still the similar to the ordinary cabinet.

2.2 Heat transfer enhancement techniques in PCM

With respect to the PCMs most common problem which is low thermal conductivity that leads to low rates of charging and discharging processes. Therefore, several approaches and schemes have been recommended in the literature to improve heat transfer, both experimentally and numerically, are necessary for most LHS applications. The most common techniques were mentioned as follows:

2.2.1 Finned tubes configurations

Some studies have been accomplished to evaluate techniques of heat transfer improvement in PCMs by including finned tubes of different configurations as shown in a study presented by (Horbaniuc, Dumitrascu, and Popescu 1999). They studied the solidification of the PCM within a finned heat pipe LH-TES system by means of an analytical method bearing in mind the angular and radial heat propagation. Two estimates (parabolic and an exponential) for the temperature profiles over the fin height were used. The location of the solid/liquid interface was plotted for different fin numbers. This method can predict the whole solidification time of the PCM for a given number of fins. Also, when the PCM must freeze in an imposed period, and conclude the required fins number to achieve this task.

Another related work was conducted by (Ismail, Alves, and Modesto 2001). They presented the results of an experimental and numerical study realized on finned-tubes in order to use them in TES systems. This model was based upon the conduction mode, the control volume approach and the enthalpy formulation method. After validation, fins number and geometry, the super heat degree and the aspect ratio of the annular spacing were found to affect the solidification time, mass fraction and the stored energy. The results confirmed the significance of the fins in postponing the unwanted effect of natural convection during the phase change process. Moreover, this study indicated the

strong effect of the annular spacing, the fin radial length and the fins number on the mass fraction and the phase change time.

2.2.2 Higher conductive porous structure

One of the heat transfer enhancement techniques is embedding of a metal matrix into the PCM to increase its conductivity. Hoogendoorn et al. (1992) performed a study on organic PCMs for TES in solar system applications. The influences of LH for these materials were gained from calorimetric differential thermal analyser measurements. Over the entire range of 25 to150 °C, appropriate organic materials are available with heat effects from 150-230 kJ/kg. The thermal conductivity of these materials was enhanced by inserting a metal matrix structure in them. A transient numerical model for the heat transfer in a PCM heat storage vessel has been set up and built-in TRNSYS.

Another study regarding metal structure was conducted by Trelles & Dufly (2003). They simulated porous LH-TES for thermal-electric cooling through a matrix-based enthalpy formulation. The system was consisted of two aluminium containers; the internal one contained the cooling objective (vaccines) in water suspension and the external one the PCM in a porous aluminium matrix. The discharging and charging processes were simulated for constant thermos-electric module cold side temperature under different porosities of the aluminium matrix. The mathematical approach simplified the analysis whereas the metal porous significantly increased the heat conduction without dropping significantly the storage capacity.

2.2.3 High conductivity particles

Using PCM dispersed with high conductivity particles is also considered as another enhancement technique which was proposed by Mettawee & Assassa (2007). They carried out experiments to examine a technique of inserting aluminium powder inside paraffin wax to improve its thermal conductivity. The particles size of the aluminium powder was 80 μm and different values of mass fractions in the PCM-aluminium composite material were used. These experiments were done by using a compact PCM solar collector in which the absorber container part achieved the absorbing function of the solar energy and storing the PCM. The results showed that the charging period was lowered by about 60% by adding aluminium powder in the paraffin. It was also

concluded that the beneficial heat gained was enhanced when adding aluminium powder as compared to the pure wax.

2.2.4 Micro-encapsulation of the PCM

A new procedure of employing micro-encapsulated PCM in energy storage systems has been established. Micro-encapsulation is the packaging of micronized material (solid or liquid) in the capsules form. The micro-encapsulated paraffin wax can reduce the reactivity of the PCM with the environment, increase the heat transfer area and allow the core material, due to coating, to resist frequent volume changes of the storage material as the phase change happens. HAWLADER et al. (2000) described results of investigation of using the coacervation method to encapsulate the PCM, where the thermal performance of the product has been evaluated. It was found that the energy storage and release capacity increased for the micro-encapsulated paraffin during its phase change depending on different ratios of paraffin to coating.

Later, Hawlader et al. (2003) carried out micro-encapsulation of PCM by two approaches, namely complex coacervation and spray drying, and compared the characteristic properties of the products. The effect of some parameters, such as encapsulation efficiency, energy storage and release capacity, on the performance of a micro-encapsulated PCM has been considered. Results showed that micro-capsules have a thermal energy storage/release capacity between 145 to 240J/g. Hence, encapsulated paraffin showed a good potential as a solar energy storage material.

PCMs are beneficial for both static and dynamic TES. By encapsulating them in a small diameter solid material, to be suspended in liquid, partially solidifying and melting slurries could be created with high heat transfer rates and effective energy densities (Griffiths and Eames 2007). Such slurries are both energy storage medium and transport medium, and can be designed for a specific set temperature. Micro-encapsulated PCM slurries with phase change temperature around 18 ºC were analysed in a test chamber containing a chilled ceiling. The results have proven that a concentration of 40% micro-capsules containing PCM could be employed as the HTF in the application of chilled ceiling. It needs a considerably slower rate of fluid flow and it

can absorb energy at a set point, thus avoiding temperature increases in panel surface as gains rise.

In the current work, two techniques for heat transfer enhancement were used. The first one was using finned-tubes HEs with Bond cabinet and finned- containers with Norpe cabinet. The second was higher conductive porous structure by employing aluminium swarf inside the PCM medium in order to increase the thermal conductivity and nucleation sites.

2.3 PCM heat exchangers

Employing the PCMs inside heat exchangers is considered one of the most common configurations used to overcome the PCMs conductivity through the charge and discharge processes. A study figures out the characteristics of PCM employed in shell-tube HE to overcome the frequency of the heat source of solar plant conducted by (M. CONTI 1996). Parallel and series connection set-ups of the storage unit were used with the heat engine. A comparison study for the parallel and series systems with respect to different design aims was implemented. It was concluded that the parallel connection looks to offer a better efficiency.

It is known that the storage effect of a PCM depends on its thermal properties including the transition temperature that occurs at a given temperature. Commercially, combinations of different PCMs are available in order to produce an appropriate transition temperature, allowing the phase changes to happen over a temperature range, i.e. the specific heat (Cp) fluctuates with the temperature providing a Cp curve, as a function of temperature. A mathematical PCM air heat exchanger (AHE) model was developed and presented (Hed and Bellander 2006). Different shapes of Cp (T) curve were considered, and model validation with experiment on a prototype HE was confirmed. The study target was to explore the possibility of using modelled PCM-HE units to fit into indoor space and energy simulation software where the thermal material properties are considered.

PCMs could be employed in applications which need to save energy due to the disparity between the supply and demand of thermal energy as in solar applications. Medrano et

al. (2009) investigated experimentally the rate of heat transfer during charge and discharge of five small HEs working as TES in order to measure their potential application in small size systems, such as home appliances or telecommunication devices, making them more efficient. These TES schemes comprised of diverse configurations of usual commercial small size HEs which have two sides; one was occupied with a PCM-R35 as a LHS and another was filled with water to circulate as heat transfer fluid (HTF). Average values of thermal energy are calculated and compared among the HEs used at different operating conditions. Results showed that the double pipe PCM-HE established in a graphite matrix has higher values. Furthermore, the compact PCM-HE was by large the one with the maximum thermal power (above 1 kW), as it has the highest heat transfer ratio of area to external volume.

Free Cooling using PCM-TES systems is particularly motivating in environments with high daily temperature differences. Although the ambient temperatures only reach low values for a few times in such environments, the rate of heat transfer between PCM and air has to be enough to freeze whole the PCM. Lazaro et al. (2009a) stated that PCM-LHS can be used for free cooling. They used a low air temperature to freeze a PCM during the night time and then cool down an indoor space during the day such that melting and freezing the PCM should happen in short times. Since the low thermal conductivity of PCM, the HE design is quite significant to satisfy free cooling needs. By conducting an experimental set-up for analysis two actual-scale prototypes of PCM–AHEs, the results illustrated that using effectively designed PCM-HE with lower total stored energy and lower thermal conductivity can give higher cooling energy and be suitable for free cooling applications.

Same researcher, (Lazaro, Dolado, Marín, et al. 2009), presented, built on experimental outcomes and an empirical model, new design conclusions for a real conditions of PCM -AHE. The empirical model was based on experimental results, allowing simulating the thermal performance in the PCM-AHE at varied circumstances. This model could be used to estimate the practical viability of its application. The PCM-AHE worked as a transient model as its thermal behaviour changes with temperature and its design has to be based time-dependent investigation. The results indicated that the criteria of PCM

selection have to take account of the power demand. Also, PCM-AHE can be used to select PCM for other HE applications for the same tested geometry.

A similar structure was explored by (Dubovsky, Ziskind, and Letan 2011). This study offered an investigation of a cross flow tube-shaped AHE that contains PCM which melts while air passes through the tube banks. The SH of the PCM liquid and the tubes material was neglected comparing to the melting LH to simplify the deriving and solving a system of partial equations which describe heat transfer of the PCM and the air for the entire system. The results of numerical and analytical solutions were obtained and compared, and simple equations were established for the whole HE parameters. Furthermore, the models estimated the results for single tubes depending on their location. The assumptions influence of the model on the outcomes and pertinence of the analytical solutions to the real HEs were verified.

In the review by (Dolado et al. 2011), the authors described models established to simulate the performance of TES system in a full-scale PCM-AHE, analysing the heat transfer between the air and slab micro-encapsulated PCM. The model was based on one-dimensional conduction analysis, utilizing FDM, and implicit formulation, using the actual PCM properties; thermal conductivity and enthalpy as functions of temperature. Two ways were followed to achieve the modelling: single plate analysis and the performance of the whole TES unit. Simulations and measurements were compared to examine the models. Average errors of lower than 12% on thermal energy were found for the whole cycle. After validation, some of variables and parameters were calculated to confirm their effect on the of the TES performance system.

Later, Campos-Celador et al. (2013) published a review on finned-plate LH-TES system integrated in cogeneration schemes. For optimization purposes, the authors presented three approaches for the same storage system: numerical, a simplified analytical and a simplified numerical models, to increase the computational efficiency of calculations. These models were employed to simulate a prototype that has been investigated experimentally by test standard for storage systems. The simplified numerical and simplified analytical models were executed by the definition of an effective coefficient of heat transfer. The results stated that all suggested models give rise to a good

agreement with the experimental outcomes. The simplified numerical approach offered quite good results for every configuration and reduced the computational time required by the numerical model from hours to minutes. However, the simplified analytical system failed to assess long configurations.

Another similar study by the same researchers (Campos-Celador et al. 2014) was presented to minimize the required volume of TES, a finned plate LH-TES system for domestic applications. This new design permits the heat transfer between the PCM (RT60) and water. To simulate that system, a mathematical model, based on a simplified numerical approach, was built and validated to be used for optimizing the final prototype, which was compared with a basic hot water tank commonly incorporated in domestic heating and hot water applications. It is found that the current design is one half of the water tank volume, providing a more compact structure which can be simply combined in the space, bringing a good chance for thermal storage particularly in applications that have limited spaces such as residential flats.

2.4 Open-type refrigerated display cabinets (ORDCs)

The absence of doors, that makes the air curtains are to be the only barrier between the warm surrounding air and the inner refrigerated space in ORDCs as well as non-uniformity of the air flow lead to entrain a considerable amount of surrounding air, increasing the temperature and energy consumption and difficulty of temperature control. As a result, ORDCs are considered the weakest link in the cold chain and better analysis and design are still vital targets to refrigeration industry and researchers. It is possible to divide the areas that were studied in ORDCs as follows;

2.4.1 Air flow and temperature distribution

Cortella et al. (2001) employed the finite element method (FEM) and sequential method for analysing air temperature and velocity distributions in ORDCs. A 2D CFD code was based on the stream-function velocity formulation, and integrated a LES turbulence model. A vertical ORDC, as an example of application, was inspected under varied operating conditions. The model results were compared and validated with experimental work conducted according to standards. The effect of different design parameters has

been considered. Another review for Cortella (2002) in which he examined the use of CFD, as an estimation tool of air flow and products temperature patterns and energy consumption inside a ORDC as CFD has actually became a very beneficial tool for a cheaper and better design of such appliances. Specific approaches are applied, since the air flow patterns and the products temperature are assessed separately and in sequence to reduce calculation time. The simulations were executed both on a horizontal and a vertical cabinet. The infiltration of ambient air on the energy balance was examined and the output was validated by comparing with experimental results. The applications stated in this work proved the model to be dependable, and of effective tool to the designers.

The study by Wu et al. (2004) introduced a dynamic approach which was based on the conservation equations for energy and mass, describing the airflow distributions and the characteristics of heat and mass transfer for a horizontal ORDC. With assistance of the PHOENICS software, the coupling problem of the convection mode of air flow with the conduction mode of products was solved theoretically. The approach was successfully experienced for an island ORDC to be used for optimizing the design and development such cabinets. The effects of the discharge air grille (DAG) diameter, the cabinet dimensions and the heights and shapes of products with the heat transfer of the air curtain were considered.

Most of ORDCs in Europe are tested in accordance with European standards in which the chilled cabinets are classified as M0, M1, M2 or H if the products temperatures are maintained between (-1 to 4 ºC), (-1 to 5 ºC), (-1 to 7 ºC) or (1 to 10 ºC), respectively. The classification M0 is usually used for display cases that keep meat. By lowering the maximum temperature by 1 K, the shelf life of fresh meat will extend to about 1.5 day. This what (Foster, Madge, and Evans 2005) tried to do when they used the a CFD code to quickly identify the required modifications to an available M2-class cabinet to reach a M0-class. Applying the adjustments on certain display cabinet lowered the energy consumption by 5% as well as minimizing the products number of high temperature (above 4 ºC) from twelve to one.

Companies of refrigeration schemes always attempt to enhance equipment performance. One development includes that operating an ORDC at higher suction of pressures and temperatures will require less power for a given refrigeration effect. Evaporator pressure regulating (EPR) valve has been employed to regulate the evaporator pressure at a level to create the preferred discharge air temperature in the cabinet. EPRs control the saturated pressure in the evaporator to deliver the accurate desired temperature at the discharge air sensor of the cabinet (Bundy, Refrigeration, and Company 2002). A comprehensive analysis of the applications of the electronic EPR valve, comparing its behaviour with the mechanical EPR valve under identical operating conditions was undertaken by (Tahir and Bansal 2005). Field experiments showed that the electronic valve has an important effect on enhancing the air temperature, lowering the evaporator frosting rate, stronger air curtain and most economic operation cost.

Chen & Yuan (2005) conducted an experimental and theoretical study of the effect of important factors on the thermal behaviour and cooling load of an ORDC, including environment air flow and temperature, inside relative humidity, air flow velocity, air velocity from perforated rear panel and night cover. The inside temperature pattern and heat load were both explored. Also, the entrainment rate factor was correlated with Richardson number and Reynolds number, from which the effects of momentum and buoyant forces on the thermal entrainment are analyzed. The results showed that the entrainment increases if the momentum force increased but decreases when the gravitational force was dominant.

Usually, air velocities are measured by devices such as anemometers or Pitot tubes, but these tools are intrusive and their measurements are affected by uncertainties. For these purposes, better instruments based on optical methods, are available such as the Laser Particle Image Velocimetry (PIV). This technique allows the characterization of the full flow field. Marinetti et al. (2012) employed the PIV to analyse the air velocity distribution inside two configurations of cabinet cooling duct and its influence on heat transfer through the evaporator. 3D flow fields at downstream and upstream the evaporator were addressed by PIV implemented on three planes accommodating the mainstream velocity vectors and positioned at various heights. It was shown the PIV

capability to highlight not sufficiently loaded evaporator sections and to evaluate the efficiency of heat transfer.

2.4.2 Air curtain configurations

The cold air is delivered to the cabinet interior through DAG situated at the top front and through holes in the perforated rear panel of the cabinet. The air then is returned back to the evaporator coil through a return air grille (RAG) positioned at the bottom front of the cabinet, creating a barrier called air curtain between the interior cold cabinet space and the warm ambient air. However, entraining between air curtains and surrounding air cannot be avoided, causing spilling a part of the cold air over the cabinet to be replaced by the ambient air. The infiltrated air into the cabinet through the RAG is responsible for most of the energy consumption. Past studies of the air curtain explained the significance of the inlet air velocity and eddy viscosity which is created as a result for turbulence as reported by (R.H. Howell 1991). This study stated that 75% of the power consumed is induced by the entrainment through the air curtain.

Designing energy efficient display case has continued to be a significant job of the industry and an essential matter for research. A significant findings by (Cui and Wang 2004) were studying the key factors affecting the cooling load of air curtain in a horizontal ORDC. In this work, a CFD model was built by employing K–ε turbulent, multiple species and radiation models, to predict the thermal performance of the air curtain for the display case and improve its design. The CFD model was validated and qualitative designs were then suggested making the air curtain more energy efficient.

In related study by Navaz et al. (2005), numerical and experimental approaches were presented to study the air curtain effectiveness and to explore parameters that affect the entrained amount of warm air in ORDC. The entrainment rate was explained as a function of these parameters which then were quantified and identified. It was concluded that the DAG velocity profile, the DAG turbulence intensity and the DAG Reynolds number have the most contribution on the entrainment. Digital particle image velocimetry was utilised to map the 2D flow field in the cabinet at the air curtain and opening areas. Validation was performed and parametric study for the entrainment rate of the ambient air into the cabinet was conducted using a CFD tool. The results pointed

out that lower Reynolds numbers will decrease the entrainment, but this will increase the products temperature on shelves. However, adequately high momentum should still exist to support the straightness of the air curtain.

An effective approach called two-fluids turbulence model was presented by Yu et al. (2007) in order to simulate the flow and heat transfer features of air curtain in a vertical ORDC. The model considered the fluid in the space as a combination of turbulent fluid which is air curtain and non-turbulent fluid which is the ambient air. Empirical relations were used to explain the exchanges of mass, energy and momentum between these two fluids. The two-fluid model results were validated with experimental data and compared with the simulation results obtained by applying the k–e model for the whole simulated space. It was found that the two-fluid model was able to calculate thermal stratification phenomenon more precisely and to show better agreement with the experimental data than the k–e model.

The two-fluid model in above was modified by same authors later, (Yu, Ding, and Chen 2008). The different from the existing model was by modifying the equation of mass transfer between the non-turbulent and the turbulent fluids, fetching the face coefficient of DAG with the volume fraction of air curtain in order to illustrate the DAG characteristics. After comparing between the simulation and experimental data, it was shown that the modified model can give better agreement with the measurements than original two-fluid and k–e models. Yu et al. (2009) presented another third different study related to thermal entrainment (TE) which is an essential factor to define the cooling performance of an ORDC. They studied a procedure of building a correlation model based on CFD to compute the TE quickly and precisely. This model can predict both the TE value and air curtain return temperature with small accepted deviations comparing with published experimental data.

To figure out some of the significant design considerations including air curtain velocity, width, discharge angle and positioning of the air curtain outlet, a computational studies based on 2&3D CFD models were conducted by Hadawey et al. (2012). The effect of chamber cross flow and the suitability of both models to perform the calculations were considered. After the validation with measurements, it was found

that 2D model could be used efficiently to carry out all the investigations saving time and cost, and the optimum flow rate of air curtain should be equal to about a third of the total air flow rate inside the cabinet.

Another interesting work regarding the flow distribution in the cooling duct of a commercial ORDC was presented by (Marinetti et al. 2014) and including an experimental and numerical investigations on a channel in which the air was driven by two fans through the evaporator. ANSYS code was employed to build a steady numerical model that can analyse the turbulence of the flow distribution. The results were compared with the three dimensions air velocity field by using the stereoscopic PIV technique. The model allowed a better comprehension of the flow maldistribution source and its influence on the air velocity field at evaporator outlet.

2.4.3 Other different operating conditions

Another challenge need to be overcome is frosting in the evaporator of cabinet. Accumulated frost affects heat transfers in the air side, energy consumption, temperature fluctuation and pressure drop coefficients, as well as minimizes the air flow through the evaporator coil and air curtain at constant fan speed. A simulation model for finned-tubes cabinet evaporator was built by (Chandrasekharan, Verma, and Bullard 2006) to be used for improving the cabinet performance during frosting times and to be able to simulate cross-counter-flow evaporator with multiple modules having totally not the same geometries. Quasi steady heat and mass transfer calculations can deliver values of relevant variables such as; air and refrigerant side pressure drop, heat and mass transfer coefficient and tube and fin frost thickness. A multi-lump procedure makes the model able to calculate both fin and tube frost thickness and surface temperature. The results were able to reveal interaction between the cabinet and air curtain, and calculate total effects of accumulated frost, simplifying the modelling of the bigger cabinet.

In the same vein, to find out the exact effect of the frost, a design of non-frosting system was described by Yu et al. (2009b). They established an experimental model for a vertical ORDC with central air supply. The refrigeration cycle of the new model, consisting of a compressor, a condenser, TEV and an evaporator, was independent of

the cabinet, and the air was cooled by the evaporator was delivered through a duct to the cabinet to realize refrigeration. Comparing with basic cabinet, it was found that the new set up offered easier control for air curtain, lower accumulated frost, longer defrost cycle and lower maximum food temperature.

A review by Gray et al. (2008) brought out improvements to enhance temperature consistency and energy performance by presenting some results derived from extensive experimental tests on ORDCs. How perforation patterns of the back panel affect the distribution of airflow between these and the front air curtain was also investigated. It was found that about 70% of total circulating air should be distributed through the front curtain. The balance of 30% passing from the back panel should be delivered horizontally between the shelves.

Stignor et al. (2009) evaluated numerically the performance potential of various designs of flat tube HEs with plain fins in indirectly cooled ORDC. One of HEs was with serpentine fins and another with continuous plate fins, both types were validated. It was resulted from this parametric study that considerable power savings that could be obtained reached up to 15% comparing with the ordinary HEs. Besides, the required temperature difference for this type of HEs was so small, allowing frost free operation that would give rise to even larger savings.

Amin et al introduced three reviews regarding to the TE rate measurement of ORDC. The first, (Amin, Dabiri, and Navaz 2009), was done by releasing a tracer gas into the air inside the discharge and return ducts and the ambient. This method depended on the concentration measurements of the tracer gas that escaped into the ambient between DAG and RAG. By applying the mass conservation around the air curtain, a relationship between the concentration of tracer gas and the TE can be recognized. The second study, (Amin, Dabiri, and Navaz 2011), targeted to universally examine the effect of the most significant variables that related to the TE of ambient air into the cabinet, identifying the relation between each of those variables and TE. The tracer gas was used for the infiltration measurement. Infiltration outcomes proved a strong relationship with the offset angle and jet exit Reynolds number and effect of each variable was described in combination of the other variables. Their last study, (Amin,

Dabiri, and Navaz 2012), was similar to previous one but associated with different, secondary, variables . The results showed that the changes in temperature and relative humidity were not significant, while the relation of infiltration rate with the turbulence intensity is nearly linear and with the product level is nonlinear.

The variation of products temperature in ORDC also was investigated by (Laguerre, Derens, and Flick 2011) as its direct influence on the quality and safety of products. This variability could be a result for different reasons such as the cabinet type (vertical or horizontal), the product arrangement and the instability of the ambient conditions. This work was implemented to study the effect of three parameters; surrounding air temperature, radiation and products position on the load temperature. The products position has the most influence comparing with the rest parameters. Experimental investigation of the instability phenomena by same researchers (Laguerre et al. 2012) were also done by analysing the heat and air flow. It was found that the convective heat coefficient at the DAG an RAG was higher than between these two locations due to the high variability of air flow close to these positions. Also, the radiative exchange at the top of the cabinet was more significant than at the bottom, and the temporal fluctuation in the air curtain temperature was a result of the on/off cycles and the introduction of surrounding air by transient vortices.

Generally, ORDCs suffer variations in the performance due to changes of ambient conditions. Gaspar et al. (2011) carried out an experimental study to figure out the effects of these conditions on the heat transfer rate and TE factor at different ambient air conditions including temperature, relative humidity and velocity. The TE was analysed and compared with the total latent and sensible heat results of the experimental tests. It was concluded that TE cannot be used indiscriminately, although its use was appropriate to design more efficient cabinet at the same climate condition. Another later comprehensive study by Gaspar et al. (2012a) was performed by modelling the heat and air flow through the internal ducts, across evaporator and fan, and considering the products thermal response in a ORDC. Experimental tests were accomplished to validate the model calculations and the results revealed the predictive capability of the model for optimization purposes and development of such equipment. Also, the

numerical calculations were used to suggest low cost functional and geometrical parametric study that were implemented later by (Gaspar et al. 2012b) to improve the ORDC performance, energy efficiency and consequently products safety. The analysis from these parametric studies developed an optimized model for the conception of an ORDC with a more acceptable configuration. The numerical calculations of this model showed a reduction in food temperature and energy consumption.

A new vertical ORDC was developed by (Song and Feng 2013) and based on ice slurry technology and central refrigeration and its thermostatic performance was experimentally considered and compared with a conventional cabinet which was chilled by using R22 directly. The results showed that the new model has good chilling effects and few temperature variations. It could essentially satisfy food keeping demand and it can operate with higher efficiency and indirectly reduce the GHG emissions.

Another study about the effect of rear panel structure on the performance of ORDC was introduced by (Wu et al. 2014) who studied the characteristics of heat and fluid flow at the different positions of the panel perforations at the same porosity, and the various flow ratios between panel and air curtain at different porosities. The results showed that less than 3% porosities can offer a better performance, and the perforations position has a slight effect on the food temperature distribution. Also, the total uniformity of food temperature and the maximum deviation values of food temperature were improved to 41% and 49%, respectively.

Recently, Wu et al. (2015) investigated and optimized the influence of the deflector structure inside DAG on the air curtain performance of vertical ORDC. This work essentially was aiming to find an optimal deflector that efficiently can lower the food temperature inside the cabinet. It was concluded that front and back food temperature reduced with increasing the inlet air curtain velocity, and the latter could enhance the disturbance inside the cabinet. While the increase in outer air curtain velocity led to weaker disturbance inside the cabinet and lower performance of air curtain. This study provided a theoretical foundation for the display cabinets design.

2.5 Summary

A background of TES in refrigeration equipment such as freezers and refrigerators, most common techniques to enhance PCM role and PCM-HEs was presented in this chapter. Furthermore, a comprehensive literature of many parameters and approaches affecting and improving the performance of open display cabinets and their air curtains were provided such as PCM-HE and micro-encapsulation. Up to the present time, there is no available work in the open literature has been devoted to the experimental and numerical investigations of the performance of ORDCs with combination of PCM. The following chapter presents experimental facilities used in this study as well as the elementary data obtained from two display cabinets.

CHAPTER 3

EXPERIMENTAL SET-UP AND TEST RESULTS

This chapter presents the experimental setup and a test facility which was incorporated control and monitoring systems and employed during this project, and is divided into five main parts. The first part gives a brief description of the British Standard ISO procedure that was followed during the assessment and testing of the cabinets under consideration. The second part is a summary of the test chamber where environmental conditions were founded for the experiments. The third one details the instrumentation and data logging systems used for both performance monitoring and control. The forth part describes two types of display cabinets which were used in this project. The experimental investigations results and discussion are also presented in the last part. All of the experiments for this research were carried out in the custom built refrigeration laboratory of Mechanical Engineering Department at Brunel University London.

3.1 ISO Test Standards

All the experimental work was carried out according to the experimentation conditions of the International Organization for Standardization (ISO 23953: 2005) for Refrigerated display cabinets, part 1; Vocabulary and part 2; Classification, requirements, and test conditions. Therefore, the requirements of the tested cabinets in the climate chamber are adjusted as follows:

Temperature Gradient: The difference in the temperatures measured between the floor and the ceiling shall not exceed 6°C, and vertical temperature gradient shall not be more than 2°C/m.

Air Distribution: The air speed at all points along the line A-B should be within 0.2-0.1 m/s, when the display cabinet switched off. The air cross flow lines must be parallel to the longitudinal axis and to the plane of the cabinet's display opening, as shown in Figure3.1a.

Chamber Conditions Measurement Points: The ambient temperature and relative humidity should be measured on the mid distance along the cabinet length, as shown in Figure3.1b.

The Measurements Accuracy: Temperature $\pm$ 0.5°C, Relative Humidity $\pm$ 1.5% and power Consumption $\pm$ 0.5%.

Radiation rate: Temperature change caused by radiation of the test chamber walls and ceiling should not exceed $\pm$ 2°C of air temperature recorded at same levels.

Tolerances: The temperature and relative humidity tolerances are $\pm$ 1°C and $\pm$ 5% respectively.

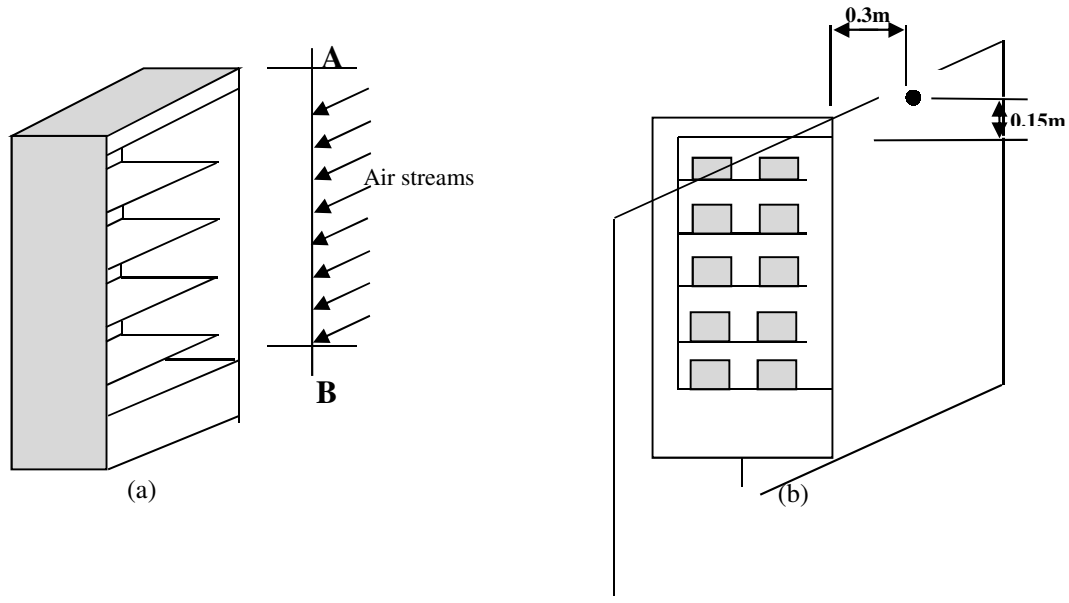

Figure3.1 Chamber conditions measurement

3.2 Climate Test Chamber

The performance of display cabinets must be classified and assessed based on consolidated test conditions that can finally be compared against a standard; therefore the need for controlled conditions to implement the testing work of the cabinets is important. The layout of this chamber is given in Figure 3.2.

3.2.1 Air Handing Unit

In order to maintain and control different experiment conditions as required by (BS EN ISO-2 2005) such as relative humidity, air temperature and air velocity, the chamber have to include an air handler unit (AHU). It can be seen, from the schematic diagram of the test chamber in Figure 3.2, that the air handler unit which includes a mixing case, a filter, a cooling coil, a heater, a humidifier and fan is located on a purpose built steel structure above the chamber roof. The chilled water of cooling coil of is supplied from a 9.9 kW chiller by a pump positioned within the chiller housing. The evaporator is shell and tube configuration and the compressor is semi-hermetic. A three-port diverting valve regulates the water flow through the coil.

This unit was designed to keep the ambient conditions inside the chamber in the range of (0- 40) °C and (35% to 100%) RH. The air handler unit controls the recirculated air through the chamber to maintain the conditions and reduce the temperature fluctuation inside the environmental chamber. The recirculating air comes from the supply air wall and blends with air curtain at the front of display cabinet and with the moist air at the back of the cabinet, then leaves the test chamber space through the return air wall to air handler unit, where the conditioned air undergoes processes of chilling, warming, moistening and blowing to reach the required values of the temperature, humidity and speed.

Moreover the temperature, humidity ratio and air circulation requirements of test chamber for the display cabinets experiments were according to (BS EN ISO-1 2005). Also, the air cross flow velocity through the chamber was kept to about 0.1-0.2 m/s and that was accomplished by adjusting the blade dampers at the air supply wall.

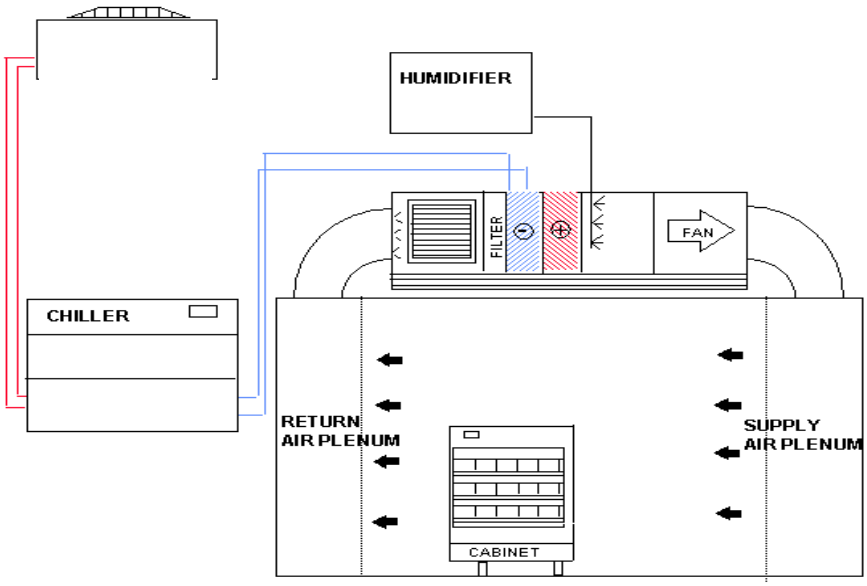

Figure 3.2 Layout of the environmental test chamber

3.2.2 Construction of the Environmental Chamber

A top view of the Environmental chamber containing the display cabinet under test is shown in Figure 3.3. The chamber size (7 m, 3.5 m and 3 m long, wide and high) is big enough to accommodate the cabinet in such the airflow nearby the cabinet will not be constrained by the chamber walls conforming to ISO Standard. The chamber walls and ceiling are built of cold chamber panels with 100 mm thickness.

Figure 3.3 also illustrates that the air-paths flow across the front side of the display cabinet without restrictions from the right to left of the test chamber and some of those air-paths interfere with the left side of air curtain. Furthermore, we can see four sections in the cabinet front left, front right, back left and back right, where the data was recorded. The back of the cabinet was positioned at 1.2 m from the rear wall of the chamber.

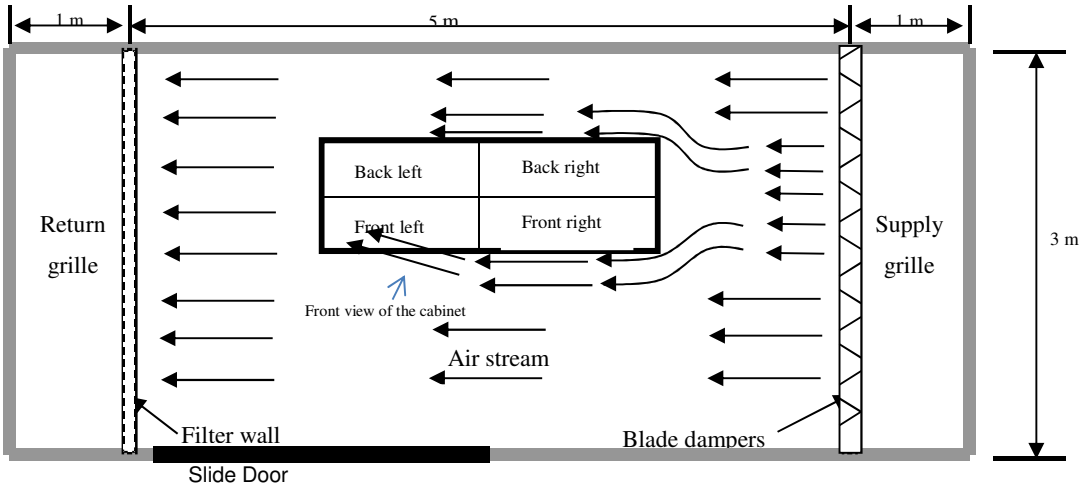

Figure 3.3 Top view of the climate chamber

The internal surfaces of those panels are made with white steel sheets, with an emissivity range (0.9 - 1.0), while the floor is made of concrete. The lighting in the chamber was provided by fluorescent lights with lighting level in the range between 500 and 650 lux which complies with the standard 600 ± 100 of lux at a height of one metre above floor level. The chamber also has a double glazed window and a slide door, 1.25 m wide and 2.5 m high. One meter spaces from both sides of the chamber, where the return and supply ducts of AHU terminated, were separated with technical walls to shape return and supply air plenums. The first space was parted with a perforated plate and filter wall reinforced by a wooden structure, making a pressure drop and thus a uniform air velocity within the test area and across the technical walls. In the same way the second space was parted with blade dampers, permitting the velocity profiles across the dampers to be regulated whenever required. Figure 3.4 shows the supply and return air plenum walls, which were designed to create an even, horizontal air flow within the test room.

Figure 3.4 Supply and return air plenum walls

3.3 Data logging system

The main measurement system included temperature, RH, and velocity sensors, data logging units (Labtech software and Data scan modules), and recording/display devices (computer set and monitor), as shown in Figure 3.5. The display cabinets were fully instrumented to measure product temperatures at different positions in the cabinet, inside-cabinet air temperatures and on and off temperatures of the evaporator air.

Figure 3.5 The main measurement system

The environmental temperature, relative humidity, cross flow velocity in the chamber, air and product temperatures in the display cabinet and compression refrigeration cycle temperatures were recorded and monitored at regular intervals by using computer-based

data logging system. The system consisted of temperature, RH, and velocity sensors; data logging system (Labtech software and Data scan modules), and recording/display system (computer set and monitor). The data logging system is comprised data acquisition modules and a recording and display system. The system is used to log the output signals from the instrumentation devices. The data acquisition systems consisted of the Data-scan 7000 series which include a Data-scan measurement processor 7320 and expansion modules 7020 from Measurement System Limited. There are 16 differential input channels, individually configurable for voltage and thermocouple measurements, in each Data-scan module and this system could be expanded up to 1000 channels. One processor and two expansion modules were prepared to cover all the instrumentation devices used in this work as shown in Figure 3.6.

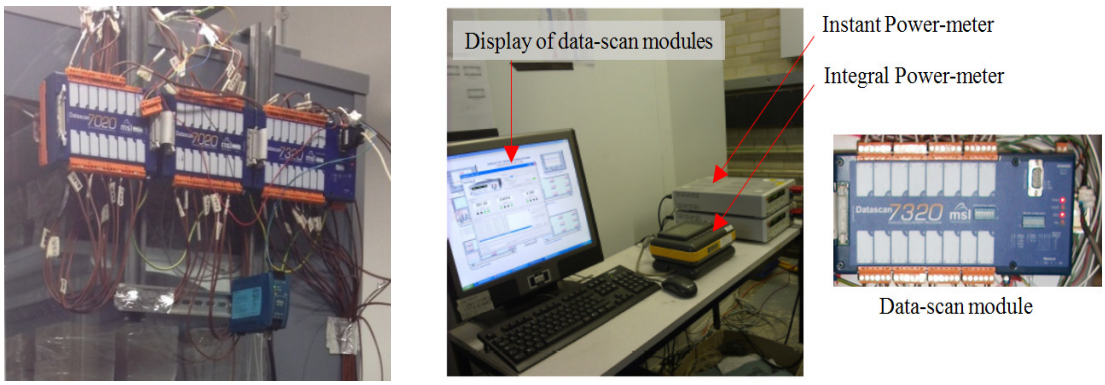

Figure 3.6 Data logging system

The recording/display system was a normal desktop computer. An RS-232 communication cables were used to transfer the signals between the computer and the Data-scan module. The computer includes Labtech, a window based icon driven data acquisition programme that saves the data into ASCII file, which is well-suited with the Data-scan module and permits a combination of more than 200 digital and analogue channels. Labtech also has ability to control a compound measurement system to be an eye-catching display for ease of monitoring.

3.4 Instrumentation devices

The instrumentation devices used on the test rig are temperature measurements, relative humidity sensor and power meter. A velocity meter was also used to measure air velocity in the test chamber and display cabinets. All measurements were recorded every 10s. This interval provided possibilities to check all temperature measurements at every 60s as specified in the standard sub-clause 5.3.1.6. The following sections provide a brief description of each device.

3.4.1 Temperature measurements

Most of temperature measurements such as products and air temperature were achieved by using T-type welded tip thermocouples with a temperature measurement range –50 °C to 200 °C with specific error (specified by manufacturer) of ± 0.2 °C. RTDs (resistance temperature detector) with model SEM105P were used for the air temperature sensor of the test chamber. All thermocouples were calibrated and it was found that all thermocouples had calibration error within the tolerance specified by the manufacturer.

3.4.2 Relative humidity measurements

Relative humidity measurements within the environmental chamber were implemented by using 'Rotronic' relative humidity and temperature probe. It incorporates a humidity sensor (Hygrometer IN-1) with measurement range from 0% to 100% and an RTD temperature sensor PT100 with range -40 °C to 60 °C. The output voltage range is 0 to 1 VDC. The measurements uncertainties are ± 1.5% and ± 0.5 °C for the humidity and temperature sensors respectively.

3.4.3 Power meter

The test rig power consumption was also monitored and recorded by using a power measurement system which is a programmable power meter (HM8115-2 from Hameg Instrument of uncertainty (±0.5%) connected in series with the main supply and a recording/display system. This meter has an LCD screen to display the measured instant power, current, voltage and power factor. RS-232 port was used to log the measured

parameters into the computer. The photograph of the instant power meter can be seen in Figure 3.6.

3.4.4 Velocity meter

The velocity meter was used to measure the air flow velocity at the air curtain and back tunnel of cabinets which is necessary for determination of the air mass flow rate of the across the evaporator coils. The meter was also used to check the velocity contour of the air flow in the test chamber to ensure that the air streams were within the ISO standard. The velocity meter is a hot wire anemometer which is Velocicalc Plus 8386A-M-GB with measurement range (0 to 50) m/s and uncertainty ± 3%. The meter can also simultaneously measure the relative humidity and temperature of the air with measurements range 0% to 90% RH – and 10 $^{\circ}$C to 60 $^{\circ}$C respectively.

3.5 Tested Multi-deck Display Cabinets

Two chilled open type vertical multi-deck of refrigerated display cabinets were tested; Bond-Group cabinet and Euromax-Norpe cabinet. They are quiet similar and the reason for using two cabinets was that we have two different energy saving techniques and each technique needs different cabinet design. The first one used with Bond cabinet was finned-tubes HEs, and the second one used with Norpe cabinet was finned-PCM container**.** The construction and dimension details for Bond and Norpe cabinets are shown in Figure 3.7 and Figure 3.8 respectively.

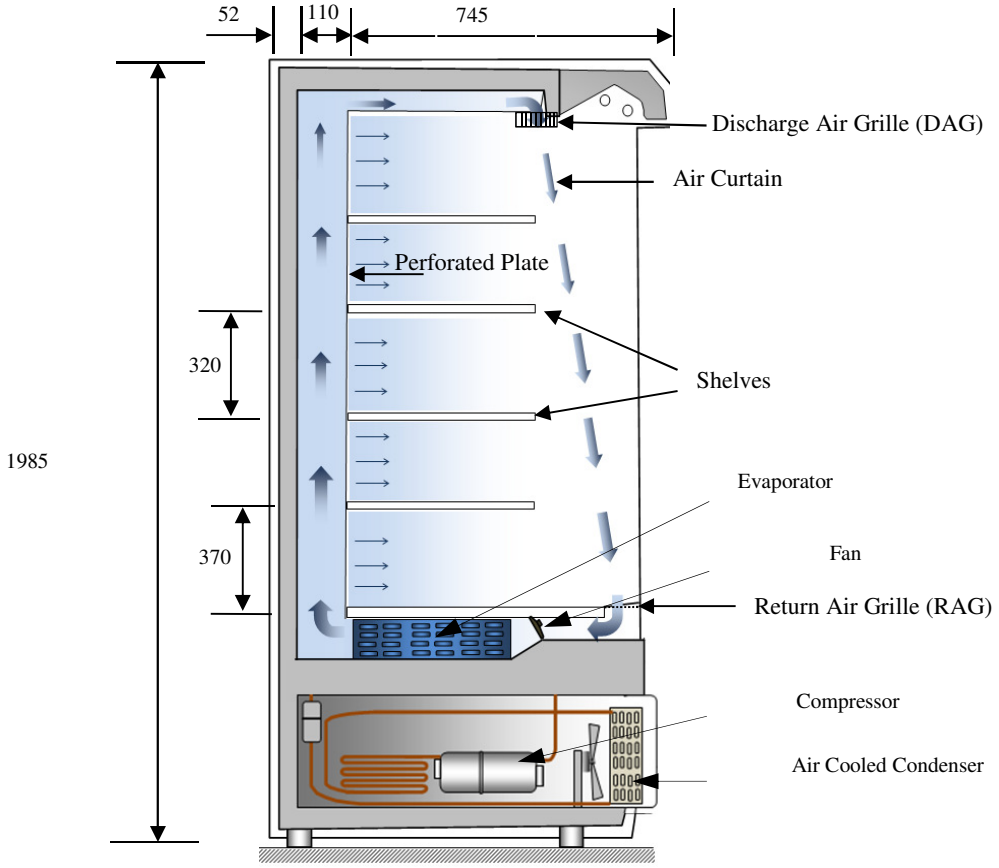

Figure 3.7 Cross section and dimensions (mm) of Bond-Group Integral Multideck cabinet

Table 3.1 Specifications of Bond-Group cabinets

Bond Asset No	Z024087	Case length	1250 mm
Case Manufacturer	B.D.C	Case Height	1985 mm
Case Model	Chicago 1250	Case Depth	910 mm
Defrost Type	Off Cycle	Display area	4.33 m^2
Elect. Load	5.5 Amps	Voltage	220v-50Hz
Refrigerant	R 1270	Op Temperature	3M2 0°C to +2°C
Gas Charge	650 gr	Shelves	Base +4

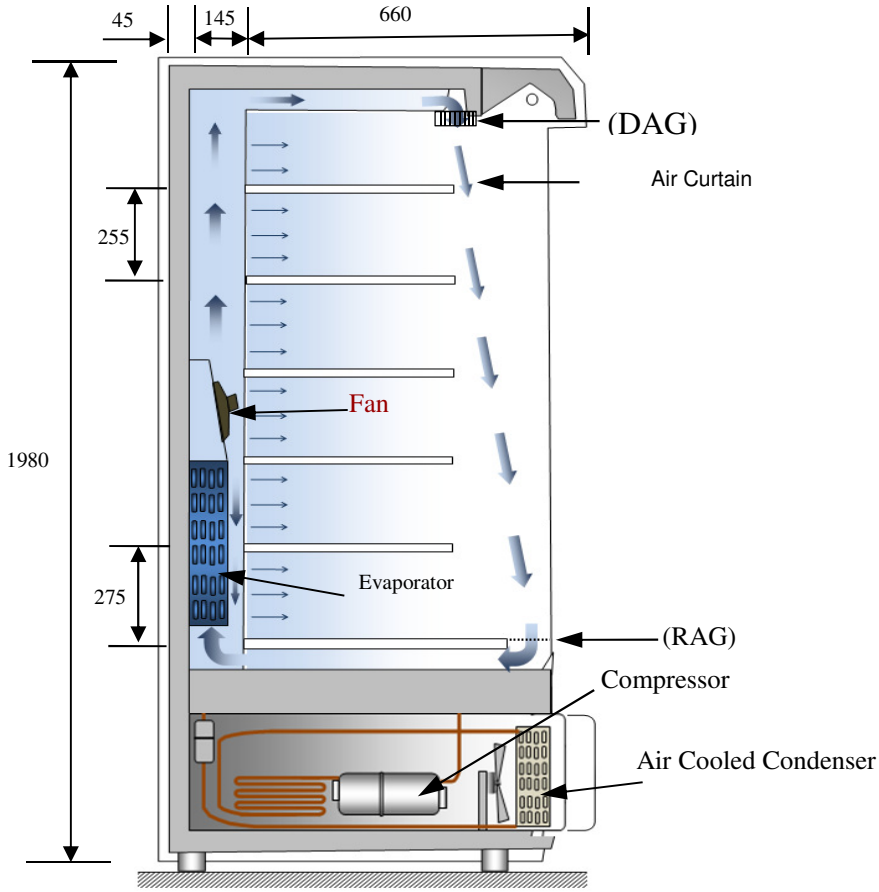

Figure 3.8 Cross section and dimensions (mm) of Euromax-Norpe cabinet

Table 3.2 Specifications of Euromax-Norpe cabinet

Description	Integral low fronted display case	Case Height	1980 mm
Case Model	EMX-125-M	Case Depth	850 mm
Defrost Type	Off-cycle	Power supply	13 amp
Capacity	810 Litres	Shelves	Base +5
Refrigerant	R 404A	Cabinet finish	White
Temperature range	0... +4ºC / M1	Display area	3,15 m^2
Case length	1250 mm	Gross weight	383 kg

The perforated plate has a specific perforation rate which is considered an important factor for the display cabinet performance because it controls the distribution of air flow rate in the cabinet. The perforation arrangement of the back panel is illustrated in Figure 3.9.

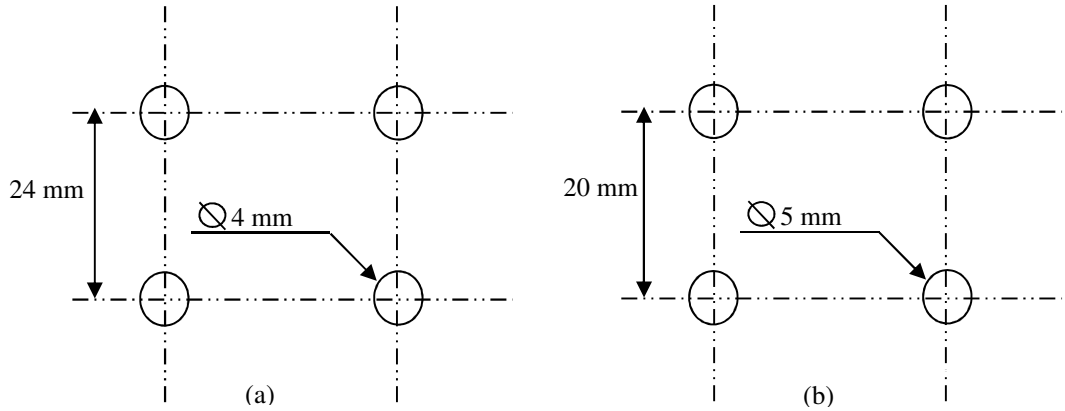

Figure 3.9 Perforation format of the back-panel for (a) Bond and (b) Norpe cabinets

The perforation ratio represents the total holes area of the back panel to the total back panel area. The opening rate of the perforation back panel for the Bond and Norpe cabinets was 0.045 and 0.032 respectively; this rate was calculated as follow:

$$\text{perforation ratio} = \frac{total\ opening\ area\ back-panel}{total\ area\ of\ back-panel} \tag{3.1}$$

3.5.1 Operation of the Display Cabinets

Bond-Group Display Cabinet: The chilled food multideck display cabinet shown in Figure 3.7 has been selected as a test prototype, with plug in cooling unit. This cabinet was old and its specifications of the cabinet are listed in Table 3.1. The evaporator is located under the bottom shelf of the cabinet. Before the evaporator coils, two of propeller fans were also equipped and suited before the evaporator in order to push the air flow through the evaporator and circulate it around the cabinet. The rest of components in the system (condenser, capillary tube and compressor) are positioned underneath. The cabinet is equipped with five shelves and one air curtain in the front.

Euromax-Norpe Display Cabinet: EMX-125-M integral low fronted multideck open display case was selected as a second test prototype in this study as shown in Figure 3.8. The cabinet was new and its specifications are listed in Table 3.2. It was equipped with single air curtain situated at the top, (base + 5) shelves, upright and top lighting, front riser for base shelf, NRC-100 control device, front bumper trim and hot gas evaporation tray. The evaporator is located at the bottom of the rear duct and divided into two parts in order to increase its performance. Above the evaporator coils, a propeller fans is also

installed in order to circulate the air flow around the cabinet. The rest of components in the system (two condensers, capillary tube and two compressors) are positioned underneath.

In both cabinets, as part of the air distribution system, the perforated back panel would allow the cooled air to flow on to the shelves and across the food products. Also, this penetrating air creates a pressure that prevents the deflection of air curtain into the display space. The back panel further stands upwards and crosses the ceiling to allow proportion of air to exit finally through the honeycomb of discharge air grille (DAG). The cold air also fall down due to gravitational force as it is heavier than the surrounding air. This generates a virtual insulation barrier called air curtain developed by the circulating air from top to the bottom at the front of the shelves. The vertical flow of air curtain will be mixed with the air coming from the surrounding environment and that penetrating from the shelves and consequently drawn into the return air grille (RAG) at the bottom of the front opening and then to the evaporator by the fans to circulate again.

To the conserve the mass flow of circulating air, a substantial amount of cold air curtain will spill onto the floor away by the RAG due the extra of mass flow rate caused by entertainment effect. Because the entertainments, a significant amount of ambient air moisture will condensate on the evaporator coil and, with the time, turn to frost. The accumulating frost needs to be regularly removed by defrosting process before blocking the air passages through the coil. The refrigerant is pumped by the compressor to high pressure side, rejecting heat to the surrounding air to allow condensation, and then letting the refrigerant to expand at lower temperature to absorb heat during the evaporation.

3.5.2 Temperature Control of the Cabinets

Both cabinets were using thermal sensors to control and monitor the air leaving the evaporator (air off), the air entering the evaporator (air on) temperature and compare them with a per-specified set point which was calculated by the controller. EVCO-221 and NRC-100 controller devices were built in for Bond and Norpe cabinets respectively. In each controller, a user interface is provided in the form of a keypad and LCD display

for the setting of different parameters, such as defrost period, set point and differential temperature. Another sensor was present in both cabinets toward the rear of the evaporator to control the defrosting termination temperature. In the Norpe display cabinet, additional sensors were presented to be used in the set point calculation, one was just before air curtain grille, and another one was on the shelf no.4.

3.5.3 Loading the Display Cabinets

Both cabinets were loaded according to ISO Standard with test packages used to simulate the thermal mass of food under real conditions. The packages of the Bond cabinet were 0.8 litre plastic containers filled with 50% propylene glycol in water solution to provide thermal capacity. The solution has a freezing temperature of -33^{o}C. The total number of those packages was 193 and the monitored packages were 24 as shown in Figure 3.10a.

Figure 3.10 Loading scheme in (a) Bond and (b) Norpe cabinets

The Norpe cabinet was loaded with different type of test packages (M-packs). The M-packs were made in the laboratory by mixing chemical compositions; hydroxyethyl methyl cellulose (Tylose), sodium chloride (salt) and 4-chloro-m-cresol (anti-bacteria),

with boiling water as specified by the supplier (Sigma-Aldrich company, Ltd). The dimension 200 x 100 x 50 mm (height x width x depth) as shown in Figure 3.10b. Its physical properties include density 1000 kg/m^3 at 0°C, thermal conductivity 0.3 W/m-K and specific heat 3500 J/kg-k. The total number of those packages was 306.

In both cabinets and to abide by the standard, a 3 cm distance was left between the packages and the side walls while a 2.5 cm distance was left between the packages rows. The loading height in each shelf was equal to the free height between each two shelves. Along the cabinet depth, the centre of the packages was located 5 cm from both the perforated panel and from the front edge of shelves.

3.5.4 Sensors Arrangements

The cabinets were fully instrumented to measure all the required parameters. The measurements of both display cabinets were carried out for the test packages in 24 products and four sections; front right, front left, rear right and rear left as we can see in Figure 3.3. These measurements were calibrated temperature sensors inserted inside geometric centre of products which were distributed in three shelves; top, middle and bottom (8 products in each shelf), in order to record and observe the average temperature variations.

The measurements also were conducted for the circulated air at three positions through the cabinet. The measurements involve; T, RH and V for air leaving the evaporator (air-off), T and V for air curtain outlet and T for the temperatures of the air entering the evaporator (air-on) as illustrated in Figure 3.11. In addition, temperatures were also measured on accessible locations of the refrigeration system piping by attaching temperature sensors before and after every part; compressor, evaporator and condenser. Simultaneously the power consumption of the cabinet was also measured. The relative humidity and temperature inside the environmental test chamber were measured using sensors located on the mid distance along the length of each cabinet as indicated in Figure3.1b.

Figure 3.11 M-packs arrangement and measurement points, (a) Bond (b) Norpe Cabinets

3.6 Test Results Summary

A series of preliminary experimental investigations were carried out at climate classes 0 (20^{o}C / 50% RH) for Bond cabinet and class 3 (25^{o}C / 60% RH) for Norpe cabinet to check the thermal performance. This was also important in order to find out whether the

manufacturer operational setting was suitable enough to obtain M-packages temperatures of M1 classification, and to deliver test data for modelling validation and inputs to the CFD model. Also the default settings of the controllers of the cabinets have appropriately been reset to determine optimum operating settings that are compatible with our work. Testing process in such cabinets is time consuming as that needs to carefully load the cabinet with a specific shape and number of test packages and some of these packages need to be instrumented with thermocouples. Moreover, all the monitored parameters need to be recorded by the logging system during all the test time, and we have to wait between three to four days till the data reach to steady state conditions. The following subsections summarise the test results for the environmental chamber and the refrigerated display cabinets.

3.6.1 Environmental Test Chamber Conditions

The boundary conditions of the environment have direct effect on the air temperature, product temperature and cooling load of the display cabinets. Environment conditions in the test chamber were tightly controlled by PD (proportional-differential) controller which is connected to the measurements system and modulates the heating system, the humidifier and the opening of the chiller system valve. The horizontal air cross flow velocity of the chamber was kept in the range (0.1 - 0.2) m/s. Figure 3.12 and Figure 3.13 illustrate the variation of the air supply temperature and relative humidity with time during stable 8 hours running period through the test chamber at climate class 0 and 3 respectively. It can be seen that the temperature and relative humidity were almost steady and maintained in the allowable range during the test. Peaks for the temperature and relative humidity curves can be seen in both Figures which are due to the defrost process of the display cabinets.

Figure 3.12 Temperature and relative humidity variation inside the test chamber at climate class 0

Figure 3.13 Temperature and relative humidity variation inside the test chamber at climate class 3

It was also found that the relative humidity slightly increases during defrost period of the display cabinet, but in general the relative humidity is well controlled. This process illustrated in Figure 3.14, the reason could be that when the defrost starts; the humidity ratio increased at constant dry bulb temperature because of the circulated air of the cabinet begins to melt and evaporate the accumulated ice between the evaporator coils. In addition, the evaporation of water from the condensate tray could be the other reason for that. This action will increase the relative humidity slightly in the ambient air which is in contact with the air cabinet, but of course the humidity controller will adjust the new value of humidity to keep it at pre-set limits.

Figure 3.14 The changes of relative humidity variation inside the test chamber at climate class 3

3.6.2 Bond-Group Display Cabinet

As we mentioned before this cabinet was not new and it has some problems such as weak air curtain. However, after some checking performance tests conducted to this cabinet, we have found that the results are acceptable to carry out our rest study. At climate class 0 (20°C and 50% relative humidity), chamber conditions, product and cabinet air temperatures and refrigeration compression cycle were measured and monitored during the test by measurement display which can be seen in Figure 3.15. This Figure shows the position and instantaneous product and air temperatures inside the cabinet. Table 3.3 shows the optimum and detailed operational settings of the cabinet obtained from the inspection stage in such those settings are adequate for the suggested modification.

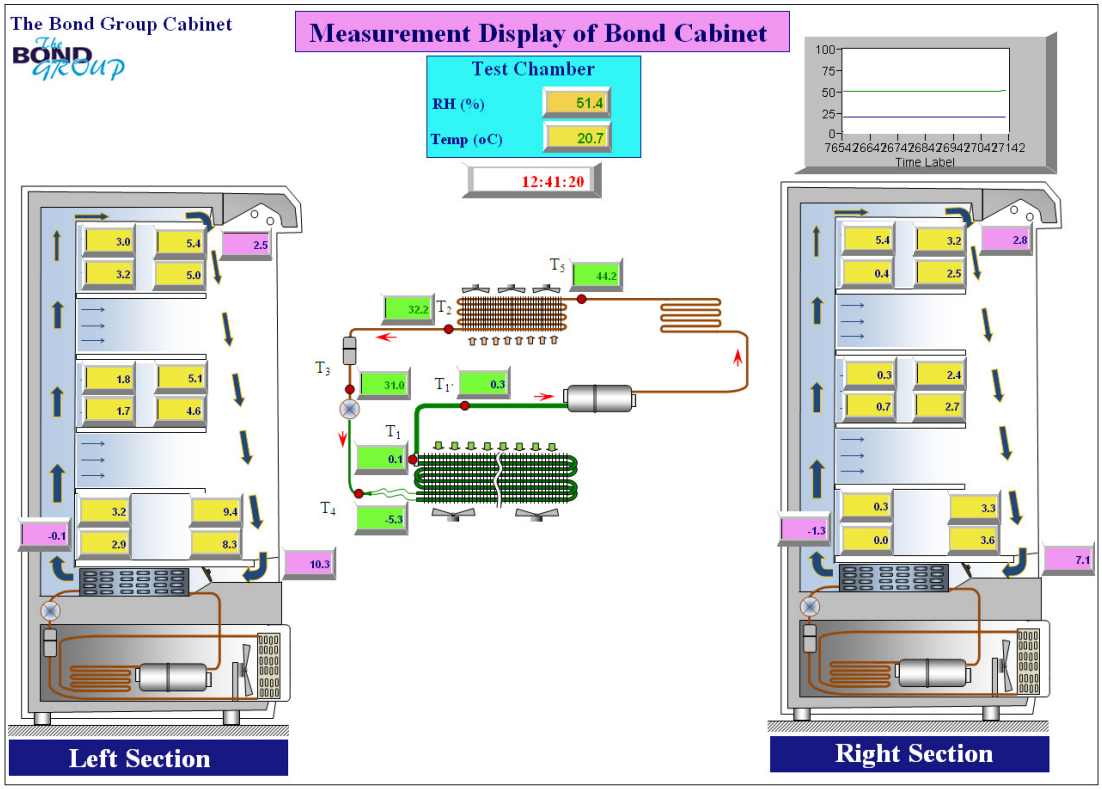

Figure 3.15 Positions for the temperature sensors inside the Bond cabinet

Table 3.3 Operational setting of the Bond cabinet

Cabinet Settings:	Value	Cabinet Settings:	Value
Set Point (ºC)	0	Defrost Intervals (h)	4
Differential Temp (ºC)	2	Defrost Termination (ºC)	8
Min Set Point (ºC)	-3	Defrost Maximum Duration (min)	45
Max Set Point (ºC)	3		

Figure 3.16 and Figure 3.17 show the product temperature variation with time of both sides; left and right for the Bond cabinet respectively. There are 12 product temperature measurements at each side represented under different names of three letters, each depending on the product simulator location in the cabinet. The first letters include T, M and B, signifying top, middle and bottom respectively; the second letters consist of R and F, indicating rear and front each; the last letters are U and L specifying upper and lower respectively. For example, TRL represents the temperature of the product at location top, rear and lower portion of the cabinet.

From these Figures, it can be seen that the product temperatures vary periodically during the test because the compressor on/off and defrost cycles over 8 hour period. It is evident that the left side of the cabinet the product has higher temperature compared to the right side. The reason could be attributed to the air stream lines across the chamber try to strongly entrain with the cabinet air curtain particularly the left side as we can see in Figure 3.3. This also was confirmed by (D'Agaro, et al 2006) who endorsed this outcome to a vortex developed on the leading wall along the direction of cross flow, creating the air bounce inward toward the display opening and hit the packages at the far end of the cabinet.

Figure 3.16 Product temperature variations for the left side Bond cabinet

Figure 3.17 Product temperature variations for the right side Bond cabinet

The bottom shelf product has the highest average temperature (3.7 ºC), while the middle shelf has the lowest average temperature (2 ºC). The reason could be that the middle shelf has more back panel holes and thus higher air flow rate coming from the back duct compared with the bottom shelf. Also the bottom shelf is wider than the rest shelves so it accommodates three products rows instead of two as shown in Figure 3.11a. The products on the rear part of the shelves has lower temperature compared to those on the front part and that could be due to the fact that, the front products are more affected by the external flow and receiving more radiation, while the rear products are less affected and closer to the cold perforated back panel and cooling coil. The highest difference of product temperature recorded on the bottom, middle and top shelves were 9.7°C, 5.2 °C and 5.4 °C respectively.

The temperature variation for air leaving the evaporator (air-off), air entering the evaporator (air-on) and air curtain outlet (air-curt) were measured with time and presented in Figure 3.18 and Figure 3.19 for the left and right sides respectively. It can be seen that fluctuations of the air temperatures are relatively wider during defrost period because the long-time of compressor absence. Also the right hand side temperatures of the display cabinet are lower than the left hand side temperature making the right side product temperature lower for the same reason mentioned in products temperature section. Also, a clear temperature rises were experienced as the air journeyed from the air-off position to the air curtain and then to the air-on to start again. This is caused by the heat gain through the side and back walls of the cabinet. The temperature differences between the left and right sides were about 1.5 °C for the air-off side, 3 °C for the air-on side and 0.5 °C for the air-curt outlet.

Figure 3.18 Temperature variation of air-off, air-on and air-curt outlet for the left side Bond cabinet

Figure 3.19 Temperature variation of air-off, air-on and air-curt outlet for the right side Bond cabinet

Figure 3.20 presents the variation of instant power with time. It can be seen that the compressor needs higher power at each restarting time and especially after defrost period. After finishing the defrost, the cabinet needs more time to reach the set point due to the temperature inside the cabinet rises by a few degrees during defrosting. Total

Energy Consumption (E_t) was calculated according to BS EN ISO 23953-2: 2005 sub-clause 5.3.5.2 as follows:

$$E_t = \sum_{n=1}^{n=N_{max}} E_n . t \qquad (kWh) \tag{3.2}$$

E_n = instant power consumption of the cabinet (kW) over 24 hours (E_n = 0 during stopping and defrost times), t = period of measurement (h).

Figure 3.20 Instant power consumption for Bond cabinet

Compression refrigeration cycle temperatures variation with time is shown in Figure 3.21. Monitoring the cycle is important to make sure it is working properly and be able to justify any errors which might be happened.

Figure 3.21 Compression refrigeration cycle temperatures for Bond cabinet

Moreover, the relative humidity and velocity of the air off temperature and the velocity of air curtain outlet were not measured by permanent sensors, we measured those couple of times by portable sensors to take the average values and make sure they are in the normal ranges to use them later in the simulation. The average relative humidity, velocity of air-off and air curtain velocity were 75%, 1.8 m/s and 0.5 m/s respectively.

3.6.3 Euromax-Norpe Display Cabinet

Although this cabinet was brand new, it was subjected to checking process and controller reset. At climate class 3 (25°C and 60% relative humidity) chamber conditions, product and cabinet air temperatures and refrigeration compression cycle were measured and monitored during the test by measurement display which can be seen in Figure 3.22. This Figure shows the position and instantaneous products and air temperatures inside the cabinet. Table 3.4 shows detailed operational setting of the cabinet obtained from the checking stage.

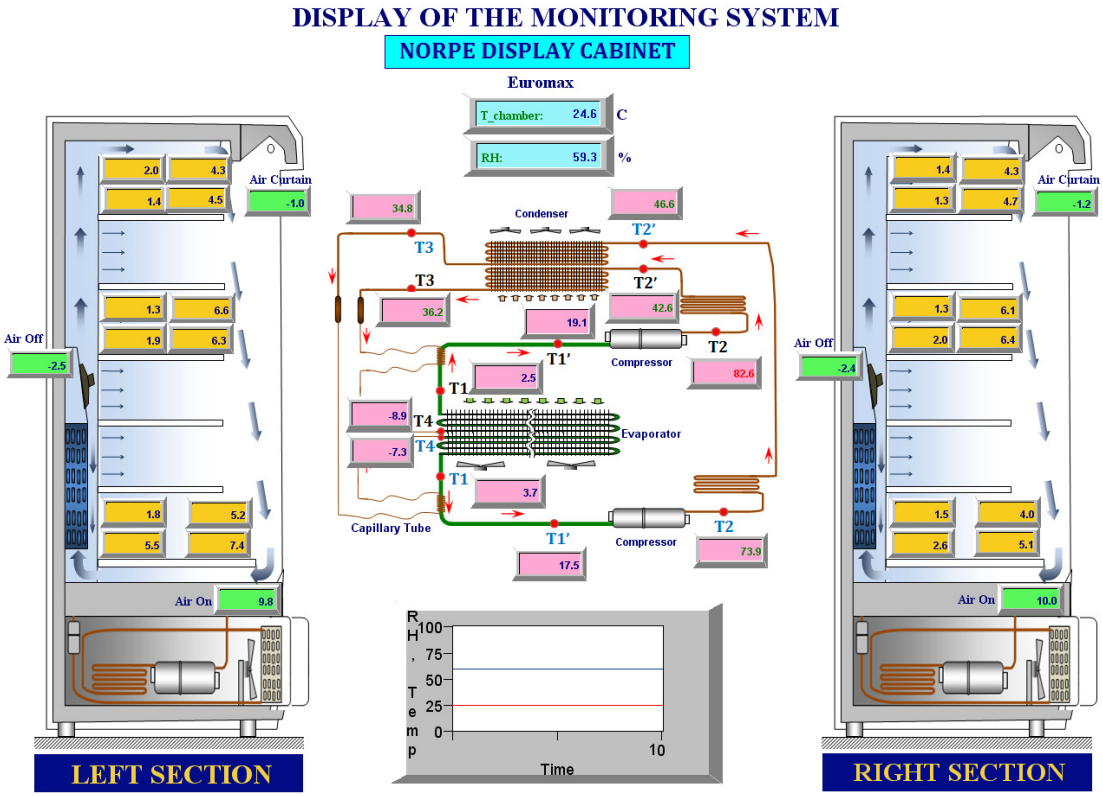

Figure 3.22 Positions for the temperature sensors inside Norpe cabinet

Table 3.4 Operational setting of the Norpe cabinet

Cabinet Settings:	Value	Cabinet Settings:	Value
Set Point (ºC)	-1.8	Defrost Intervals (h)	4
Differential Temp (ºC)	2.2	Defrost Termination (ºC)	11
Min Set Point (ºC)	-3	Defrost Maximum Duration (min)	35
Max Set Point (ºC)	3		

Figure 3.23 and Figure 3.24 show product temperature variation with time of both sides; left and right for the Norpe cabinet respectively. Again there are 12 product temperature measurements at each side represented under different names of three letters similar to naming system for previous cabinet. From these Figures, it can be seen that the product temperatures vary periodically during the test because the compressor on/off and defrost cycles over 8 hours period. On the left side of the cabinet the product slightly has higher temperature compared to the right side for the same reason mentioned in previous cabinet. The bottom shelf product has the highest average temperature 4.2C, while the top shelf has the lowest average temperature 3C because the top shelf has

been least affected by chamber stream lines where the air curtain is more strong and it has fewer products, and vice versa for the bottom shelf. This was also approved by (Al-Sahhaf 2011), the variation in products temperature was found to gradually increase from top to bottom shelves.

Figure 3.23 Product temperature variations for the left side

Figure 3.24 Product temperature variations for the left side Norpe cabinet

Again the product on the rear part of the shelves has lower temperature compared to the product on the front part of the shelves as mentioned before. The highest difference of

product temperature recorded on the bottom, middle and top shelves were 6.8°C, 5.8 °C and 3.9 °C respectively.

The temperature variation for air-off, air-on and air-curtain outlet were measured with time and presented in Figure 3.25 and Figure 3.26 for the left and right sides respectively. Again it is clear that the right hand side temperatures of the display cabinet are lower than the left side and the temperature increases with moving of circulated air for the same reason mentioned in the previous cabinet. The temperature differences between the left and right sides were about 1 °C for the air-off side, 2 °C for the air-on side and 0.5 °C for the air-curt.

Figure 3.25 Temperature variation of air-off, air-on and air-curt outlet for the left side Norpe cabinet

Figure 3.26 Temperature variation of air-off, air-on and air-curt outlet for the right side Norpe cabinet

Figure 3.27 presents the variation of instant power with time. Energy consumption was calculated according to BS EN ISO standard sub-clause 5.3.5.2. From this Figure, it can be noticed that the compressor needs higher power at the starting of each running time and especially after defrost period. After finishing the defrost, the cabinet needs more time to reach the set point due to the temperature inside the cabinet rises by a few degrees during defrosting. It is also noticed that during the defrost time the instant power higher than normal off cycle because the off cycle defrost method in which the evaporator fan will be running using room air to defrost the evaporator block.

Figure 3.27 Instant power consumption for Norpe cabinet

Compression refrigeration cycles temperatures variation with time is shown in Figure 3.28 and Figure 3.29 . Monitoring the cycles is important to make sure they are working properly and be able to justify any errors which might happen. We have two compression cycles in this cabinet to increase the performance. We can clearly see the temperature differences (between the inlet and outlet) were 65 $^{\circ}$C and 10 $^{\circ}$C for the compressor and condenser respectively.

Figure 3.28 First compression refrigeration cycle temperatures for Norpe cabinet

Figure 3.29 Second compression refrigeration cycle temperatures for Norpe cabinet

Again, the relative humidity and velocity of the air off temperature and the velocity of air curtain were not measured by permanent sensors, we measured those couple of times by portable sensors to take the average values and make sure they are in the normal ranges to use them later in the simulation. The average relative humidity and velocity of air-off and air curtain velocity were 80%, 2.8 m/s and 1.3 m/s respectively.

3.7 Summary

The test standards, environmental test chamber, data acquisition system, tested display cabinets and sensors arrangements of the tests have been presented in this chapter. In addition, the performance test results of the display cabinets were discussed. The data of both cabinets showed a variation in readings from right to left sides, rear to front sections and top to bottom shelves. Since 2D-CFD model is to be used to model the air flow and heat transfer inside the display cabinets, the related data was collected for validation purposes, and to utilise as actual boundary conditions for the simulations employed for the optimisation scheme.

Chapter 4 will present experimental PCM integration and results comparison of both display cabinets.

CHAPTER 4

EXPERIMENTAL PCM INTEGRATION AND RESULTS COMPARISON

The experimental performance for two types of refrigerated open-type multi-deck display cabinets with and without integrated phase change materials (PCMs) was investigated in this chapter. To examine and optimize different types of PCMs (in terms of quantity and quality), the integration was implemented by using two different configurations; heat exchangers and containers, at different locations inside the cabinets.

4.1 Introduction

To satisfy the maximum transient load, supermarket refrigeration equipment, such as display cabinets, is normally oversized. Both the utilization of compressor capacity control and application of thermal energy storage (TES) within the equipment are considered to be the most common techniques in assuring the system's operation at part-load conditions. Using PCMs for thermal energy storage has played a key role in refrigeration systems through their direct integration into the system components or cabinets for energy savings and control. Such integrations have been studied over many years in different ways and acquired substantial attention recently.

Most of the studies cited in literature review focused on the effects of PCM application on the performance of closed type cabinets, such as freezers and refrigerators or a conventional refrigeration system, but there is only one study was applied on open type

display cases as was mentioned in chapter 2. It is the purpose of this chapter to experimentally investigate the effect of PCM integration on the performance for two types of open multi-deck display cabinets in terms of energy savings, food product temperature improvements, and comparisons with conventional units.

4.2 PCM integration in Bond Cabinet

This cabinet was the first option for modification study as the second cabinet was not arrived yet. All specifications and description for this cabinet are mentioned in chapter 3. It was not new and its modification took about six months from whole research period, all modifications stages are described in the following sections.

4.2.1 Experimental setup

PCM integration through this cabinet was suggested to evaluate and improve the overall efficiency of the display cabinet, and to be the first stage that will outline and specify the direction of the whole project. There are several suggested positions to integrate the PCM through this cabinet, and choosing the most effective position depends on some criteria. The first factor is the volume and density of latent heat as there is wide range of PCMs available with different characteristics. The type of PCM is associated with required volume for a given application due to the density of latent heat stored. The required volume of PCM for this cabinet will be calculated in later section. The second important issue that should be taken in the account is the freezing and melting temperature. It is well known that the cabinet air temperatures are different from position to another through the cabinet so that deciding where the PCM should be located highly depends on all thermal-physical properties of circulating air at individual locations such as temperature and air velocity.

Figure 4.1 The Left side view of the Bond cabinet with installed PCM-HEs

Furthermore, the configurations and arrangements suggested to employ the PCM is another significant consideration to efficiently benefit from PCM function. One of the common PCM configurations is PCM heat exchanger (PCM-HE) that could contribute to decrease the required quantity of TES as was mentioned in literature review. We have chosen this technique with the current cabinet due to its design (evaporator at the bottom) that provide an appropriate space at air flow duct in the rear side in order to install the finned tubes HE containing the PCM as shown in Figure 4.1. The base of this duct found to be the best suggested position for the PCM due to the ease of installing the PCM-HE on the cabinet base just after the evaporator where the air velocity at its maximum value.

Figure 4.2 Front view of the cabinet with fans and evaporator coil (Back panels were removed)

Figure 4.3 The air flow duct dimensions

After many experimental investigations and analysing the primary results that mentioned in chapter 3 for Bond cabinet, the modification stage started by removing all products, shelves, back and base panels and instrumentation devices as depicted in Figure 4.2. The exact dimensions were taken with required allowance to specify the HE's dimensions later on.

4.2.2 Proposed PCM

As mentioned in the previous section, characteristics of integrated PCMs such as transition temperature and volume and density of latent heat will depend on their position in the display cabinet (i.e. before or after evaporator). After series of experimental tests, we have found that air temperature before evaporator (Air-On) was in the temperature range of 6°C to 13°C. According to the cabinet design, this temperature value is appropriate to evaporator capacity. However, for the current design, there are few options to install the PCM before the evaporator as illustrated in Figure 4.1.

Air cabinet temperature after evaporator (Air-Off) was found to be in the range of -4°C to +4°C to maintain low Air-curtain temperatures during Off-cycles. For the given data and design, the focus will be on PCMs applied after evaporator coils. Hence based on the Air-Off temperature range, the suggested PCM transition temperature must be within the Air-Off temperature range to guarantee appropriate temperature for phase changing process. Molten paraffin RT (-2) was selected and identified as potential PCM for this stage of research with thermodynamic properties shown in Table 4.1 for small differential scanning calorimetry (DSC) sample as shown in Figure 4.4, PCM temperatures are satisfactory. This figure clearly showed us the amount of heat flow that can be released and absorbed during the freezing and melting processes respectively and at which temperature those two processes are starting and finishing.

Figure 4.4 differential scanning calorimetry for RT (-2)

RT is pure organic PCM and has good properties such as no sub-cooling effect, chemical stability, long term product, stable performance over the cycles of phase change. However, its latent heat capacity and thermal conductivity are lower compared to water.

Table 4.1 Thermal properties for RT

Characteristics	Value
Density (liquid) (kg/m^3)	880
Density (solid) (kg/m^3)	770
Volume expansion (%)	12
Thermal conductivity(both phases) (W/m K)	0.2
Specific heat (kJ/(kg K)	2
Melting temperature (K)	271.35
freezing temperature (K)	270.35
Latent heat of fusion (kJ/kg)	125
Temperature difference	3
Maximum operation temperature (K)	303.15

4.2.3 Nucleation

The initial stages that occur in the crystallization process from a thermodynamic phase (solution, liquid or vapour) via self-assembly are called nucleation. It is also defined as the process that determines the required time before the new self-organized phase appears (Kalikmanov 2012). The kinetic of nucleation process in a solution requires sub-cooling which can be obtained by decreasing the temperature. The solution molecules then attempt to nucleate achieving thermodynamic balance.

Figure 4.5 Aluminium swarf

Moreover, If a solid particles of foreign material are added to the solution, the crystallization will be faster and easier (Mersmann 2001), especially when these particles have higher thermal conductivity than the PCM medium itself (Sahan and Paksoy 2014). Therefore, all the heat exchanger tubes were filled with about 5% of aluminium swarf in order to increase the thermal conductivity inside the PCM medium as well as create the nucleation sites. Different types of swarf were investigated such as thin rings of copper pipe. The Aluminium swarf which is illustrated in Figure 4.5, showed the best performance among all tested swarf types.

4.2.4 PCM heat exchangers

In this work, we did not use ready PCM-HE as our application needs special specifications of HE design which are not available in the market as well as making PCM-HE design was one of the our research goals.

It was suggested to reuse two different types of HEs as shown in

Figure 4.6 and as follows;

a) Twin 15mm copper tubes with aluminium fins, 90mm x 40mm.

b) An evaporator coil with 23mm steel tube and aluminium fins.

Figure 4.6 PCM-Heat Exchangers parts

All HEs were not ready for direct use and needed a lot of work to be used in building and sizing a PCM-HEs and integrating them within the cabinet. First, the evaporator

coil was cut and formed into a set of finned tubes, and pipe connections and plates at the two ends were removed and the coil was cut into 3 pieces. After the cutting process, fins were cut to achieve the 10 cm width according to the 10 cm available gap at the back of the display cabinet as shown in Figure 4.7. Then, two fined tubes pieces were connected to each other using four small copper pipes as shown in Figure 4.8.

Figure 4.7 (a) cutting the ends and (b) adjusting the fins for evaporator coil

However, this work was not ideal as there were not fins in the middle and the leakages inside the welded pipes were difficult to deal with. Based on the available space at the air flow duct of the cabinet, only two parts of the suggested HEs were then used; twin tubes with fins and modified four finned tubes HEs. Finally, all HE parts are ready for the next steps which include filling them with aluminium swarf and then pouring the PCM inside the HE tubes at room temperature with specific amount and leaving a space for expansion purposes of PCM solid phase as follows.

Figure 4.8 (a) one piece of the prepared finned tube (b) 2 connected fined tubes pieces (c) Ready four pipes HE

Twin copper tubes were filled with 0.27L of RT (-2), this amount represents 210 g. The modified four finned tube was filled with 1.32L of RT (-2) this amount represents 1160 g. The total amount of RT (-2) used was 1370 g. 14% volume expansion in phase change range was considered in calculations. The location of each finned tubes PCM-HE inside the cabinet was just after the evaporator as shown in Figure 4.9.

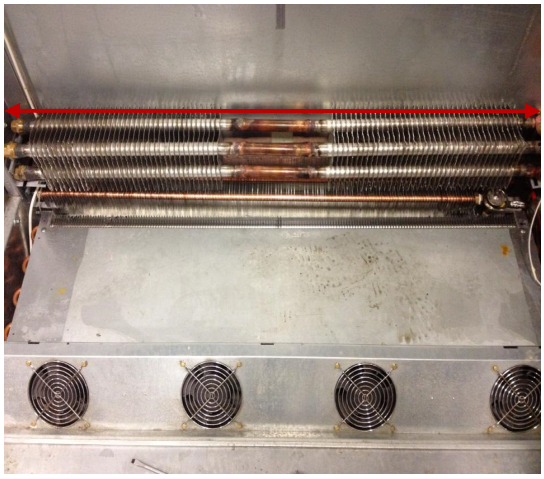

Figure 4.9 (a) one installed HEs, (b) two Installed HEs and (c) closer view for both HEs inside the cabinet

4.3 Bond cabinet results and discussion

The test results are presented in two groups; tests for the cabinet without PCM and preliminary tests for the cabinet with RT (-2) as PCM. The test results include; product temperatures, cabinet air temperature, Energy consumption and performance comparison. With M-packs and water-glycol as test packages load arrangement and at test conditions climate class 0: 20^{o}C / 50% RH.

4.3.1 Product temperature

The cabinet product temperatures with and without PCM-HEs were measured during 8 hours test period for the left and right side as shown in Figure 4.10 and Figure 4.11

respectively. In each side, there are 12 product temperature measurements represented under different names of three letters as mentioned in chapter 3.

Figure 4.10 Product temperature variations for the left side Bond cabinet with and without PCM

Figure 4.11 Product temperature variations for the right side Bond cabinet with and without PCM

It can be seen from both Figures; the product temperatures stay stable with small fluctuations in response to the compressor On, Off and defrost cycles. For the cabinet without PCM, the product temperature variation ranges (ΔT) were higher than those

with PCM. This reduction in temperature range reduces the temperature differences of products temperature and allows them to be more convergent. However, as predicted, the outcome of adding PCM was not strong in achieving an effective increase in whole average of product temperatures within standard limits. This small increase was caused by a subsequent rise in cabinet air temperatures, which are in immediate contact with the products. The main temperature differences between the both tests are summarized in Table 4.2.

Table 4.2 Experimental products temperature for Bond cabinet

Experimental parameters	Left Side		Right Side	
	Without PCM	With PCM	Without PCM	With PCM
Average temperature (ºC)	4.215	4.296	1.47	1.513
Maximum temperature (ºC)	9.459	8.28	3.78	3.137
Minimum temperature (ºC)	1.013	1.707	-0.379	-0.305
Temperature range (ºC)	8.446	6.569	4.159	3.042

Moreover, it is clear form this table that the average temperature is slightly higher for modified cabinet and this was expected as the PCM-HEs were considered as an extra load. However, this increase was not high enough to get considerable energy saving.

4.3.2 Cabinet air temperatures

Figure 4.12 and Figure 4.13 obviously show the influence of PCM with time on the cabinet air temperatures; air off, air on and air curtain outlet at both left and right sides respectively. It can be seen from figures that all the maximum temperatures in the original cabinet are higher than those with the PCM setup. The effect of PCM on the off cycle periods was very small for this cabinet, and thus the off period time was nearly constant at around 3 minutes for both cases. However, the overall effect appeared, as expected, during defrost period when the temperature values significantly increased for longer periods. Defrost duration gave enough time for PCM to melt absorbing a heat and, then decrease the maximum temperature values. This reduction affects the product temperatures as mentioned in the previous section. Furthermore, it is evident that the cabinet air temperatures are more stable and homogenous when PCM is integrated

Figure 4.12 Cabinet air temperature variations for the left side Bond cabinet with and without PCM

Figure 4.13 Cabinet air temperature variations for the right side Bond cabinet with and without PCM

4.3.3 Average instant power consumption

The variations of instant power with time for the system employing PCM-HEs and the basic one is shown in Figure 4.14. Total energy consumption of each cabinet was calculated according to BS EN ISO 23953-2: 2005. For the basic system, the power required with time is around 0.5% higher than that obtained from the modified cabinet.

It should be noted that adding the PCM has slightly affected the defrost duration as the cooling capacity supplied by the PCM-HEs was not enough to maintain the cabinet temperature during the PCM discharge (melting) process. Energy consumption was calculated by using complete cycle method. The average instant power, running time and energy consumption of the cabinet at both tests are shown in Table 4.3.

Figure 4.14 Average instant power consumption for Bond cabinet with and without PCM

Table 4.3 Energy parameters of Bond cabinet

parameters	**Cabinets**	
	without PCM	**with PCM**
Average instant power (KW)	1.15	1.15
Running time (h)	19.65	19.54
Experiment time (h)	24	24
Energy Consumption (kWh)	22.603	22.476
Compared to without PCM (%)	-	0.5%

4.3.4 Finned Tube Surface Temperatures

Finned tube (FT) surface temperatures of PCM-HEs at four locations (BL, BR, TL and TR) were recorded with time as shown in Figure 4.15a and b. It is clear that the lower HE has slightly lower temperature due to its location is closer to the evaporator coil. Generally, not all of the PCM was utilized during the working time as the cabinet performance was not good enough.

Figure 4.15 (a) Sensor locations on PCM_HEs, (b) Surface temperatures variation with time for PCM-HEs

4.3.5 Quantification of PCM

We did not calculate the required amount of the PCM that can make considerable energy saving and substitute the evaporator role during the defrost time. The reason for that were the experimental limitations which provided us with small spaces to add the PCM so we were not sure the available PCM amount was satisfactory. However, we have done the experiment to get indication about the PCM effect. After the current encouraging results, it is necessary to find out the amount of PCM to be integrated in this cabinet for energy saving purposes.

For the current work; the mass of PCM used in the experimental test = 1.37 kg and the latent enthalpy = 125 kJ/kg then the total latent heat will be 171.25 kJ as follows;

$$PCML_t(KJ) = M_{pcm}(Kg) \times \Delta h_{pcm}(KJ/Kg) \tag{4.1}$$

Minimum temperature reached by PCM = -3.9°C, and PCM freeze is -2.8 thus, ΔT of PCM = 1.1°C, but to utilize from the whole PCM enthalpy, the total range should equal 3°C as shown in Table 4.1. Therefore, the actual amount of PCM enthalpy used in the experiment was 62.8KJ according the following equation:

$$PCML_a(KJ) = PCML_t(KJ) \times \frac{\Delta T_a}{\Delta T_t} \tag{4.2}$$

To know the required amount of PCM for the current cabinet conditions, we should consider the temperature difference for the evaporator coil (ΔT for air on/off) =11°C and measured mass flow rate through the coil = 0.1008 kg/s to be able to calculate the sensible cooling capacity of the evaporator as follows;

$$Q_s = m_a \times cp_a \times (t_{on} - t_{off}) \tag{4.3}$$

From Eq. (4.3), the evaporator capacity is 1.11 KJ/s. The effective defrost period (DEF_{eff}) was 7.5 mins which starts after 5 mins of the average whole defrost period which is 12.5 mins, when all the coil ice has been melted. During this period the PCM role comes to substitute the evaporator role. Therefore, amount of cooling energy required from PCM (E_R) through the effective defrost time is about 500 kJ according to following equation:

$$E_r(KJ) = Q_s(KJ/s) \times \mathrm{DEF}_{eff}(s) \tag{4.4}$$

That means the current effective amount of the used PCM = 12.5 % of optimum amount, which needs to be increased in future tests. Moreover, the temperature measurements on the finned tube surfaces showed that only some of the employed PCM was utilised. Therefore, energy saving of the cabinet with PCM was found to be very small and the use of water based PCM will be investigated with the new cabinet in next part of this project.

4.4 PCM integration in Norpe Cabinet

The second open type display cabinet in this project was arrived. It was EMX-125-M integral low-fronted multi-deck open display cabinet as seen in Figure 4.16. It was new

and the main cabinet in our research as all modification studies and the rest of this research will depend on it. All specifications and description for this cabinet were mentioned in chapter 3. It was better than previous one in terms of thermal performance and construction design, all modifications stages are described in the following sections.

Figure 4.16 Tested Norpe display cabinet

4.4.1 Experimental setup

The display cabinet, with or without PCM integration, was then mounted in the same air-conditioned chamber and tested at the same operating conditions to measure and compare the performances of the system and components.

Table 4.4 Experimental measurements data

Experimental parameters	Value
Fan pressure Jump (Pascal)	25
Ambient Temperature (K)	298.15
Food products properties	ρ= 1000 kg/m^3 , CP= 3500 (J/Kg-K), K=1W/m-k
Instant power consumption(kW)	1.6
Time step (s)	10
Experiment duration (h)	24

Various thermal parameters and experimental measurements such as fan pressure jump were detailed in Table 4.4. PCM integration through this cabinet was suggested to be in different place comparing to the first cabinet. As it was mentioned before the cabinet construction plays a main role in specifying the possible suggested positions to install the PCM through the cabinet. For the current cabinet the evaporator position was at the back duct and this forced the designer to make the back duct a little wider to accommodate the evaporator size. For instance, the back duct is the first option and most appropriate place to integrate the PCM as seen in Figure 4.17.

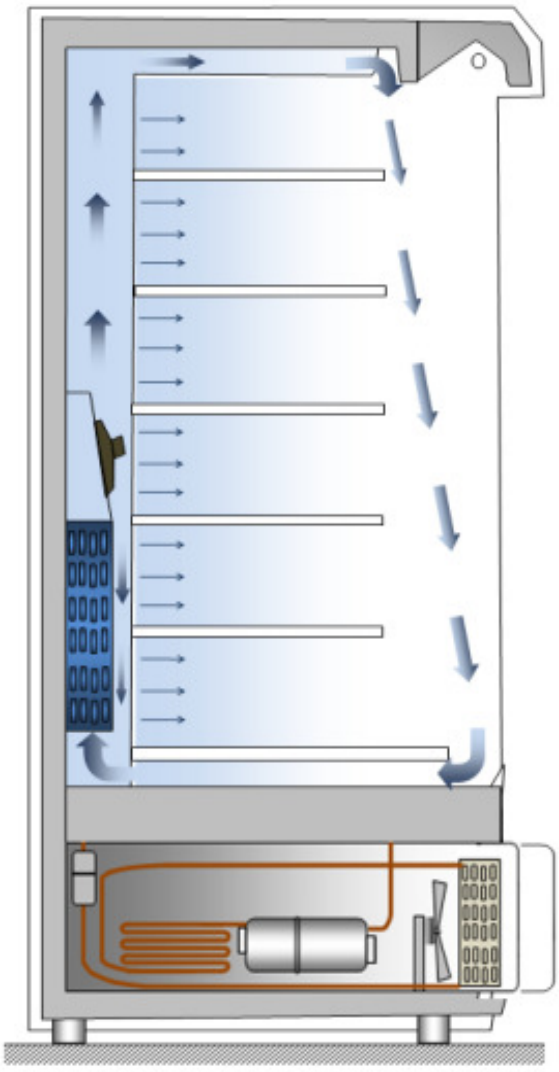

Figure 4.17 Left side view of the Norpe cabinet with PCM containers

After many experimental investigations and analysing the primary results that were mentioned in chapter 3 for Norpe cabinet, the PCM integration stage started by removing all products, shelves, back and base panels and instrumentation devices and all the necessary dimensions were taken to specify the PCM containers later on as depicted in Figure 4.18. It is obvious from this figure that the air flow duct at the back of the cabinet, above the evaporator provides an appropriate space in order to install the containers holding the PCM.

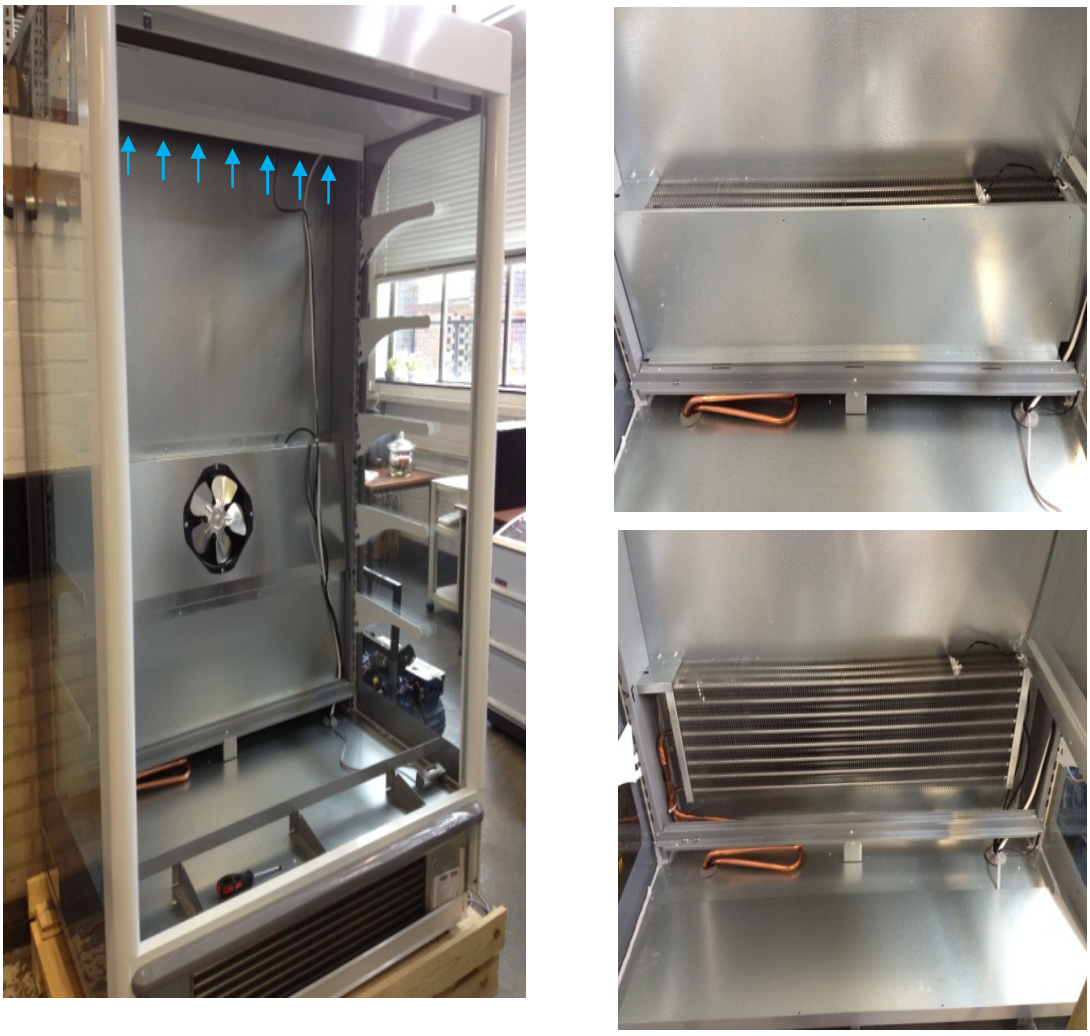

Figure 4.18 Front view of the cabinet with fan and evaporator coil (Back and base panels were removed) with dimensions

4.4.2 PCM selection

The key principle to choose a PCM for a specific application is its melting /solidification temperature. However, other essential parameters must be also considered for an accurate decision. These parameters include: thermal conductivity, stability to cycling and latent heat.

Water based PCMs with a nucleate agent was used in this stage of work. It is known that water starts to freeze at a temperature less than 0°C causing a sub-cooling (about -5 °C) and melt at 0°C, with a large latent heat of 334 kJ/kg. This sub-cooling of water can be reduced by adding silver iodide (AgI). Figure 4.19 demonstrates that the freezing onset temperature of tap water increases significantly with an increase in the amount of silver iodide (Lu, 2013). Therefore, water with a high latent heat has a good potential for usage as a PCM. Water gel PCM was purposely selected and made by mixing different compositions at specific mass ratios to obtain the appropriate melting and freezing temperatures for this particular application. It was composed of deionised water, silver iodide, guar and sodium tetraborate as shown in Figure 4.20. The freezing onset of PCM depends on the location installed inside the cabinet. Currently, the focus is on PCMs applied just after evaporator coils. Therefore based on the air-off temperature range, a water gel PCM was prepared with a freeze onset of around -2.0°C. It was then charged into two single panel containers, installed immediately after the cabinet evaporator in the main back flow channel enabling the cooled air to flow through external containers surfaces.

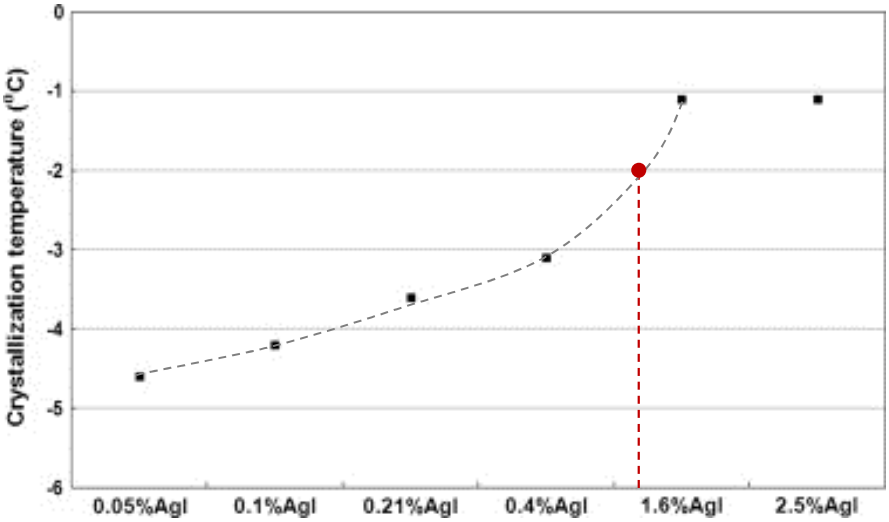

Figure 4.19 Freezing onset temperature of tap water (10 mg) with different percentages of (AgI) in DSC (Lu, 2013)

Figure 4.20 The component of PCM

4.4.3 PCM containers

As illustrated in Figure 4.21, two similar single panel containers were used in this test as PCM-HEs. The manufacturer specifications of these two containers are listed in Table 4.5. Choosing radiators to work as a PCM-HE was because the their suitability for that purpose in terms of high heat transfer supported by surface area of fins, good internal space to accommodate the amount of PCM as well as fast and cheap option., Using central heating radiators was not ideal for our application, however they can at least do the HE function with acceptable level. The supplied air duct at the back of the cabinet, above the evaporator, will accommodate these two containers charged with the proposed PCM as seen in Figure 4.22. Four long bases (3 cm) were attached behind each container in order to maintain a gap at the back such that the cooled air flow from the evaporator exit can thus pass through both container sides externally as shown in Figure 4.23.

The containers were installed such that their fins were facing the front side due to the air mass flow rate will be more at that side into the rear duct. The purpose of using the PCM container is to enable it to function as an 'auxiliary evaporator' or cooling coil during the defrost period when the compressor is switched off. Accordingly, the PCM charge in the containers should be enough to maintain cabinet temperatures within an acceptable range as if the evaporator is still working during defrost period.

Figure 4.21 single panel radiators with dimensions

Figure 4.22 The containers and their position inside the cabinet

Figure 4.23 Attaching long bases at the back of each container

Table 4.5 Specifications of the containers.

Parameters	Value
Type	11-single Panel
Height (mm)	600
Length (mm)	500
BTU	1356
Projection (mm)	76
Weight (kg)	8.4
Finish	Epoxy polyester powder coat
Certification	Manufactured to ISO 90001
Colour	White

4.4.4 Quantification of PCM

According to the experience acquired from the first cabinet, quantification the required PCM is quite important step that should be done at the beginning of modification stage. The evaporator cooling capacity can be calculated from Eq. (4.3). From the measurements, the evaporator capacity was calculated to be 2.2475 kW. It was found from test results that the defrost period was on average 7 minutes and after this time the cabinet temperature would reach the defrost termination temperature.

Moreover, during defrost time the high cabinet temperature gradually increased before reaching its peak value. In the first two and half minutes of defrost period, the cabinet air temperature was within normal range as there was still some ice that need to melt on the evaporator surface. Therefore, this part of the defrost time was considered as a normal off cycle. Accordingly, the effective time (DEF_{eff}) for the evaporator to be out of the duty was around 4.5 minutes (270 s) at each defrost period, and the calculated and designed PCM amount should be sufficient to cover this time span.

That means the cabinet temperature will be within the normal range during the whole seven minutes of each defrost time period. After that, the whole PCM will be melted and the temperature starts to increase, causing an extra defrost time which will be about five minutes. To achieve that, the energy required (E_R), to charge the PCM containers during the (DEF_{eff}), needs to be calculated from Eq. (4.4) to be 621.2 KJ.

The amount of PCM charge in the containers is therefore determined as 1.86 kg based the following calculation:

$$M_{pcm} = E_r / PCML_a \tag{4.5}$$

In Eq. (4.5), the PCM latent heat (PCML) was measured by the differential scanning calorimeter (DSC). The average temperature that will be reached by the water gel is 4ºC where the PCM fluid density is around 1000.0 kg/m^3. If a 15% volume expansion in the phase change range was considered in the designs, each radiator should be charged with 0.93 L of water gel PCM at room temperature.

4.5 Norpe cabinet results and description

The test results include temperatures of products, evaporator air on and off, air curtain outlet, and power consumption and performance comparison. They are presented in two categories: tests for the cabinet without and with PCM with M-packs as test packages load arrangement and at test conditions climate class 3: 25°C / 60% RH. The display of the monitoring system for the cabinet with PCM containers installed is shown in Figure 4.24.

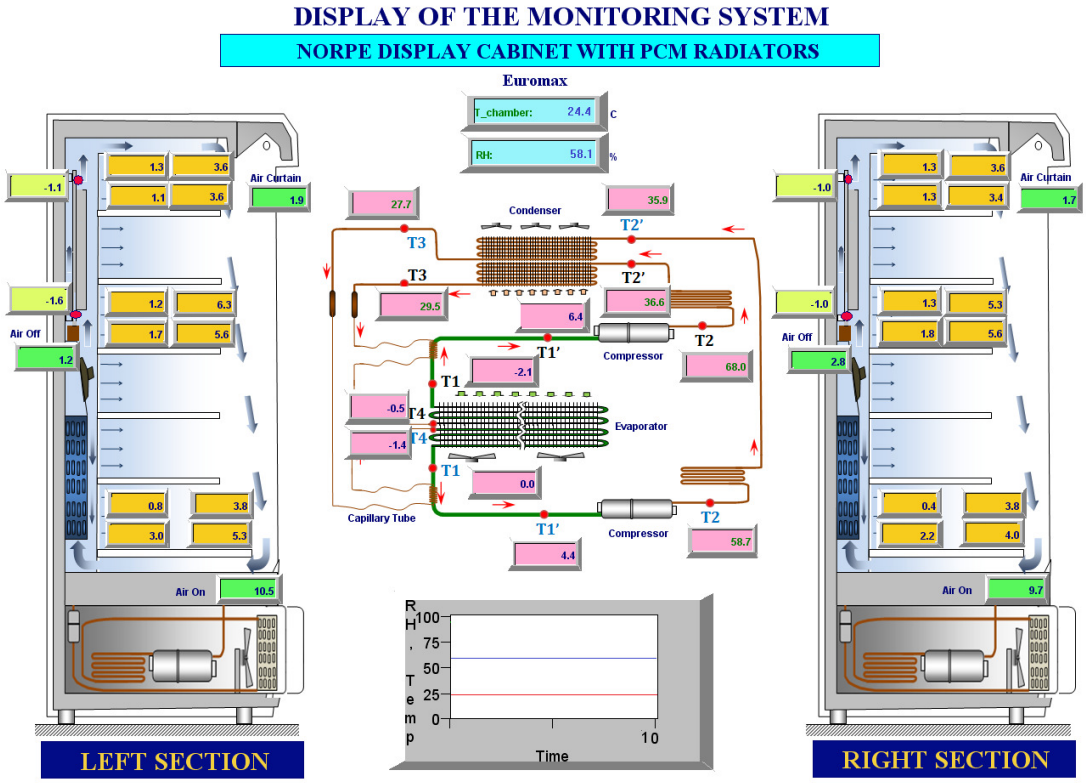

Figure 4.24 Monitoring system for the modified Norpe cabinet

4.5.1 Product Temperature Measurements

The cabinet product temperatures without and with PCM containers were measured during a 8 hours test period for the left and right sides as shown in Figure 4.25 and Figure 4.26 respectively. In each cabinet side, there are 12 product temperature measurements represented under different names of three letters, each depending on the product simulator location in the cabinet as mentioned in chapter 3. It can be seen from those figures, for both circumstances, the product temperatures remain steady with very small fluctuations in response to the compressor On, Off and defrost cycles over test period.

For the cabinet without PCM, the product temperature variation ranges (ΔT) were behaving similar to the first cabinet as indicated in section 4.3.1. . The main temperature differences between the both tests are summarized in Table 4.6.

Figure 4.25 Product temperature variation for the left side Norpe cabinet with and without PCM

Figure 4.26 Product temperature variations for the right side Norpe cabinet with and without PCM

Table 4.6 Experimental products temperature for Norpe cabinet

Experimental parameters	Left Side		Right Side	
	Without PCM	With PCM	Without PCM	With PCM
Average temperature (ºC)	3.91	4.26	3.35	3.6
Maximum temperature (ºC)	7.97	6.85	6.49	6.01
Minimum temperature (ºC)	0.87	1.53	0.93	1.21
Temperature range (ºC)	7.1	5.32	5.56	4.80

4.5.2 The cabinet air temperatures

Figure 4.27 and Figure 4.28 obviously show the influence of PCM on the cabinet air temperatures; air off, air on and air curtain outlet at both left and right sides respectively. It can be seen from figures that all the maximum temperatures in the original cabinet are higher than those with the PCM setup. The effect of PCM on the off and on cycle periods was very similar for the first cabinet, and thus the off period times were nearly similar at both cases. Again, the whole PCM effect appeared during defrost durations when the cabinet air temperature values considerably increased for longer periods as the compressor is off. Defrost periods gave enough time and wide temperature range for PCM to melt and solidify, absorbing and releasing a heat from the cabinet, and then affect the air temperatures by decreasing and increasing their maximum and minimum values respectively. This reduction in temperature range

affects the product temperatures as mentioned before. Moreover, it is evident that the cabinet air temperatures are more stable and homogenous when PCM is integrated.

Figure 4.27 Cabinet air temperature variations for the left side Norpe cabinet with and without PCM

Figure 4.28 Cabinet air temperature variations for the right side Norpe cabinet with and without PCM

4.5.3 The defrost period

As seen in Figure 4.29, the defrost period for the cabinet without PCM was about 7 minutes, and for the cabinet with PCM it was about 12 minutes. The increase ratio

(70%) during this period was a result of the heat transfer that took place between the PCM and cabinet air. The energy extracted from the PCM provided the cooling capacity needed when the compressor was stopped. This leads to a reduction in energy consumption which, with optimization, will be even higher than the basic one without PCM. In another hand the on cycles also increased with adding PCM as it is considered as an extra load. However the increase ration was less than that for off cycles. It is also noticeable from the same figure that the maximum air off temperature in case with PCM was lower by around 2ºC and the reason for that is the position of radiator was before the air off sensor so that the effect of PCM was clear on that temperature.

Figure 4.29 The defrost duration at air-off left temperature

4.5.4 Average instant power consumption

The variation of instant power with time for the system employing PCM containers and the basic one is shown in Figure 4.30. Total energy consumption of each cabinet was calculated according to BS EN ISO 23953-2: 2005. For the basic system, the power required with time is around 5% higher than that obtained from the modified cabinet. When the cooling capacity supplied by the PCM containers was able to maintain the cabinet temperature during the PCM discharge (melting) process. In this period, the compressor was off, and the PCM containers acted as an extra evaporator by keeping the air off temperature below the admissible higher temperature limit for a longer time.

When the PCM completely was melted, the cabinet air temperature rises gradually and the compressor restarts. With the compressor on, the PCM progressively refroze. Energy consumption was calculated by using complete cycle method. The average instant power, running time and energy consumption of the cabinet at both tests are shown in Table 4.7.

Figure 4.30 Average instant power consumption for Norpe cabinet with and without PCM

Table 4.7 Energy parameters of Norpe cabinet

parameters	**Cabinets without PCM**	**with PCM**
Average instant power (KW)	1.6176	1.6066
Running time (h)	20.17	19.09
Experiment time (h)	24	24
Energy Consumption (kWh)	33.01	31.35
Compared to cabinet without PCM (%)	-	5%

4.5.5 PCM radiator surface temperatures

The variation of PCM radiator surface temperatures with time is shown in Figure 4.31a. Four sensors were situated at the bottom and top of both containers, as illustrated in Figure 4.31b. It can be seen that the PCM temperatures decrease gradually after each defrost period, and after one hour they reach the desired temperatures of -2ºC (freeze onset). At this point, the actual function of the PCM begins to maintain the energy during the on cycles and release it during the off and defrost cycles. It is clear that the

top surface temperatures are higher than the bottom ones during the defrost time since the top parts are filled just as the whole PCM becomes solid. When the melting stage finished, this part will be empty quickly because the PCM levels go down. Also, the top temperature is further from the air off temperature. It is clear that whole the PCM was utilized.

Figure 4.31 (a) Surface temperatures variation with time, (b) Sensor locations on PCM-radiator

4.6 Summary

The experimental study for two types of chilled food multi-deck display cabinets equipped with PCM in a form of heat exchangers installed on the available spaces of the main rear ducts was described and detailed. An enhancement of system performance and reduction in the cabinet air temperatures were achieved. Tests were carried out for those cabinets without PCM integration first, then with PCM-HEs. Modification stages, used tools, assumptions and boundary conditions and other related issues have been discussed and illustrated. Simulation model and the simulation outcomes with validation against experimental measurements are the next steps, which is the topic of the following chapter.

CHAPTER 5

2D CFD MODEL SETUP AND VALIDATION

In this chapter, 2D model have been developed by employing a finite volume method using ANSYS 16.2 software for a prototype refrigerated open-type multi-deck display cabinet (Norpe). The model can predict the cabinet performance, the temperature distributions and the air flow patterns inside the cabinet for a range of operating conditions. This chapter provides a vision into the theory and mechanism behind the computational approach and relate this to how the model is developed inside ANSYS. Also, some of the sub-models used will be clarified and their influence on calculating an accurate solution evaluated. Another objective for this chapter is to present a preliminary 2D CFD model and then to validate it against experimentally derived results.

5.1 Introduction

The expression of Computational Fluid Dynamics (CFD) has been around for decades and now is common in different fields of industry, academia and many research centres. According to Versteeg, H. and Malalasekera 2007, CFD is the study of a system involving heat transfer, fluid flow and other related phenomena by means of computer-based simulations. Appropriate employment of CFD can efficiently analyse complex flow patterns including turbulence, transient, three-dimensions, and buoyancy with complicated geometries of actual applications (A. Al-Sahhaf 2011).

CFD approach has become one of the main primary investigation tools of many new suggested designs due to its capability to deliver reasonably qualitative, quantitative and inexpensive results for different flow configurations. Moreover, unlike many experimental and theoretical approaches, all parameters of results can be obtained instantly at any time and point through the study field. This will provide a full understanding of the flow regimes simultaneously occurring in the entire domain. Consequently, this leads to vital advantage during the study of display cabinets, since their performance depends on airflow patterns and their thermal properties. Thus, by using CFD techniques, better design and more efficient cabinet could be achieved when the airflow mechanism around and within the whole domain was well realised (Xia and Sun 2002).

The ability of CFD application to predict the air thermodynamics situations in wide applications of refrigeration including display cabinets was proved by many reviews such as (Smale, et al, 2006) and (Norton and Sun 2006). However, there are still some limitations in such software as simulation cannot represent 100% of reality. Hence, in order to confirm the accuracy of the simulation, the CFD results need to pass the validation stage against experimental outcomes. Moreover, a sufficient experience and comprehensive understanding of this technique is necessary to create dependent results.

5.2 Air and heat flow modes of display cabinets

The circulating air through open display cabinets is the key to evaluating their performance and efficiency. As a working fluid, this air transfers the sensible and latent heat from the products and the ambient air to the evaporator coils. A full CFD description of all physical processes that take place in the cabinet needs appropriate modelling to interpret various heat phenomena, including conduction, convection, and radiation. The display opening causes enormous interaction between the cabinet and the surrounding space and is by means of free and forced convection heat transfer between the cabinet constricted air and the environment air.

Heat conduction modes usually occur across the cabinet walls as a result of relatively high gradient in temperature. While heat radiation modes take place due to the big

temperature difference between the products and the nearby environment. Air flow modes include both laminar and turbulent, driven by either buoyancy force or momentum. All simulation techniques employed together with such air and heat flow regimes and their solution will result in a demanding and complex solution process. The following sections will briefly explain the CFD approach and provide the stages occupied in the modelling setup.

5.3 The CFD approach

The modelling process starts by dividing our domain into a large number of control volumes (elements) to build the mesh covering the whole domain geometry. The information is stored in the central node of each element within the domain. Even though modelling software differs depending on the producer, all approaches are based on the governing equations of fluid flow. The mathematical equations of fluid dynamics, describing the moving fluid for each element through the field, are called the governing equations, namely the continuity, momentum, energy equations, along with an equation of state. These equations take the non-linear partial differential form (no analytical solution) and are iteratively solved in a computer to calculate estimated solutions.

Each equation defines the conservation of one variable inside the field and this means that a balance among the various factors affecting this variable must be achieved. In CFD approach, all partial equations must convert into discrete algebraic equations in a process called as discretisation. This process is performed by finite volume method which usually employed in CFD since flow visualisation is easier with this method as well as it requires fewer computer resources. The main function of finite volume method is the integration of all the equations in differential form to equations in discretised form over a control volume at the nodal point. Then, all discretised equations are organised into form algebraic equations system that can be resolved by means of matrix procedures until the specified convergence criteria are met at each nodal point.

5.4 The CFD code

Any CFD model should involve three steps; the pre-processing, processing and post-processing. Figure 5.1 illustrates the sequence of those steps inside the CFD code. All these stages were accomplished using ANSYS v.16.2 platform which is capable of creating, managing and solving the whole project in one display place.

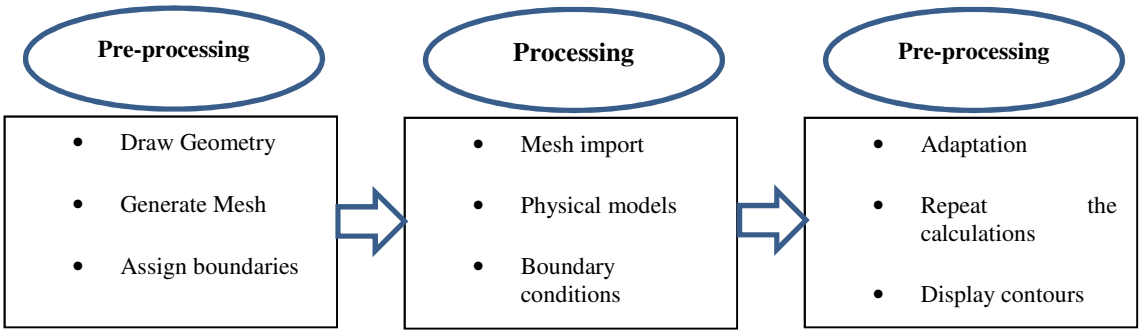

Figure 5.1 Basic programme structure

The geometry drawing stage is performed using ANSYS DesignModeler application which is used as a geometry editor of existing CAD. Then, ANSYS Meshing application is employed to generate the mesh and the physics preference will be set based on the type of system being edited. Next, ANSYS Fluent provides complete ability to solve the flow problems using specific meshes that were generated in geometries. It also enables to coarsen or refine the mesh based on the flow solution. All other processing tasks are implemented during the Fluent solution mode, including setting fluid properties, executing the solution, defining boundary conditions, refining the mesh, executing the solution, and post-processing the preliminary results. ANSYS post-processor is a flexible tool that designed to enable simple results visualization and quantitative analysis.

5.5 Pre-processing

5.5.1 ANSYS Workbench

ANSYS Workbench is a platform that combines the strength of essential simulation tools with the tools required for managing the whole project on the main project workspace. The project is driven by a schematic workflow that is represented visually

on the Project Schematic. Any analysis should be built by adding blocks called systems to the Project Schematic; each system is a block of one or more components called Cells, which represent the sequential steps necessary for the specific type of analysis. After adding systems, we can link them together to share and transfer data between systems see Figure 5.2. From the cells, you can work with various ANSYS applications and analysis tasks. ANSYS applications allow you to specify parameters such as geometry parameters, material properties and boundary conditions. Parameters can be defined within the application and managed at the project level in the Workbench environment. Also, it is easy to investigate design alternatives by modifying any part of an analysis, and then automatically update the project to see the effect of the change on the simulation result.

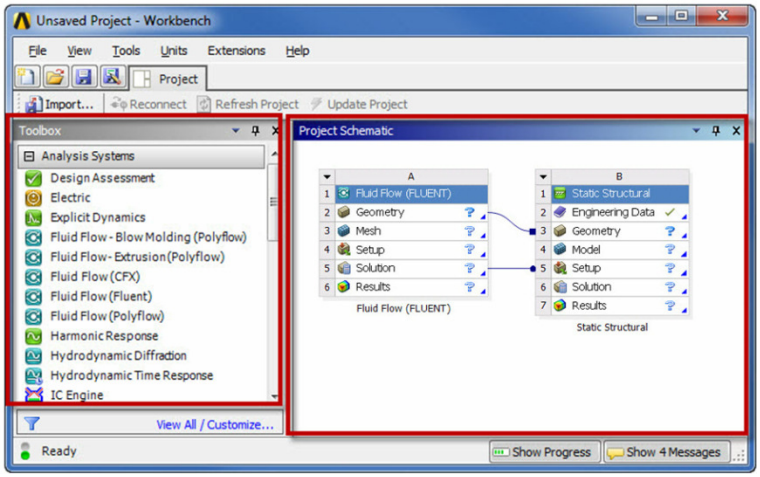

Figure 5.2 Workbench platform

5.5.2 Geometry

Definition and creation the geometry is the first step of any CFD model. The model geometry of the display cabinet is built using dimensions taken from the actual Norpe cabinet in the laboratory as illustrated in Figure 5.3. To simplify the model, no need to represent the exact geometry. For instance, only significant geometry features which are of interest have been modelled to avoid a large number of grids. This leads to a stable, faster and more accurate solutions (Stribling 1997). It is also important to specify whether the model will be analysed in 2D or 3D domain since this should be addressed at the starting due to its main effect on the computer resources required and the results accuracy. Through this work, the model used and analysed is only 2D since our

parameters of interest are not highly dependent on the third dimension as well as our study is mainly a comparison between two cases in terms of PCM effect so that eliminating a common factor could be a reliable simplifying method.

For the current project, the designs of the evaporator, fan, DAG, RAG and rear panel will stay unchanged since the purpose of this study is to focus on accumulated PCM effect on the air circulating in closed cycle inside the cabinet. Most of the previous studies carried out on the display cabinets performance, such as (Stribling, 1997), (Ge, 2010), (Foster, 2005) and (Howell 1993), were based on the 2D model. However, in stores, display cabinets are influenced by indoor air motion, and to simulate this, test chamber requires air flow across the face cabinet with a velocity between 0.1 and 0.2 m/s. (A. Hadawey 2006) showed that the influence of the side draught covers up to 33% of the length of the front cabinet side. Furthermore, a comparison between 2D and 3D model results, in terms of cooling power, was done by (D'Agaro, 2006) who determined that the third dimension is important only at the side walls of short cabinets that subjected to cross-flow.

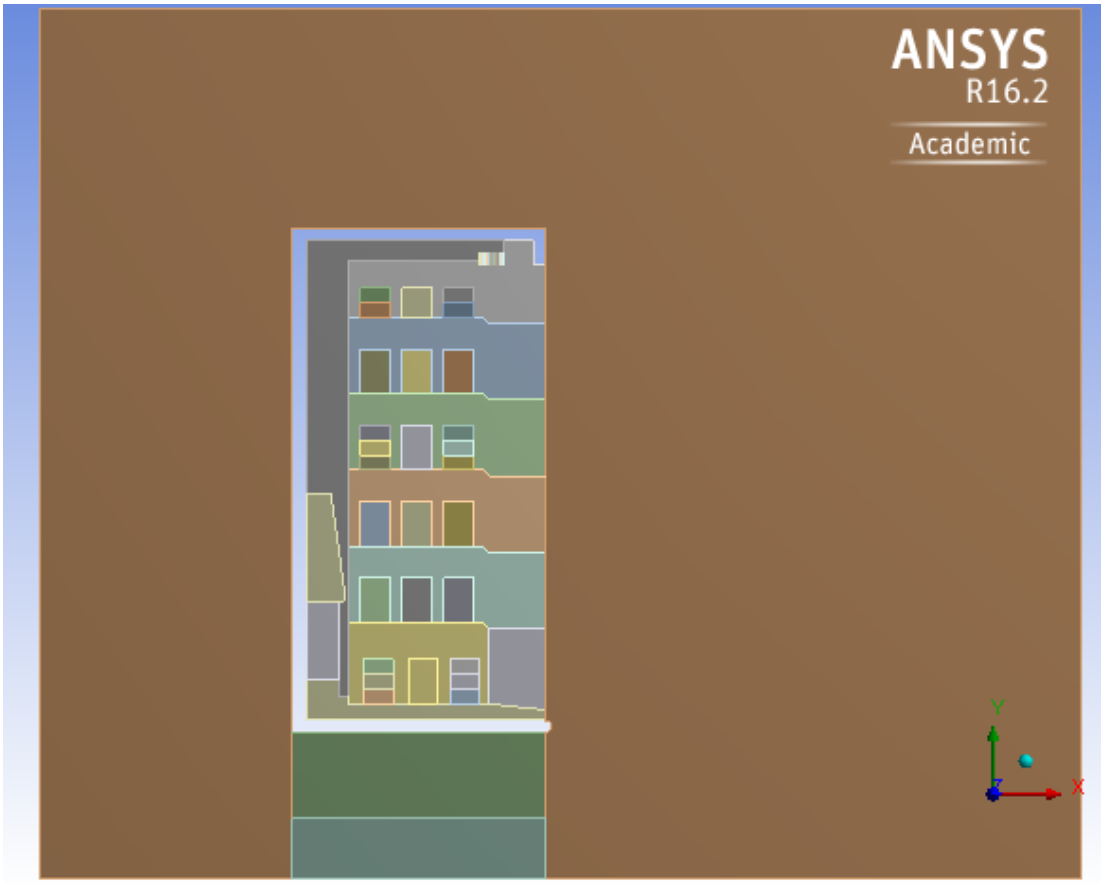

Figure 5.3 Whole computational domains for the cabinet loaded with products inside the test chamber

5.5.3 Mesh

The second task during the pre-processing stage is a generation of mesh which is considered prolonged and important. The size, shape and amount of elements employed in the mesh are responsible for the solution accuracy, the convergence, stability and calculation time. In spite of the fact that providing more accuracy and flow details are revealed by a big number of cells, the simulations are restricted by the cost and time of calculation. The grid type of any region through the domain is usually dependent on the flow behaviour and the complexity of geometry. Due to the structured type of mesh typically enhances the solution conversion, triangles structured mesh is employed in this work to define the geometry of the calculation domain, exempting products assigned as squares elements, as depicted in Figure 5.4. The total nodes numbers reached 67426 and 121367 elements and grid adaption has been considered and the number of grid points is progressively increased from one simulation to another. During mesh generation,

smaller grid have been purposely employed in regions where important air flow and high temperature gradient were likely such as internal space, cabinet edges, rear back panel, air curtain outlet, DAG, RAG and the front of the opening area of the cabinet as illustrated in Figure 5.4. All the dimensions and details of the mesh are illustrated in Table 5.1.

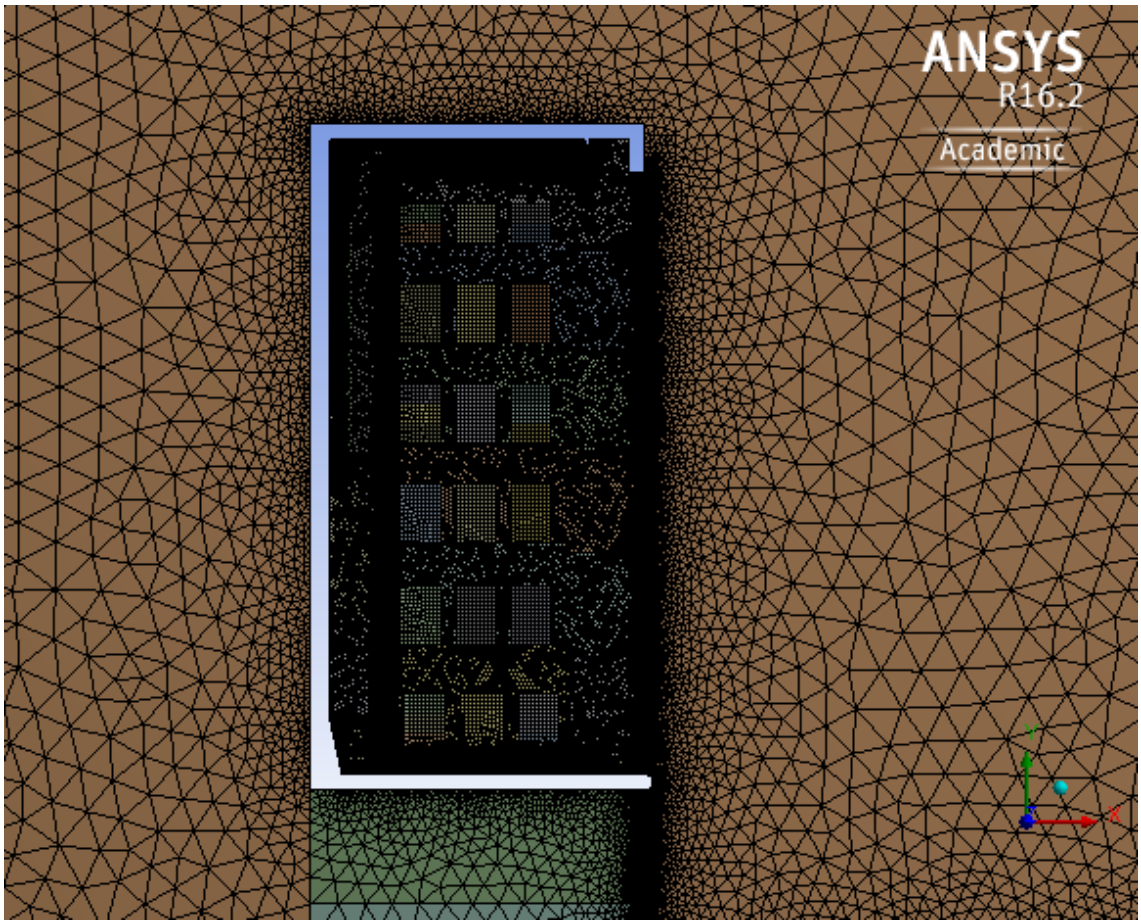

Figure 5.4 Computational grids for the 2D CFD model

Table 5.1 Mesh details

Use Advanced Size Function	On: Curvature	Max Face Size	$9.5e^{-002}$ m
Relevance Centre	Medium	Use Automatic Inflation	None
Initial Size Seed Active	Assembly	Inflation Option	Smooth Transition
Smoothing	Medium	Transition Ratio	0.272
Span Angle Centre	Fine	Maximum Layers	2
Curvature Normal Angle	Default (18.0 °)	Growth Rate	1.2
Min Size	Default($1.136e^{-003}$ m)	Inflation Algorithm	Pre
Nodes	64802	Elements	114339

5.6 Processing

The set-up and solution processes are done within the Fluent application window by initialising, controlling, monitoring, calculating and checking the solutions. At the beginning and to save time, all the flow properties values should be initialised with actual values. The calculations were executed using a single-precision option that uses seven decimal digits only. At each iteration run, an imbalance exists in the simulation process called residual that monitors the numerical behaviour of convergence. In the current work, the solution process is completed when the residual value touched $1x10^{-8}$.

To make sure that convergence has been reached, all important variables were observed for the duration of the calculations which will be finished when no considerable change in results is detected. Besides, to confirm property conservation, the overall imbalances in all domain variables were regularly tested to be as small as possible. The solver properties used in this model were the pressure based type, absolute velocity formulation and planar 2D space. The following conservation equations were applied in the 2D CFD model.

Pressure-based assumes the fluid is incompressible, $\rho = constant$, independent of space and time, so that $\partial\rho/\partial t = 0$. The continuity equation will be:

$$\frac{\partial U}{\partial x} + \frac{\partial V}{\partial y} = 0 \tag{5.1}$$

Momentum equations:

$$\rho\frac{\partial u}{\partial t} = -\frac{\partial p}{\partial x} + \mu\left(\frac{\partial^2 u}{\partial x^2} + \frac{\partial^2 u}{\partial y^2}\right) \tag{5.2}$$

$$\rho\frac{\partial v}{\partial t} = -\frac{\partial p}{\partial y} + \mu\left(\frac{\partial^2 v}{\partial x^2} + \frac{\partial^2 v}{\partial y^2}\right) \tag{5.3}$$

Energy equation:

$$\frac{\partial T}{\partial t} + U\frac{\partial T}{\partial x} + V\frac{\partial T}{\partial y} = \frac{q}{\rho Cp} + \alpha\left(\frac{\partial^2 T}{\partial x^2} + \frac{\partial^2 T}{\partial y^2}\right) \tag{5.4}$$

State equation

$$\rho = \frac{P}{RT} \tag{5.5}$$

5.6.1 Turbulence modelling

The air flow of open display cabinets is categorised as a transitional mode in which the turbulent kinetic energy is shaped and damaged, driving to rotational flow structures, usually named as eddies. Those eddies endorse the transported quantities of energy, momentum, and species concentration to fluctuate and mix. Buoyancy and the shear forces of the main flow are responsible for this phenomenon. The beginning of turbulence depends on the value of Reynolds number which is the ratio of the inertia force to viscous force. The general transport equation for the conservation of mass, momentum, energy, and turbulent quantities can be presented by the following form:

$$\frac{\partial \emptyset}{\partial t} + \frac{\partial (u\emptyset)}{\partial x} + \frac{\partial (v\emptyset)}{\partial y} + \frac{\partial (w\emptyset)}{\partial z} = \frac{\partial}{\partial x}\left[\Gamma \frac{\partial \emptyset}{\partial x}\right] + \frac{\partial}{\partial y}\left[\Gamma \frac{\partial \emptyset}{\partial y}\right] + \frac{\partial}{\partial z}\left[\Gamma \frac{\partial \emptyset}{\partial z}\right] + S_{\emptyset} \tag{5.6}$$

Where $\emptyset$ is a general variable that could be mass, momentum, energy, turbulent kinetic energy, or turbulent dissipation rate, by choosing suitable values for the diffusion coefficients (Γ) and source terms $S_{\emptyset}$, the partial differential equations for the conservation of mass, momentum, energy, turbulent kinetic energy and turbulent dissipation rate can be found. Turbulence models are commonly categorised depending on the number of their partial differential equations. The Prandtl model, for example, has no equations and, therefore, called a zero-equation model. The k-ε model is called a two-equation model and the Reynolds Stress Model (RSM) is a three to five-equation model. Turbulence presentation is divided into three sets: Large Eddy Simulations (LES), Direct Numerical Simulation (DNS) and Reynolds Averaged Navier-Stokes (RANS).

Most CFD applications use the RANS turbulent models due to offering the most economic approach for calculating complex turbulent flows. Also, this model is appropriate for various engineering applications and typically provides the required level of accuracy (Ansys 2011). The user should decide which model is the most suitable for a given applications as no one of those models is universal. A turbulent model is further classified, depending on how the heat and diffusion fluxes and Reynolds stresses are modelled, into Reynolds stress and eddy viscosity models.

A simple Reynolds Stress Model was described by (Launder 1989) and common eddy viscosity model is called k-ε model summarised by (Launder and Spalding 1974). The Reynolds-stress model is superior to the eddy-viscosity one but, there is a drawback in terms of less stable numerical algorithm and more computational time required. Thus, the standard k–ε two-equation model is employed as shown in Eqs.(**5.7**) and (**5.8**).

$$\frac{\partial(\rho k)}{\partial t}+\frac{\partial(\rho u k)}{\partial x}+\frac{\partial(\rho v k)}{\partial y}=\frac{\partial}{\partial x}\left(\rho \Gamma_k \frac{\partial k}{\partial x}\right)+\frac{\partial}{\partial y}\left(\rho \Gamma_k \frac{\partial k}{\partial y}\right)+S_k \quad \textbf{(5.7)}$$

$$\frac{\partial(\rho \varepsilon)}{\partial t}+\frac{\partial(\rho u \varepsilon)}{\partial x}+\frac{\partial(\rho v \varepsilon)}{\partial y}=\frac{\partial}{\partial x}\left(\rho \Gamma_\varepsilon \frac{\partial \varepsilon}{\partial x}\right)+\frac{\partial}{\partial y}\left(\rho \Gamma_\varepsilon \frac{\partial \varepsilon}{\partial y}\right)+S_\varepsilon \quad \textbf{(5.8)}$$

5.6.2 Assumptions and boundary conditions

Although the geometry and an appropriate grid design are of significance in the modelling, the boundary conditions have the highest impact on the result nature. The solutions accuracy of the governing equations is commenced from initial values of boundary conditions and dependent on those specified values. Then, most of the boundary conditions and assumptions in this study are those come from experiments in order to improve the reality of physical representation of the fluid flow in the cabinet.

5.6.2.1 Wall boundary conditions

During the CFD set-up, the boundary conditions assigned as a wall are two types. First are the test chamber's walls (ceiling and floor) and external cabinet walls which were defined as one-sided and adiabatic walls. Second are the rest of cabinet edges and products' covers (two-sided) which are modelled as conducting walls (coupled thermal conditions). Wall boundaries are solid surfaces used to bound and separate solid and fluid regions to frame the real computational domain. At those boundaries, the tangential velocity component is considered to be zero (no-slip boundary).

5.6.2.2 Inlet/ Outlet boundary conditions

Introducing the air to the computational domain requires defining all its thermal and physical properties such as; temperature, velocity, evaporator fan and turbulence magnitudes which either calculated or identified from preceding experimental work. The left and right walls of the test chamber were modelled as pressure inlet and pressure outlet respectively. Those variables are frequently assumed to be distributed in a

uniform pattern crossing the inlet edge. It is also required a fan model to simulate the fan with its real pressure jump. The inlet type for circulating air is a fan with constant pressure jump profile.

5.6.2.3 Radiation modelling

The phenomenon of interaction the electromagnetic waves with the surrounding is called radiation that includes absorption and scattering within the fluid medium, and absorption and reflection at walls. This effect is usually ignored in the simulation of display cabinets unless there is big difference in temperature between the products and the ambient. Orphelin, (1997) stated that the radiation share in the energy balance in the display cabinet is equivalent to that of conduction and convection, and could donate to 7% of the sensible load through heating the visible part of the products along with the internal cabinet body. While ANSYS offers different radiation models, only the Discrete Ordinates (DO) model by Oliva, (2004) and the Discrete Transfer Radiation (DTR) model by Shah, (1979) are appropriate for the our study. The suitability of each model is dependent on the problem physics and solution needs. Although the DTR model could provide good results, it is not used in this study as its procedure is rather time consuming. For that reason, The DO model is applied through radiation modelling to simulate the coupling of radiation and convection. In addition, the boundary temperature is used to identify internal emissivity, and the external black body temperature is assumed to be constant

5.6.2.4 Evaporator modelling

The evaporator section of the display cabinet is modelled as a heat sink to the cabinet with a porous media to pretend the evaporator coils. Accumulating frost on the evaporator will affect both the air off temperature and air flow rate of the rear panel. However, this would be a dispensable complexity and it is adequate to assume a clear evaporator coil and thus, constant air velocity (Xiang 2003). As we know the capacity of evaporator consists of sensible and latent heat parts, however only the sensible part will be taken in the calculations as the moisture content of air is ignored in this model for the reason mentioned in section 5.6.2.6 . For instance, the heat source that will play

the evaporator role should be integrated inside the model by using user defined function (UDF) macro and calculated from the following equations;

$$Q_s = -mcp(t_{on} - t_{off}) \quad \textbf{(5.9)}$$

$$Q_{source} = Q_s / V_{evap} \quad \textbf{(5.10)}$$

After finding the sensible capacity from Eq. (**5.9**), the latter will be divided by the evaporator volume to find the heat sink value per unit volume as shown in Eq. (**5.10**).

5.6.2.5 Products modelling

The products in the cabinet must be involved into the dynamical model of the display cabinet. In a real-world store, different types and shapes of products are displayed in such cabinets. However, to study the display cabinet performance, M-packs (similar to meat) with one rectangular shape are chosen as products. The products arrangements can be stacked in different and random patterns due to the costumers' use, however all products were modelled as conducting solids with real thermal properties and specific stack pattern according to the EN-411 standards as shown in Figure 5.3 Whole computational domains for the cabinet loaded with products inside the test chamber

5.6.2.6 The other boundary conditions

The cross section of the entire air conditional chamber contained the cabinet is considered as a computational domain. The examination conditions of the cabinet defined in Chapter 3 will be used as boundary conditions in the CFD models. Various thermal parameters such as fan pressure jump were obtained from the experimental measurements and the turbulence data from assumptions.

The cabinet air should be assigned as negative buoyant by taking the gravitational acceleration, as an additional physical quantity due to the temperature difference between the ambient air and the cabinet air. Throughout the calculation in this work, and according to (Ansys 2013) the use of species model is not possible as it cannot be used together with solidification/melting model which is essential to study the PCM behaviour later. So that, the effect of moisture on the air content of the test chamber is not considered. Besides, including moisture model is insignificant in terms of simulating the air temperature pattern (D'Agaro, 2006b), as well as, for comparison

purposes, the humidity will be the common factor between the two cases with and without PCM. The lost weight of the product is not considered too as the load is only packaged as chilled products. The temperature and velocity contours were assumed as uniform with reasonable approximation because of the effect of the honeycomb curtain.

5.6.3 Modelling the back panel

Modelling of the perforated panel (also known as rear grille) plays an essential role in the calculation of air amount passed to the DAG, the cabinet flow distribution, and also products temperature. The perforated back panel was modelled by many researchers in different methods depending on the nature of the parameters of interest. Some investigators have tried to consider the entire back panel either as small separated divisions along to represent the holes (Yu, 2007) or as an inlet-velocity (Foster, 2005). Both of those strategies could give the real amount of penetrating air. However, they could cause a high dropping in the pressure and flow rate through the back duct. Another common assumption was accomplished by using porous jump model (A. Al-Sahhaf 2011). But this is mostly appropriate for the case in which the flow is exactly vertical to the porous jump surface. Instead, in this work, the real geometry of the back panel is modelled by drawing the actual holes along the panel since drawing holes in 2D model is relatively easy. This is adopted since it is simple and effective way to simulate the flow patterns of air infiltrating from the rear panel as shown in Figure 5.3.

5.6.4 Modelling the DAG

The honeycomb shape of the discharge air grille (DAG) has an important effect on the initial shape of the air curtain, which responsible for the entrainment ratio of ambient air. Through this Modelling, the actual geometry of the side view (series of narrow slots) for DAG is also considered during the geometry building stage as this will enhance the reality of the simulation. However, this requires high number and smaller size of cells to accommodate this zone and the transition zone from DAG to the domain see Figure 5.3.

5.6.5 Mesh adaption

The mesh size has a big influence on the convergence, accuracy and stability of the numerical calculations and results. Consequently, it is important to make sure that the

final results are not affected by grid resolution. ANSYS Fluent has the solution-adaptive mesh refinement feature which allows us to refine and/or coarsen our mesh based on geometric and numerical solution data (Canonsburg 2013). By using this feature properly, extra cells can be added where necessary, thus enabling the features of the flow field to be better resolved. In the meantime, computational resources are not wasted by the inclusion of unnecessary cells, as occurs in the conventional grid independence approach (Chila and Kaminski 2008). Furthermore, this technique will save time as we do not need to go back to mesh generation stage for additional grid improvement. For this purpose, three different grids number were studied by using increasingly fine grids till the maximum product temperature difference is about 0.3 ℃. Two adaptions were adopted through calculations and the final grid number is 121367 which were used for further computation. The product temperatures of each adaption are depicted in Figure 5.5. The areas affected by the second adaption were shown in Figure 5.6.

Figure 5.5 Mesh adaption based on product temperatures

Figure 5.6 Modified mesh after the second adaption

5.6.6 Steady and transient simulations

At the beginning, the model has been implemented in the steady state condition and therefore all the boundary conditions will remain constant through the calculation. This stage of simulation is important to gain primary validation with the experimental results and also to use it as initial conditions for the transient simulation later on. In this stage, we only need to use the DEFINE_SOURCE macro.

In reality, the display cabinet is not a steady state application therefore and after reaching the steady state results, a time-dependent model is then developed to study the trend of cabinet air temperatures and of energy consumption with time (Mastrullo et al. 2014), taking also into account defrost effect (Bansal et al. 2010). This stage of the modelling is started by integrating all UDF codes to the main boundary conditions. All other boundaries are still the same. The calculations will continue for three days to give enough time for the transient data to stabilise. All product temperatures, air curtain, return grill, air on temperatures, air curtain velocity were monitored and recorded to separate files during the transient calculations to be ready for analysis later on.

5.7 Post-processing

Presenting the simulation results successfully supports to enhance, visualise and analyse the thermal and physical features of the air flow. In this study, the ANSYS CFD post-processor application is occupied for the graphic illustration of the computational results. This built-in software provides high quality graphs through analysing data and visualising processes.

5.8 User-defined functions

User-defined functions (UDFs) are C functions that can be dynamically loaded with the ANSYS solvers to improve their standard features. UDFs are capable for customizing boundary conditions, material properties and source terms, and enhancing existing ANSYS models (Ansys Inc 2013). The need for UDFs in this simulation is necessary because the calculations will be time dependent with temperature controller. This model is quite similar to the real cabinet as we have added thermostatic controller to control the Off and On periods of the compressor and also to govern defrost processes at specific times. To achieve that, we need three types of predefined DEFINE macros that we will use to define our UDF.

The first one is DEFINE_SOURCE macro that will specify a heat source in the evaporator region to play the evaporator role inside the cabinet by removing the heat from the circulating air. The value of this source is calculated according to the sensible capacity of the real cabinet evaporator as shown in Eq. **(5.10)**. The second type is EXECUTE_AT_END macro which will check the cabinet temperature after each time step and work as a thermostatic controller. This macro will be responsible for the On/Off and defrost periods of the cabinet. The last macro is DEFINE_INIT that is used to set initial values of flow quantities.

5.9 Model validation with the Experimental Results

To validate the cabinet models, the prototype cabinet was mounted in an air-conditioned chamber and extensive experiments were conducted at constant space air temperature and relative humidity. The cabinet models have therefore been validated through comparison with experiment results for cabinet air and products temperatures at

different locations of the airflow path and specific food products. The products were numbered as shown in Figure 5.7. As mentioned before, the simulation process is divided into two parts; the first one is steady state analysis to prepare appropriate initial conditions for the second part which is transient analysis so that the validation process is also divided into two stages; steady and transient.

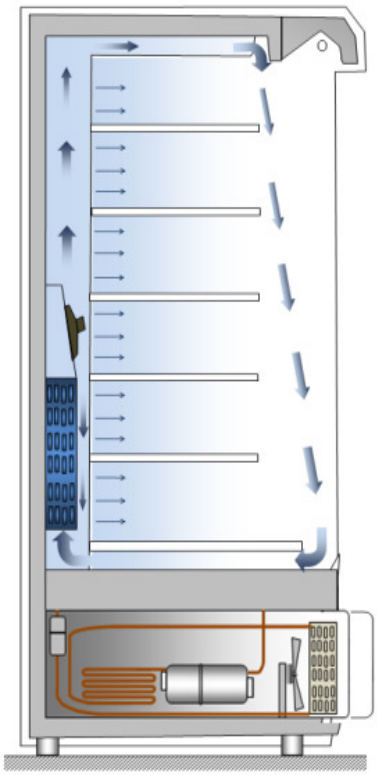

Figure 5.7 Left side view of the cabinet with products

5.9.1 Steady state validation

Of course this stage of simulation is for the cabinet without PCM since it is not beneficial to add PCM to the steady calculation. The contours of air and product temperature at steady state are depicted in Figure 5.8. It can clearly identify the heat exchange around the air curtain, where the air curtain efficiently stands as an obvious heat transfer barrier between the internal display cabinet space and the indoor space air. The food packages in vicinity close to the air curtain have relatively higher temperatures

than those nearer to the perforated back panel because of the interaction between the cold back panel flow and the air curtain

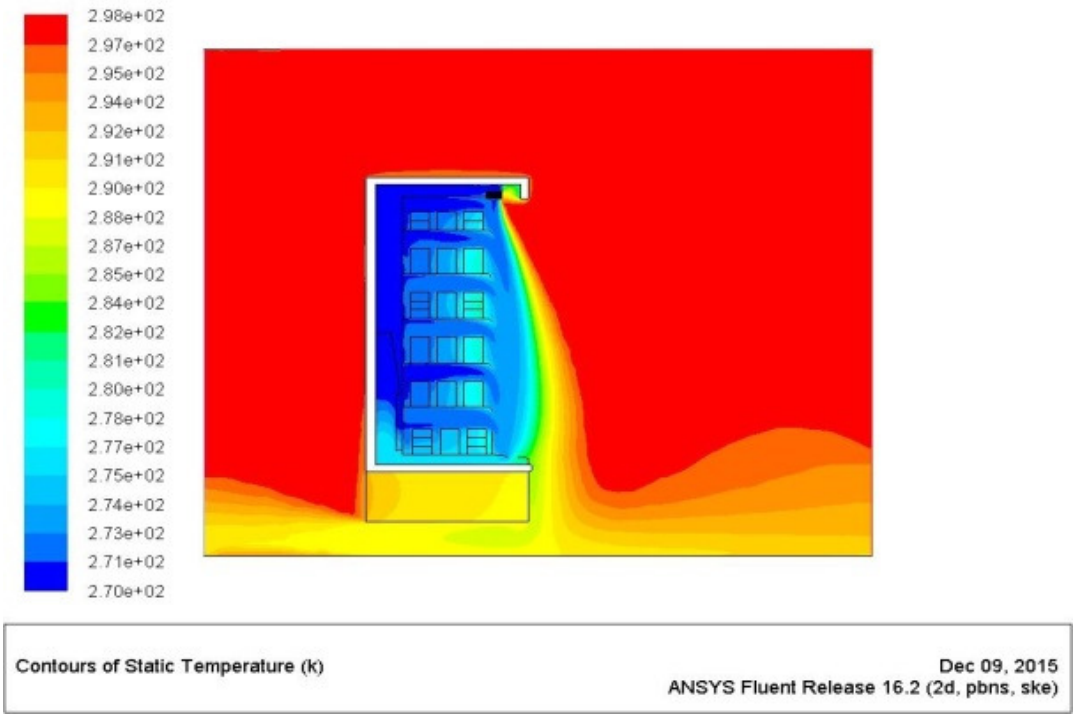

Figure 5.8 Air and product temperature contours for steady model

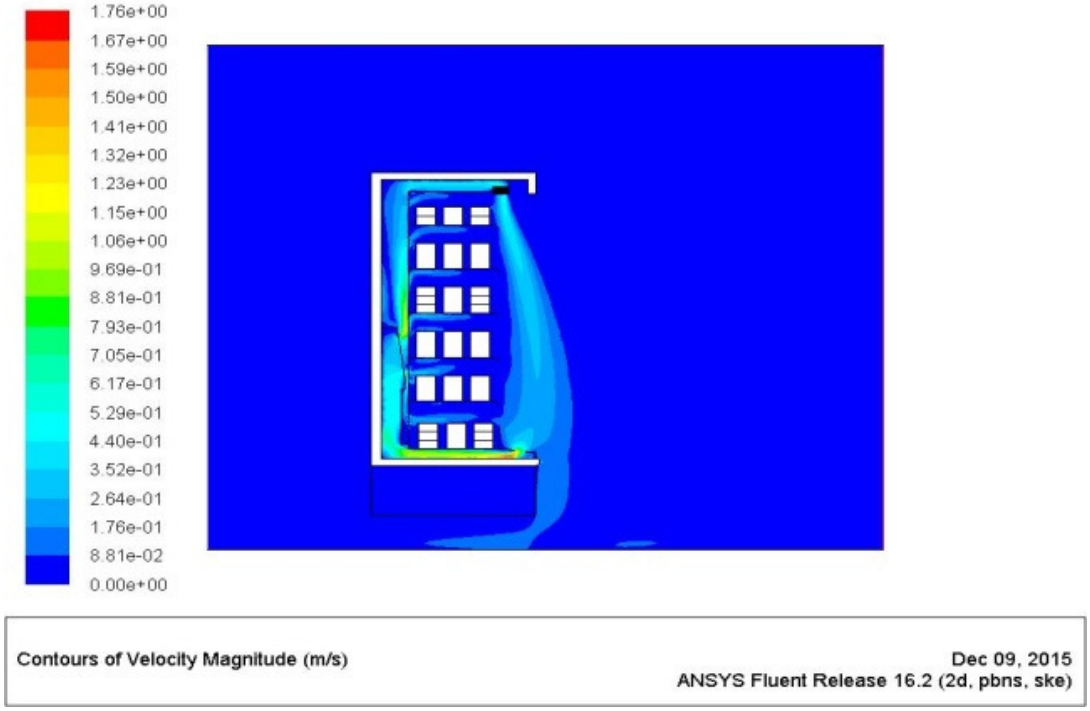

Figure 5.9 Air velocity contours for steady model

Figure 5.9 showed the air velocity contours for the steady state simulation. It is clear that the maximum air velocities are in the bottom duct as a result for the suction side of the fan. Another high air velocity area is noticed after the fan and close to the back panel as a result for the inclined fan position. It is obvious that the velocity inside the evaporator decreased because the porous media which represent the evaporator coils. It can also be observed from the same Figure that an air curtain is formed between discharge air grille and return air grille, as well as the air flow paths coming from the holes of the perforated panel are clear.

Similarly, the graph in Figure 5.10 shows the steady state simulation and experiment results without PCM for temperatures of products numbered in Figure 5.7. It should be noted that the simulation temperatures of those numbers of 1 to 4 products are maintained at around 274.5 K, which are quite close to the experimental results. However, for the rest of products, the numerical results are slightly higher than those of the experimental measurements because the limitations of steady state assumption. Then, the numerical results show good agreement with the experiments, indicating that

the present computational method can efficiently simulate the heat transfer performance of the display cabinet.

Figure 5.10 Validation of products temperature for Steady model without PCM

5.9.2 Transient validation

As the temperature difference of every two close mounted products is quite small, they are thus integrated into six instead of twelve product temperatures in Figure 5.11 by taking the average temperature of those two close products. As shown in this Figure for the variations of six product temperatures without PCM for stable measurement and calculation, we can see the validation of our transient simulation by comparing experimental product temperatures with simulation results. By matching the colours, we can see good agreement between both data in which the maximum temperature difference between the simulation and experiment results is about 0.8 °C. Also, it is noticed that the temperature of product numbers 1-4 are much lower than others since they are closer to the highest flow rate of cold air coming through the back panel holes.

Figure 5.11 Validation of products temperature for transient model without PCM

5.10 Summary

An outline for the assessment and construction of the CFD model for the display cabinet was presented by this chapter. Model processing stages, used software, assumptions and boundary conditions and other related issues have been discussed and illustrated. The validation task also was included in this chapter for the cabinet before and after modification.

The simulation outcomes against experimental measurements for the cabinet with and without PCM will be the topic of the following chapter.

CHAPTER 6

THEORETICAL PCM INTEGRATION AND RESULTS COMPARISON

In this chapter, the second part of simulation study for the Norpe display cabinet performance is performed by integrating PCM container inside the cabinet in order to investigate its effect on the cabinet in terms of products and cabinet air temperatures, power consumptions and thermal performance. To inspect and optimize the PCM effect, different conditions for this modification are studied. The incorporation was applied by using water based PCM, at different conditions inside the cabinet.

6.1 Introduction

After the experimental modification that has been done in previous chapters, it is important to study the possibility of simulating the PCM integration through display cabinets. One of the most important benefits of simulation studies is that they can deliver users with practical feedback when designing actual world structures. This permits the designer to decide the efficiency and perfection of a design before constructing the system. However, our system already was constructed so that the simulation function will be dedicated to establish a unique display cabinet model, simulating of PCM integration similar to the experimental one and exploring the qualities of alternative designs without building actual and physical systems. Accordingly, theoretical investigation of specific scheme choices during the simulation

stage rather than the manufacture stage will considerably diminish the total cost of constructing the system. Another advantage of simulation study is that it permits designers to investigate a problem at some varied levels of abstraction. For example it is possible in simulation to study an effect of one parameter on the system by forcing the other parameters to be constant. However, some complex simulations are considered costly as they could need to use expensive computer resources with a super processor.

In this chapter, 2D CFD models have been developed for a prototype refrigerated open-type multi-deck display cabinet with and without integrated PCM. The models predicted the effect of adding a PCM container on the cabinet efficiencies, the temperature distributions and the air flow patterns inside the cabinet for a range of operating conditions (PCM thickness, ambient temperature, air velocity). The cabinet models have therefore been validated through comparison with experiment results for temperatures at different locations of the airflow path and of food products.

6.2 Simulation set-up

The display cabinet model, with and without PCM integration, is then built in the same conditions for the real environmental chamber and tested at the same operating conditions in order to measure and compare the performances of the two systems and components with and without PCM. Various thermal parameters and measurements assumption are used in the simulation to enhance the calculations as shown in Table 6.1. Simulation of PCM integration through this cabinet was suggested to be in the same place like the experimental one to be validated with experiment results later on. All the simulation assumptions with and without PCM are the same. The only difference was adding a new model which is solidification/melting model to execute the charge and discharge processes that happen inside the PCM container and benefit from its stored latent heat.

Table 6.1 Simulation assumption data

Assumption parameters	value
Initialization method	Standard
Reference frame	Relative to Cell Zone
Time step size (S)	0.25
Number of time steps	2880
Time stepping method	Fixed
Maximum iteration/time step	20

6.3 Proposed PCM

It is important to select the optimal quality and quantity of PCM in any particular thermal application to fulfil terms of operation and cost. PCM based water is one of the most comprehensively studied PCMs in low temperature applications considering its availability, stability and the best thermal properties (E. Oró, de Gracia, et al. 2012). Long term performance and stable thermal characteristics of PCMs are the prerequisite for longer equipment life (Behzadi and Farid 2014). In addition, the latent heat should be as high as possible to decrease the size of the PCM container.

Many numerical studies regarding maximize the PCM storage performance have been carried out (Sciacovelli et al. 2015). In this model, water is used as a PCM and the heat transfer to and from the PCM involves convective mode. Then, the PCM properties were quite similar to those of water as shown in Table 6.2. The PCM storage is modelled as a rectangle container unit with fins on the back panel flow duct after the evaporator and indirect contact with the circulating air through the cabinet. The phase transition temperature is constant (0^0 C) and matches to the air cabinet temperature (Borderon et al. 2015). The energy will then be released from or stored in the PCM during solidification and melting processes depending on the temperature.

Table 6.2 Thermal properties of the PCM based water.

Characteristics	Value
Density (kg/m^3)	998.2
Thermal conductivity (W/m k)	0.6
Specific heat (kJ/(kg K)	4.182
Melting and freezing temperature (K)	273.15
heat of fusion (kJ/kg)	334

6.4 PCM model

The method used for modelling the solidification/melting process in ANSYS Fluent is the enthalpy-porosity technique (Voller et al. 1989). In this approach, a quantity called the liquid fraction, which represents the fraction of the cell volume that is in liquid form, is associated with each cell in the domain. The liquid fraction is computed at each iteration, based on an enthalpy balance. The enthalpy of the material is also calculated as the sum of the sensible enthalpy, h, and the latent heat, ΔH:

$$H = h + \Delta H \tag{6.1}$$

Where

$$h = h_{ref} + \int_{T_{ref}}^{T} C_P dT \tag{6.2}$$

The liquid fraction, β, is defined as

$$\beta = \begin{cases} 0 & \text{if } T < T_s \\ 1 & \text{if } T > T_l \\ \dfrac{T - T_s}{T_l - T_s} & \text{if } T_s < T < T_l \end{cases} \tag{6.3}$$

The latent heat content can now be written in terms of the latent heat of the material, L:

$$\Delta H = \beta L \tag{6.4}$$

The latent heat content can vary between zero (for a solid) and L (for a liquid). For solidification/melting problems, the energy equation is written as:

$$\frac{\partial}{\partial t}(\rho H) + \nabla.(\rho v H) = \nabla.(K \nabla T) + S \tag{6.5}$$

The solution for temperature is essentially iterated between Eq. **(6.3)** and Eq. **(6.5)**. The simulation process of PCM integration is divided into two parts; the first one is steady state analysis which was necessary to prepare appropriate initial conditions for the second part which is transient analysis.

6.5 Steady model with PCM

As mentioned before for simulation without PCM, at the commencement, the model with PCM has been executed in the steady state condition and therefore all the boundary conditions will be constant through the calculation. This stage of simulation is important to gain primary validation with the experimental results and also to use it as initial conditions for the transit simulation with PCM later on. In this stage, we only need to use the DEFINE_SOURCE macro. Although the solidification/melting model was active in this stage, it is impossible to see the PCM effect on the operating conditions due to the charge and discharge processes will not occur as the temperature is constant. However, there is a few differences between the temperature contours comparing the without PCM steady state model.

6.6 Transient model with PCM

After steady state simulation with PCM was converged, a transient model with PCM was built and developed to study the PCM effect on the interested parameters such as cabinet air temperatures, phase change temperature and energy consumption with time, taking also into account defrost effect which supposed to be the most affected parameters as the discharge/charge PCM processes should happen at that time. This stage of the modelling was started by integrating all UDF codes to the main boundary conditions. All other boundaries are still the same. The calculations will jump from the steady state results and continue for longer time than the transient model without PCM. The reasons for that are adding another model to the simulation (solidification/melting) and PCM liquid fraction needs extra time to become stable. All-important parameters were monitored and recorded into separate files during the transient calculations to be ready for analysing later on.

6.7 Model validation with PCM

The validation process for the simulation model with PCM is also based on the experimental results for the cabinet with PCM integration. This stage includes validation of both models; steady and transient.

6.7.1 Steady validation

The steady stage of simulation with PCM will not show us the PCM effect since the evaporator will be considered to work continuously during steady calculations. However, the validation for this stage still necessary in terms of air flow pattern which is influenced by adding such size of PCM in the way of circulating air. The contours of static temperatures for the cabinet air and products at steady state results with PCM are seen in Figure 6.1. It can clearly identify the same observations as in Figure 5.8.

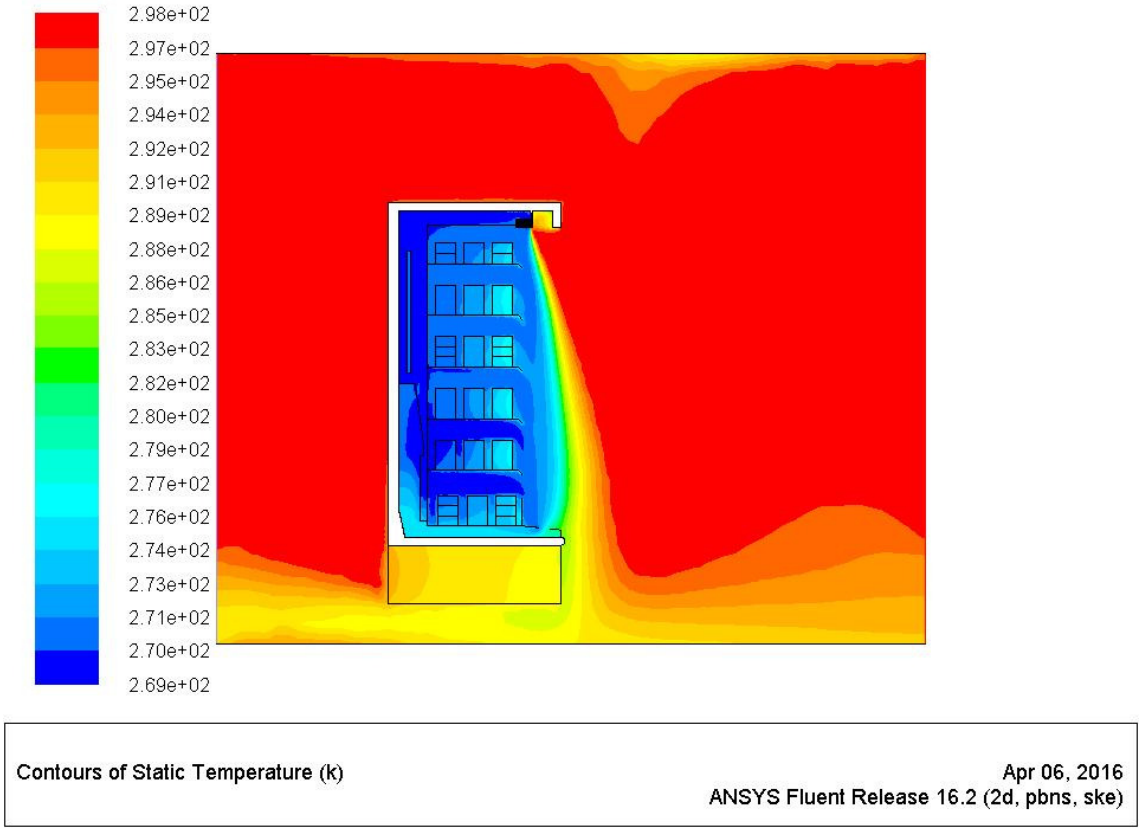

Figure 6.1 Air and product temperature contours for steady model with PCM

Figure 6.2 shows the air velocity contours for the steady state simulation with PCM. It can be observed from that velocity contours are quite similar to the steady model without PCM. It is clear that the maximum air velocities are in the bottom duct as a result for the suction side of the fan as was mentioned in description of Figure 5.9. It

could also be observed from this Figure that the air flow at the back panel around the PCM container was achieved to make sure that the heat transfer rate at the highest level.

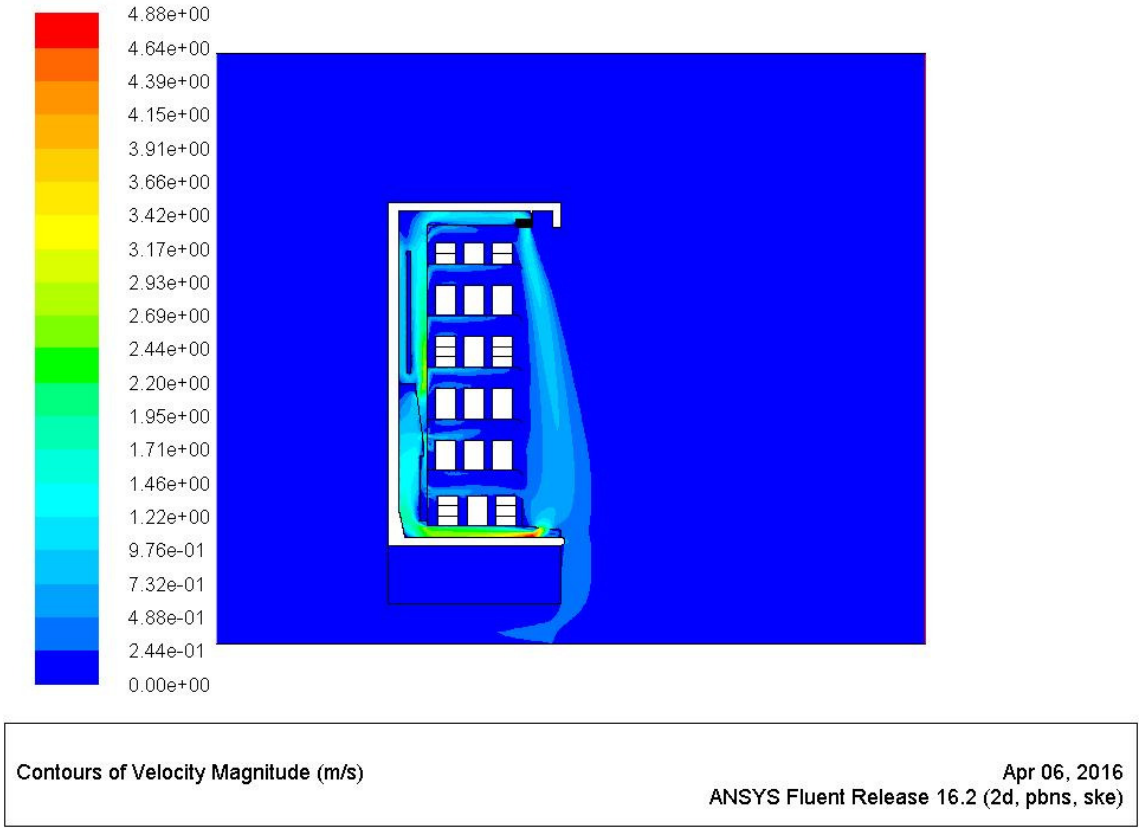

Figure 6.2 Air velocity contours for steady model with PCM

The air velocity is another important factor for this study due to its impact of convection heat transfer on charging and discharging of PCM. For instance, Figure 6.3 validates the values of air velocities for the simulation and measurements results during steady state model with PCM. Also, this validation is important as it illustrates that the air flow pattern at the main points, in the circulating air path, is slightly influenced by the PCM container size.

Figure 6.3 Validation of air velocity for Steady model with PCM

6.7.2 Transient validation

Another important validation of the transient simulation results for the cabinet with PCM is cabinet air temperature as shown in Figure 6.4. It shows validation of the air-curtain outlet temperature with time. It is noticed that there is a good agreement with the measurement results. However, some inconsistencies are observed between simulation and measurements results particularly for the cycle numbers. This could be argued that not all PCM was effective during the experiment such that the defrost period for the test was shorter than that of simulation.

Figure 6.4 Validation of curtain-outlet temperature for Transient model with PCM

Liquid fraction contours for the melting process of big (defrost) cycle for the PCM are demonstrated in Figure 6.5 in which the average liquid fraction contours are taken at 0%, 25%, 50%, 75% and 100% and the discharge and charge processes take place every big and short cycle. Although not all PCM is transformed into liquid in small cycles, we could still notice some good effects of the PCM integration on the cabinet air temperatures as depicted in the results. In addition, it is clear that liquid fraction ratio is higher at the PCM container or cabinet top due to air temperature. It can be readily acknowledged that the simulation and experiment results of the cabinets with and without PCM match fairly well.

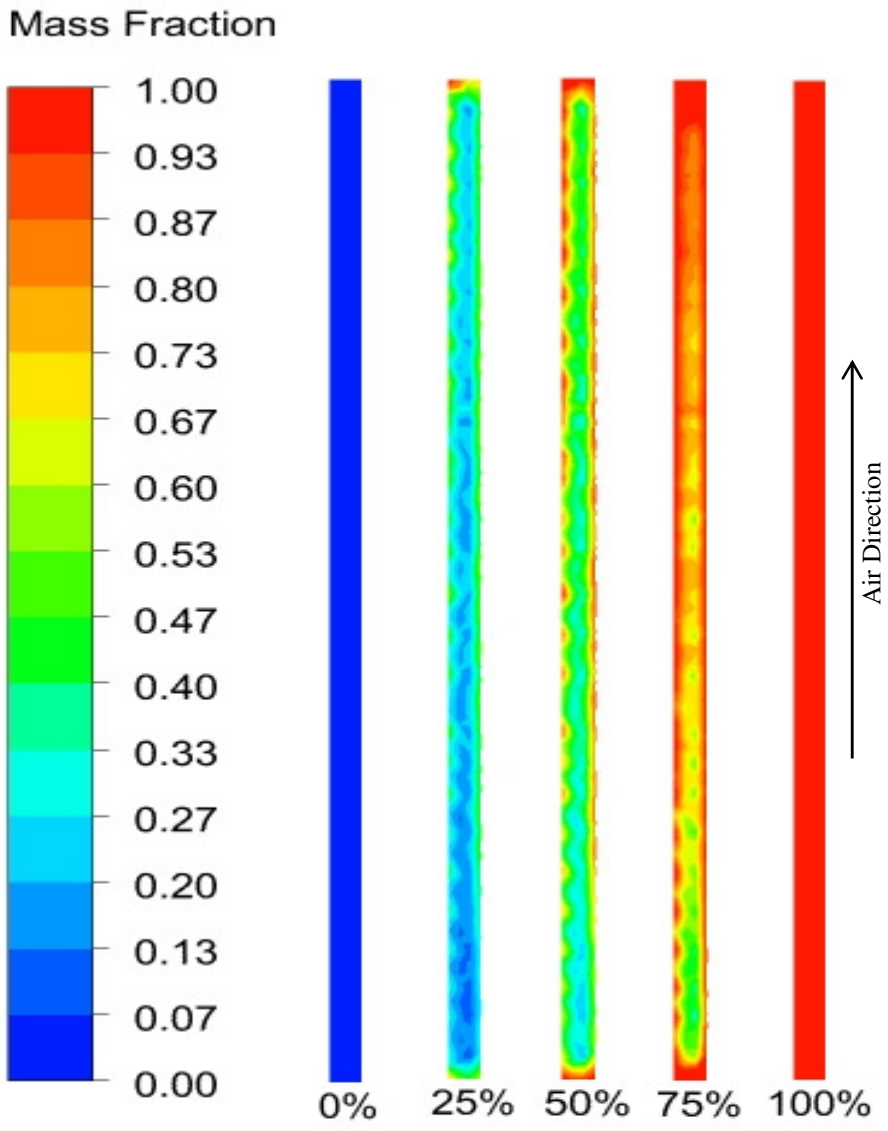

Figure 6.5 Liquid fraction Contours for PCM container

6.8 Result and discussion

Due to the complexity of the developed CFD model, it would take a few days for the simulation to approach stabilisation and until then the simulation results could be collected. The simulation results include mostly the performance comparisons for the cabinet with and without PCM integration.

6.8.1 Cabinet air temperatures

Figure 6.6 distinctly shows the influence of PCM on the cabinet air temperatures at evaporator air-off, curtain outlet and air-grille. It can be observed from this Figure that the maximum temperatures of cabinet air in the original cabinet are higher than those with PCM setup because the PCM absorbs some heat from the circulated air during the system off periods. Also, the minimum temperatures of original cabinet are lower than those corresponding ones with PCM due to the PCM is considered as an extra load in the on periods while the cooling capacity maintains constant. Another PCM effect demonstrates that the number of small on /off cycles decreases considerably from 11 to 8 due to the duration increase of each cycle. In addition, the defrost time period also shows increase for the modified cabinet with PCM. All these positive effects of the improved cabinet will contribute the reduction of cabinet power consumption as described below.

Figure 6.6 Variations of cabinet air temperatures with time during period of 8 hrs with and without PCM

6.8.2 Defrost and normal operation cycles

There are two operational cycles for the cabinet compressor on and off, defrost (big) and normal (small). Every four hours, the unit is switched off for defrost until the monitored (thermostat) temperature is higher than the limitation or the defrost period is

complete. Apart from the defrost period, the unit compressor enters into the normal (small) cycles and is controlled on and off based on the thermostat temperature redaction and settings. The temperature variations at the thermostat point for the cabinet with and without PCM in the period of defrost and normal are predicted and shown in Figure 6.7. It is noted that the temperature variation is more convergent for the cabinet with PCM which will be helpful for the temperature uniformity of food products stored. In addition, the addition of PCM has a significant impact on the total working time of the cabinet compressor in which the big and small cycle durations for the cabinet with PCM increase about 55% and 26% respectively. These are the reasons of the continuous heat transfer processes between the cabinet air flow and the integrated PCM. For any defrost or normal cycles, both on and off periods are increased for the modified cabinet. However, the increase rate for off period is more significant than that of on period due to the heat sink and source roles of PCM in these periods respectively. This leads to longer off period for the unit compressor and thus saving energy.

The energy extracted from the PCM provides the cooling needed when the compressor was stopped, which, with optimization, may achieve more energy reduction than the basic cabinet without PCM.

Figure 6.7 Defrost, Off and On durations with and without PCM

6.8.3 Product temperatures

The food product temperatures for the cabinet without and with PCM storage container were recorded during 8 hours of stable calculation period as shown in Figure 6.8 a and b respectively. In each figure, there are 12 product temperatures represented under different product numbers. Generally, it can be noticed from these figures, for both circumstances, the range of each product temperature remains stable with very slight variation in response to the compressor on, off and defrost. For the modified cabinet, the whole variation range of product temperatures is more moderate than that without PCM signifying more uniformity in product temperatures. However, as predicted, the outcome of adding PCM shows an increase in the whole average of product temperatures because the extra load from PCM, but still within standard limitation as shown in Table 6.4. These simulation results of product temperatures correspond to the predicted air temperatures shown in Figure 6.6 since the air flows are in immediate contact with the products.

(a)

(b)

Figure 6.8 Variations of products temperature with time during 8 hrs (a) without and (b) with PCM

Table 6.3 Theoretical products temperature for Norpe cabinet

Simulation parameters	Without PCM	With PCM
Average temperature (K)	276.7	277.2
Maximum temperature (K)	279.6	279.3
Minimum temperature (K)	274.5	275.4
Temperature range (K)	5.1	3.9

6.8.4 Compressor working time

Starting from defrost, the compressor on (1) and off (0) states for the cabinet with and without PCM are predicted and shown in Figure 6.9. When the PCM is integrated, the cabinet has fewer frequencies for both on and off states but has longer total off period. This is because that when the compressor is off, the PCM acts as an air cooler by carrying on absorb the heat from the air flow and consequently postpones the increase speed of cabinet air temperatures until the PCM is mostly melted. When the compressor is on, the PCM starts to solidify progressively and acts as an additional load such that the on period of each cycle for the cabinet with PCM is also longer. Nevertheless, the total on period is still less for the cabinet with PCM considering of its fewer on states. The reduced on times for the compressor can also lead to longer compressor operation life. It can also bring further energy savings since the compressor needs higher power at starting point from our measurement as illustrated in Figure 6.10. We can find the

percentage of energy saving after adding the PCM container to the cabinet during about one day running fluent time from Table 6.4. It is found about 6.4% energy saving plus the saving percentage resulted from reducing the number of compressor starts.

Figure 6.9 Working state variations with time for cabinet with and without PCM

Figure 6.10 Instant power consumption of experiment with time

Table 6.4 Energy consumption of the cabinet in one fluent day

Energy parameters	**Without PCM**	**With PCM**
Average instant power (kW)	1.6	1.6
Whole running time (h)	0.6	0.6
Total On time (h)	0.4875	0.45
Total Off time (h)	0.1125	0.15
Energy consumption (kW h)	0.78	0.72
No of compressor starts	72	54
Energy saving (%)	**6.4**	

6.8.5 PCM solidification rate

The variations of PCM container average temperature, thermostat temperature and the PCM average liquid fraction with time are shown in Figure 6.11 for 8 hours stable calculation. For PCM to be beneficial during defrost and normal compressor off times, the PCM temperature needs to stay close to its transition temperature (273.15 K) for longer periods. This is achievable as it lies within the cabinet air temperature range. It can be seen that all and part of PCM latent heat are used respectively during the defrost off and normal off time periods. It is clear that the liquid fraction increases (discharging) gradually during the defrost period until its highest value of one when the whole PCM turns to liquid. Whereas only small part of PCM turns to liquid during a normal off period as there is no enough time to change whole PCM phase. After the off point, the liquid fraction starts to decrease (charging) and then increase (discharging) during the on and off working cycles, respectively.

Figure 6.11 Variation of Melting/Solidification and transition temperature with time

6.8.6 Variation of ambient air temperature and air velocity

The variations of PCM liquid fraction and predicted thermostat temperature with time at different values of evaporator fan pressure jumps (or air flow rates) are illustrated in Figure 6.12. It is obvious that at 20 Pascal fan pressure jump, the PCM takes longer time to solidify after defrost as the low air velocity will decrease the transfer rate between the PCM and the circulated air flow compared to the effect of higher fan pressure jump. In this case, it will take shorter time for the thermostat sensor to reach its setting point and then switch off the compressor and thus more small cycles appeared. While the higher air velocity at 30 Pascal pressure jump will solidify the PCM quickly such that more cooling capacity is needed for the PCM solidification and thus leading more time for the thermostat sensor to reach the setting point.

Figure 6.12 Melting/Solidification and thermostat temperature at different fan pressure jumps

Figure 6.13 indicates how the solidification process and thermostat temperature are affected by indoor space air temperature. The higher space air temperature (30ºC) means higher thermal load and that will make the evaporator cooling capacity not sufficient for the thermostat sensor to reach its setting point (no small cycles) and maintain product temperature at the same time. Thus, the compressor will be switched on all the time till next automatic defrost. Conversely, the lower space temperature (20 ºC) will decrease the cabinet cooling load and allow the thermostat to reach the setting point easily but have reduced compressor off periods and more small cycles.

Figure 6.13 Melting/Solidification and thermostat temperature at different indoor space air

6.8.7 PCM Thickness optimization

From simulation results it appears that the cabinet performance is sensitive to the PCM thickness as presented in Figure 6.14. The Off time saving is the percentage ratio of the extra off time resulted from using PCM and the off time without PCM. The best thickness (used in this study) was 16 mm which gave us 29.6% off time saving. However, the thickness parameter has negative impact on the off time when exceed 16 mm, due to the fact that the big thickness of PCM container will highly affect the air flow configurations in the back duct as well as the high latent heat will increase the thermal load on the cabinet.

Figure 6.14 Off time increase at different thicknesses of PCM

6.9 Summary

The theoretical study of a display cabinet with a PCM-HE fitted on the existing space of the main back duct was illustrated in this chapter. This PCM incorporation demonstrated an enhancement of thermal system performance and reduction in the cabinet air temperatures when the cabinet is off. Calculations are carried out for this cabinet first without PCM integration, then with a container filled with pure water as a PCM. The next chapter will summarize the conclusions and recommendations of this study.

CHAPTER 7

CONCLUSIONS AND RECOMMENDATIONS FOR FUTURE WORK

The preceding chapters examined experimentally and theoretically the proof of concept of LH-TES to minimize the increase of the environmental impacts of supermarkets and presented approaches to quantify them. The concept benefits from the advantages latent heat stored in the PCM in reducing the energy required by cabinets in supermarkets. This work is done into experimental and theoretical parts.

The experimental study of two chilled food multi-deck display cabinets equipped with PCM HEs installed on the available space of the main rear duct shows an enhancement in terms of system performance and cabinet temperature. Analytical investigations to determine the quality and quantity of the required PCM in each cabinet used in the experimental part were carried out while the performance of each cabinet and its integration with the TES system were evaluated.

Tests were carried out for this cabinet without PCM integration first, then with two single plate containers holding water gel PCM. The experimental results achieved from this work were used to compare and validate a CFD simulation model that was developed later. The model was then used to predict and optimise cabinet performance with PCM by changing various parameters such as climate class and the type, quantity and location of the PCM and PCM heat exchangers throughout the cabinet.

The outcomes arising from the whole thesis and recommendations for future work aiming at reducing the energy consumption of such cabinets are summarised by this chapter. The following are the main conclusions of this work:

7.1 Conclusions

1. The simulation and test results indicated that the response of the cabinet with PCM was positive in minimizing the power consumption, product and cabinet air temperatures when the cabinet was off and improving thermal performance.

2. It was found that with PCM the energy saving potentials of the Norpe cabinet significantly improved experimentally and theoretically, to around 5% and 6.4 % respectively at climate class 3 conditions (25ºC and 60% RH).

3. In terms of cabinet air temperatures, both test and model results showed considerable benefit from reductions of maximum temperatures and temperature range.

4. The whole variation range of product temperatures has become more moderate after modification signifying more uniformity in product temperatures. Also, adding PCM showed an increase in the whole average of product temperatures.

5. The defrost intervals were the most affected factors for the modified cabinet. They were increased experimentally and theoretically by approximately 70% and 98% respectively compared to those with the basic cabinet.

6. A significant decrease (27%) in the number of starts/stops of the compressor was observed for the theoretically modified cabinet, and this will directly affect the compressor life.

7. PCM effectiveness was highly sensitive to the indoor space air temperature and fan pressure jump and the optimum values of those parameters should be chosen accurately for a given operating conditions and certain PCM.

7.2 Recommendations for future work

It is worth noting that energy savings are a function of the ambient temperature, relative humidity, operational settings of the cabinet and PCM freezing point, all of which should be considered for future models.

This thesis has covered many alternative parameters related to the design of the PCM-TES system, and their effect on the thermal performance and energy savings of display cabinets. However, other design aspects may be as beneficial to the energy consumption in such cabinets, and may further enhance their performance. Research must be conducted to assess the feasibility of using different types of more efficient and purpose built HEs which could be used to accommodate the PCM in the back panel duct of the cabinet instead of the containers employed in this study. In addition, the energy saving could be more as the material and the capacity of such HEs will be much better.

After experimentally and theoretically demonstrate the PCM effectiveness in refrigerated display cabinets for saving energy in the current study, a simulation and experimental work for integrating the PCM in different locations through the cabinet walls such as top air duct, bottom duct and through the shelves could be alternative options to be explored and compared with the current results.

Also, optimization study could be applied to find out the more efficient option of the suggested locations to integrate the PCM such that this model could be appropriate for manufacturing purposes to be commercially applicable. Further benefits include high energy saving when all proposed locations of integrated walls have been used at the same time for the modified display cabinet.

All the numerical work in this thesis has been conducted using 2D simulations. However, 3D simulation for the cabinet with the PCM container must be conducted to faithfully represent more realistic situation and find out the effect of the third dimension on the current results. Achieving that allows for studying the 3D liquid fraction tendency through PCM container rather than 2D.

REFERENCES

A. Al-Sahhaf. 2011. “Investigation of the Entrainment and Infiltration Rates through Air Curtains of Open Low-Front Refrigerated Display Cabinets REFRIGERATED DISPLAY CABINETS.” PhD thesis, Brunel University London.

A. Hadawey. 2006. “Design of Chilled Food Display Cabinets for Better Temperature Integrity and Longer Product Shelf Life.” PhD thesis, Brunel University London.

A. Raeisi, IN. Suamir, S. A.Tasso. 2013. “Energy Storage in Freezer Cabinets Using Phase Change Materials.” in *2ndIIR International Cold Chain Conference*. Paris.

Ahmed, Mashud, Oliver Meade, and Mario A. Medina. 2010. “Reducing Heat Transfer across the Insulated Walls of Refrigerated Truck Trailers by the Application of Phase Change Materials.” *Energy Conversion and Management* 51(3):383–92.

Al-Sahhaf, A. 2011. “INVESTIGATION OF THE ENTRAINMENT AND INFILTRATION RATES THROUGH AIR CURTAINS OF OPEN LOW-FRONT REFRIGERATED DISPLAY CABINETS.”

Alzuwaid, F., Y. T. Ge, S. A. Tassou, A. Raeisi, and L. Gowreesunker. 2015. “The Novel Use of Phase Change Materials in a Refrigerated Display Cabinet: An Experimental Investigation.” *Applied Thermal Engineering* 75:770–78.

Amin, Mazyar, Dana Dabiri, and Homayun K. Navaz. 2009. “Tracer Gas Technique: A New Approach for Steady State Infiltration Rate Measurement of Open Refrigerated Display Cases.” *Journal of Food Engineering* 92(2):172–81.

Amin, Mazyar, Dana Dabiri, and Homayun K. Navaz. 2011. “Comprehensive Study on the Effects of Fluid Dynamics of Air Curtain and Geometry, on Infiltration Rate of Open Refrigerated Cavities.” *Applied Thermal Engineering* 31(14–15):3055–65.

Amin, Mazyar, Dana Dabiri, and Homayun K. Navaz. 2012. “Effects of Secondary Variables on Infiltration Rate of Open Refrigerated Vertical Display Cases with Single-Band Air Curtain.” *Applied Thermal Engineering* 35(1):120–26.

Ansys, Inc. 2013. “ANSYS Fluent Theory Guide.” 15317(November):514.

Ansys, Inc. 2011. “ANSYS FLUENT User ’ S Guide.” 15317(November):2498.

Ansys Inc. 2013. “ANSYS Fluent UDF Manual.” 15317(November):724–46.

Azzouz, K., D. Leducq, and D. Gobin. 2008. “Performance Enhancement of a Household Refrigerator by Addition of Latent Heat Storage.” *International Journal of Refrigeration* 31(5):892–901.

Azzouz, K., D. Leducq, and D. Gobin. 2009. “Enhancing the Performance of Household

Refrigerators with Latent Heat Storage: An Experimental Investigation." *International Journal of Refrigeration* 32(7):1634–44.

Azzouz, K., D. Leducq, J. Guilpart, and D. Gobin. 2005. "Improving the Energy Efficiency of a Vapor Compression System Using a Phase Change Material." Pp. 1–11 in *2nd Conference on PCM & Slurry*. Switzerland.

Bansal, Pradeep, David Fothergill, and Ryan Fernandes. 2010. "Thermal Analysis of the Defrost Cycle in a Domestic Freezer." *International Journal of Refrigeration* 33(3):589–99.

Behzadi, S. and M. M. Farid. 2014. "Long Term Thermal Stability of Organic PCMs." *Applied Energy* 122:11–16.

Borderon, Julien, Joseph Virgone, and Richard Cantin. 2015. "Modeling and Simulation of a Phase Change Material System for Improving Summer Comfort in Domestic Residence." *Applied Energy* 140(0):288–96.

BS EN ISO-1. 2005. "Refrigerated Dispaly Cabinets-Part 1: Vocabulary."

BS EN ISO-2. 2005. "Refrigerated Dispaly Cabinets-Part 2: Classifications, Requirments and Test Conditions."

Bundy, By Pat, Senior Application Engineer-supermarket Refrigeration, and Sporlan Valve Company. 2002. *Reducing Pressure Drop in Suction Lines Suction Regulating Valves , in Conjunction with Step Motors , Can Reduce Pressure Drop in Suction Lines and Increase Efficiency*.

Cabeza, L. F., H. Mehling, S. Hiebler, and F. Ziegler. 2002. "Heat Transfer Enhancement in Water When Used as PCM in Thermal Energy Storage." *Applied Thermal Engineering* 22(10):1141–51.

Campos-Celador, A., G. Diarce, I. González-Pino, and J. M. Sala. 2013. "Development and Comparative Analysis of the Modeling of an Innovative Finned-Plate Latent Heat Thermal Energy Storage System." *Energy* 58:438–47.

Campos-Celador, Lvaro et al. 2014. "Design of a Finned Plate Latent Heat Thermal Energy Storage System for Domestic Applications." *Energy Procedia* 48:300–308.

Canonsburg, Technology Drive. 2013. "ANSYS Fluent Meshing User ' S Guide." 15317(November):724–46.

CCC. 2010. *The Fourth Carbon Budget, Reducing Emissions through the 2020s*.

Cerri, G. 2003. "Identification of Domestic Refrigerator Models Including Cool Storage." in *20th International Congress of Refrigeration*. Washington D.C.

Chandrasekharan, Ramesh, Parmesh Verma, and Clark W. Bullard. 2006. "Development of a Design Tool for Display Case Evaporators." *International*

Journal of Refrigeration 29(5):823–32.

Chen, Yun Guang and Xiu Ling Yuan. 2005. "Experimental Study of the Performance of Single-Band Air Curtains for a Multi-Deck Refrigerated Display Cabinet." *Journal of Food Engineering* 69(3):261–67.

Cheng, Wen Long and Xu Dong Yuan. 2013. "Numerical Analysis of a Novel Household Refrigerator with Shape-Stabilized PCM (Phase Change Material) Heat Storage Condensers." *Energy* 59:265–76.

Cheng, Wen-Long, Bao-Jun Mei, Yi-Ning Liu, Yong-Hua Huang, and Xu-Dong Yuan. 2011. "A Novel Household Refrigerator with Shape-Stabilized PCM (Phase Change Material) Heat Storage Condensers: An Experimental Investigation." *Energy* 36(10):5797–5804.

Chila, Ronald J. and Deborah a. Kaminski. 2008. "Grid Independence Via Automated Unstructured Adaptation." *Journal of Fluids Engineering* 130(12):121403.

Cortella, Giovanni. 2002. "CFD-Aided Retail Cabinets Design." *Computers and Electronics in Agriculture* 34(1–3):43–66.

Cortella, Giovanni, Marco Manzan, and Gianni Comini. 2001. "CFD Simulation of Refrigerated Display Cabinets." *International Journal of Refrigeration* 24(3):250–60.

Cui, Jingtan and Shengwei Wang. 2004. "Application of CFD in Evaluation and Energy-Efficient Design of Air Curtains for Horizontal Refrigerated Display Cases." *International Journal of Thermal Sciences* 43(10):993–1002.

D'Agaro, Paola, Giovanni Cortella, and Giulio Croce. 2006a. "Two- and Three-Dimensional CFD Applied to Vertical Display Cabinets Simulation." *International Journal of Refrigeration* 29(2):178–90.

D'Agaro, Paola, Giovanni Cortella, and Giulio Croce. 2006b. "Two- and Three-Dimensional CFD Applied to Vertical Display Cabinets Simulation." *International Journal of Refrigeration* 29(2):178–90.

DEFRA. 2005. *The Validity of Food Miles as an Indicator of Sustainable Development*.

Demirbas, M.Fatih. 2006. "Thermal Energy Storage and Phase Change Materials: An Overview." *Energy Sources, Part B: Economics, Planning, and Policy* 1(1):85–95.

Dolado, Pablo, Ana Lazaro, Jose M. Marin, and Belen Zalba. 2011. "Characterization of Melting and Solidification in a Real Scale PCM-Air Heat Exchanger: Numerical Model and Experimental Validation." *Energy Conversion and Management* 52(4):1890–1907.

Dubovsky, Vadim, Gennady Ziskind, and Ruth Letan. 2011. "Analytical Model of a PCM-Air Heat Exchanger." *Applied Thermal Engineering* 31(16):3453–62.

El-Dessouky, Hisham and Faisal Al-Juwayhel. 1997. “Effectiveness of a Thermal Energy Storage System Using Phase-Change Materials.” *Energy Conversion and Management* 38(6):601–17.

F. Bruno. 2005. “USING PHASE CHANGE MATERIALS (PCMs) FOR SPACE HEATING AND COOLING IN BUILDINGS .” Pp. 26–31 in *performance enhanced buildings environmentally sustainable design conference*.

Faramarzi, Ramin. 1999. “Efficient Display Case Refrigeration.” *ASHRAE Journal* 41(11):46–54.

Farid, Mohammed M., Amar M. Khudhair, Siddique Ali K. Razack, and Said Al-Hallaj. 2004. “A Review on Phase Change Energy Storage: Materials and Applications.” *Energy Conversion and Management* 45(9–10):1597–1615.

Foster, A. M., M. Madge, and J. A. Evans. 2005. “The Use of CFD to Improve the Performance of a Chilled Multi-Deck Retail Display Cabinet.” *International Journal of Refrigeration* 28(5):698–705.

Gaspar, Pedro Dinis, L. C. Carrilho Gonçalves, and R. A. Pitarma. 2011. “Experimental Analysis of the Thermal Entrainment Factor of Air Curtains in Vertical Open Display Cabinets for Different Ambient Air Conditions.” *Applied Thermal Engineering* 31(5):961–69.

Gaspar, Pedro Dinis, L. C.Carrilho Gonalves, and R. A. Pitarma. 2012a. “CFD Parametric Studies for Global Performance Improvement of Open Refrigerated Display Cabinets.” *Modelling and Simulation in Engineering* 2012.

Gaspar, Pedro Dinis, L. C.Carrilho Gonalves, and R. A. Pitarma. 2012b. “Detailed CFD Modelling of Open Refrigerated Display Cabinets.” *Modelling and Simulation in Engineering* 2012.

Ge, Y. T., S. A. Tassou, and A. Hadawey. 2010. “Simulation of Multi-Deck Medium Temperature Display Cabinets with the Integration of CFD and Cooling Coil Models.” *Applied Energy* 87(10):3178–88.

Gin, B., M. M. Farid, and P. K. Bansal. 2010. “Effect of Door Opening and Defrost Cycle on a Freezer with Phase Change Panels.” *Energy Conversion and Management* 51(12):2698–2706.

Gin, Benjamin and Mohammed M. Farid. 2010. “The Use of PCM Panels to Improve Storage Condition of Frozen Food.” *Journal of Food Engineering* 100(2):372–76.

Gray, I. Luscombe, P., McLean, L., Sarathy, C S P., Sheahen, P., Srinivasan, K. 2008. “Improvement of Air Distribution in Refrigerated Vertical Open Front Remote Supermarket Display Cases.” *International Journal of Refrigeration* 31(5):902–10.

Griffiths, P. W. and P. C. Eames. 2007. "Performance of Chilled Ceiling Panels Using Phase Change Material Slurries as the Heat Transport Medium." *Applied Thermal Engineering* 27(10):1756–60.

Hadawey, Abas F., Tawfiq J. Jaber, Waleed Abdul Ghaffar, and Abu Dhabi. 2012. "Air Curtain Design Optimization of Refrigerated Vertical Display Cabinet Using CFD." *International Journal of Scientific Engineering and Technology* 1(4):76–88.

Hawlader, M. N. A., M. S. Uddin, and Mya Mya Khin. 2003. "Microencapsulated PCM Thermal-Energy Storage System." *Applied Energy* 74(1–2):195–202.

HAWLADER, M. N. A., M. S. UDDIN, and H. J. ZHU. 2000. "Preparation and Evaluation of a Novel Solar Storage Material: Microencapsulated Paraffin." *International Journal of Solar Energy* 20(4):227–38.

Hed, G. and R. Bellander. 2006. "Mathematical Modelling of PCM Air Heat Exchanger." *Energy and Buildings* 38(2):82–89.

Hoogendoorn, C. J., G. C. J. Bart, and The Nethedands. 1992. "Performance a N D Modelling of Latent Heat Stores." 48(I):53–58.

Horbaniuc, Bogdan, Gheorghe Dumitrascu, and Aristotel Popescu. 1999. "Mathematical Models for the Study of Solidification within a Longitudinally Finned Heat Pipe Latent Heat Thermal Storage System." *Energy Conversion and Management* 40(15):1765–74.

Howell, R. H. 1993. "Effects of Store Relative Humidity on Refrigerated Display Case Performance." *ASHRAE Transactions* 99(pt 1):667–78.

IEA. 2010. "World Energy Outlook 2009." *World Energy Outlook* 23(4):326–28. Retrieved (www.iea.org/weo/2010.asp).

IN. Suamir. 2012. "INTEGRATION OF TRIGENERATION AND CO2 BASED REFRIGERATION SYSTEMS FOR ENERGY CONSERVATION IN THE FOOD RETAIL INDUSTRY." PhD thesis, Brunel University London.

IRENA and ETSAP. 2013. "Thermal Energy Storage. Technology Brief." (January):24. Retrieved (www.irena.org/Publications).

Ismail, K. A. R., C. L. F. Alves, and M. S. Modesto. 2001. "Numerical and Experimental Study on the Solidification of PCM around a Vertical Axially Finned Isothermal Cylinder." *Applied Thermal Engineering* 21(1):53–77.

Kalikmanov, Vitaly. 2012. *Nucleation Theory*. Springer. Retrieved March 31, 2016 (https://books.google.com/books?id=GKC5BQAAQBAJ&pgis=1).

KENISARIN, M. and K. MAHKAMOV. 2007. "Solar Energy Storage Using Phase Change Materials." *Renewable and Sustainable Energy Reviews* 11(9):1913–65.

Laguerre, O., M. H. Hoang, V. Osswald, and D. Flick. 2012. "Experimental Study of Heat Transfer and Air Flow in a Refrigerated Display Cabinet." *Journal of Food Engineering* 113(2):310–21.

Laguerre, Onrawee, Evelyne Derens, and Denis Flick. 2011. "Temperature Prediction in a Refrigerated Display Cabinet: Deterministic and Stochastic Approaches." *Electronic Journal of Applied Statistical Analysis* 4(2):191–202.

Launder, B. E. and D. B. Spalding. 1974. "The Numerical Computation of Turbulent Flows." *Computer Methods in Applied Mechanics and Engineering* 3(2):269–89.

Launder, Brian E. 1989. "Second-Moment Closure: Present... and Future?" *International Journal of Heat and Fluid Flow* 10(4):282–300.

Lazaro, Ana, Pablo Dolado, Jose M. Marin, and Belen Zalba. 2009. "PCM-Air Heat Exchangers for Free-Cooling Applications in Buildings: Empirical Model and Application to Design." *Energy Conversion and Management* 50(3):444–49.

Lazaro, Ana, Pablo Dolado, Jose M. Marín, and Belen Zalba. 2009. "PCM-Air Heat Exchangers for Free-Cooling Applications in Buildings: Experimental Results of Two Real-Scale Prototypes." *Energy Conversion and Management* 50(3):439–43.

Liu, Ming, Wasim Saman, and Frank Bruno. 2012. "Development of a Novel Refrigeration System for Refrigerated Trucks Incorporating Phase Change Material." *Applied Energy* 92:336–42.

Lu, W. and S. A. Tassou. 2013. "Characterization and Experimental Investigation of Phase Change Materials for Chilled Food Refrigerated Cabinet Applications." *Applied Energy* 112:1376–82.

Lu, Y. L., Zhang, W H., Yuan, P., Xue, M D., Qu, Z G., Tao, W Q. 2010. "Experimental Study of Heat Transfer Intensification by Using a Novel Combined Shelf in Food Refrigerated Display Cabinets (Experimental Study of a Novel Cabinets)." *Applied Thermal Engineering* 30(2–3):85–91.

Lunt, Mark F. et al. 2015. "Reconciling Reported and Unreported HFC Emissions with Atmospheric Observations." *Proceedings of the National Academy of Sciences of the United States of America* 112(19):5927–31.

M. CONTI, C. H.CHARACH. 1996. "Thermodynamics of Heat Storage in a Pcm Shell-and-Tube Heat Exchanger in Parallel or in Series With a Heat Engine." *Solar Energy* Vol. 57(1):59–68.

Marinetti, Sergio, Giovanna Cavazzini, Laura Fedele, Francesco De Zan, and Pierluigi Schiesaro. 2012. "Air Velocity Distribution Analysis in the Air Duct of a Display Cabinet by PIV Technique." *International Journal of Refrigeration* 35(8):2321–31.

Marinetti, Sergio, Giovanna Cavazzini, Igor Lauri, Samuele Testa, and Silvia Minetto. 2014. "Numerical and Experimental Analysis of the Air Flow Distribution in the Cooling Duct of a Display Cabinet." *International Journal of Refrigeration* 42(0):8–13.

Marques, A. C., G. F. Davies, J. A. Evans, G. G. Maidment, and I. D. Wood. 2013. "Theoretical Modelling and Experimental Investigation of a Thermal Energy Storage Refrigerator." *Energy* 55:457–65.

Marques, A. C., G. F. Davies, G. G. Maidment, J. A. Evans, and I. D. Wood. 2014. "Novel Design and Performance Enhancement of Domestic Refrigerators with Thermal Storage." *Applied Thermal Engineering* 63(2):511–19.

Martínez, P.J., Pinazo, J.M., Veláquez, A. 2003. "Passive Thermal Energy Storage in Refrigerated Trailers." *ASHRAE Transactions* 324–328.

Mastrullo, R., A. W. Mauro, L. Menna, A. Palma, and G. P. Vanoli. 2014. "Transient Model of a Vertical Freezer with Door Openings and Defrost Effects." *Applied Energy* 121:38–50.

Medrano, M. et al. 2009. "Experimental Evaluation of Commercial Heat Exchangers for Use as PCM Thermal Storage Systems." *Applied Energy* 86(10):2047–55.

Mersmann, A. 2001. *Crystallization Technology Handbook*. CRC Press.

Mettawee, E. B. S. and G. M. R. Assassa. 2007. "Thermal Conductivity Enhancement in a Latent Heat Storage System." *Solar Energy* 81(7):839–45.

Navaz, Homayun K., Brenda S. Henderson, Ramin Faramarzi, Ahmad Pourmovahed, and Frederic Taugwalder. 2005. "Jet Entrainment Rate in Air Curtain of Open Refrigerated Display Cases." *International Journal of Refrigeration* 28(2):267–75.

Norton, Tomás and Da-Wen Sun. 2006. "Computational Fluid Dynamics (CFD) – an Effective and Efficient Design and Analysis Tool for the Food Industry: A Review." *Trends in Food Science & Technology* 17(11):600–620. Retrieved January 11, 2016 (http://www.sciencedirect.com/science/article/pii/S0924224406001981).

Oliva, A., G. Colomer, M. Costa, and R. C. 2004. "Three-Dimensional Numerical Simulation of Convection and Radiation in a Differentially Heated Cavity Using the Discrete Ordinates Method." 47:257–69.

Oró, E., A. de Gracia, A. Castell, M. M. Farid, and L. F. Cabeza. 2012. "Review on Phase Change Materials (PCMs) for Cold Thermal Energy Storage Applications." *Applied Energy* 99:513–33.

Oró, E., L. Miró, M. M. Farid, and L. F. Cabeza. 2012. "Improving Thermal Performance of Freezers Using Phase Change Materials." *International Journal of Refrigeration* 35(4):984–91.

Oró, Eduard, Alvaro De Gracia, and Luisa F. Cabeza. 2013. “Active Phase Change Material Package for Thermal Protection of Ice Cream Containers.” *International Journal of Refrigeration* 36(1):102–9.

Oró, Eduard, Laia Miró, Mohammed M. Farid, and Luisa F. Cabeza. 2012. “Thermal Analysis of a Low Temperature Storage Unit Using Phase Change Materials without Refrigeration System.” *International Journal of Refrigeration* 35(6):1709–14.

Orphelin, M. and D. Marchio. 1997. “Computer-Aided Energy Use Estimation in Supermarkets.” *Building Simulation Conference, Prague, Czech Republic*. Retrieved (http://www.ibpsa.org/proceedings/BS1997/BS97_P088.pdf).

Pielichowska, Kinga and Krzysztof Pielichowski. 2014. “Phase Change Materials for Thermal Energy Storage.” *Progress in Materials Science* 65:67–123.

R.H. Howell, P. A.Adams. 1991. *Effects of Indoor Space Conditions on Refrigerated Display Case Performance, ASHRAE—596RP*. Tampa, FL.

Sahan, Nurten and Halime O. Paksoy. 2014. “Thermal Enhancement of Paraffin as a Phase Change Material with Nanomagnetite.” *Solar Energy Materials and Solar Cells* 126:56–61.

Sciacovelli, A., F. Gagliardi, and V. Verda. 2015. “Maximization of Performance of a PCM Latent Heat Storage System with Innovative Fins.” *Applied Energy* 137:707–15.

Shah, N.(1979). 1979. “New Method of Computation of Radiation Heat Transfer in Combustion Chambers.” University of London.

Sharma, Atul, V. V. Tyagi, C. R. Chen, and D. Buddhi. 2009. “Review on Thermal Energy Storage with Phase Change Materials and Applications.” *Renewable and Sustainable Energy Reviews* 13(2):318–45. Retrieved July 10, 2014 (http://www.sciencedirect.com/science/article/pii/S1364032107001402).

Smale, N. J., J. Moureh, and G. Cortella. 2006. “A Review of Numerical Models of Airflow in Refrigerated Food Applications.” *International Journal of Refrigeration* 29(6):911–30. Retrieved March 9, 2016 (http://www.sciencedirect.com/science/article/pii/S0140700706000971).

Song, Wen Ji and Zi Ping Feng. 2013. “One New Type Vertical Open Display Cabinet and Its Thermostatic Performances.” *Research Journal of Applied Sciences, Engineering and Technology* 6(23):4370–74.

Stignor, Caroline Haglund, Bengt Sundén, and Per Fahlén. 2009. “Energy-Efficient Flat-Tube Heat Exchangers for Indirectly Cooled Display Cabinets.” *International Journal of Refrigeration* 32(6):1460–71.

Stribling, David. 1997. “INVESTIGATION INTO THE DESIGN AND

OPTIMISATION OF MULTIDECK REFRIGERATED DISPLAY CASES." PhD thesis, Brunel University London.

Stribling, David, Savvas A. Tassou, and Douglas Marriott. 1997. "Two-Dimensional CFD Model of a Refrigerated Display Case." *ASHRAE Transactions* 103(1):88–94.

Tahir, A. and P. K. Bansal. 2005. "MEPR versus EEPR Valves in Open Supermarket Refrigerated Display Cabinets." *Applied Thermal Engineering* 25(2–3):191–203.

Tassou, S.A., and Suamir, IN. 2010. "Trigeneration – a Way to Improve Food Industry Sustainability." in *Proc. SEEP 2010 Conference*. Bari, Italy.

Tassou, S. A., I. Chaer, N. Sugiartha, Y. T. Ge, and D. Marriott. 2007. "Application of Tri-Generation Systems to the Food Retail Industry." *Energy Conversion and Management* 48(11):2988–95.

Tassou, S. A., G. De-Lille, and Y. T. Ge. 2009. "Food Transport Refrigeration - Approaches to Reduce Energy Consumption and Environmental Impacts of Road Transport." *Applied Thermal Engineering* 29(8–9):1467–77.

Tassou, S. A., Y. Ge, A. Hadawey, and D. Marriott. 2011. "Energy Consumption and Conservation in Food Retailing." *Applied Thermal Engineering* 31(2–3):147–56.

Trelles, Juan P. and John J. Dufly. 2003. "Numerical Simulation of Porous Latent Heat Thermal Energy Storage for Thermoelectric Cooling." *Applied Thermal Engineering* 23(13):1647–64.

Ure, Z. 2001. "Positive Temperature Eutectics TES System." *AIRAH J.* 31–35.

Versteeg, H. and Malalasekera, W. 2007. *An Introduction to Computational Fluid Dynamics-the Finite Volume Method*. 2nd ed.

Voller, V. R., A. D. Brent, and C. Prakash. 1989. "The Modelling of Heat, Mass and Solute Transport in Solidification Systems." *International Journal of Heat and Mass Transfer* 32(9):1719–31.

WANG, FUQIAO. 2003. "THE PASSIVE USE OF PHASE CHANGE MATERIALS IN REFRIGERATION SYSTEMS." PhD thesis, London South Bank University.

Wang, Fuqiao, Graeme Maidment, John Missenden, and Robert Tozer. 2007a. "The Novel Use of Phase Change Materials in Refrigeration Plant. Part 1: Experimental Investigation." *Applied Thermal Engineering* 27(17–18):2893–2901.

Wang, Fuqiao, Graeme Maidment, John Missenden, and Robert Tozer. 2007b. "The Novel Use of Phase Change Materials in Refrigeration Plant. Part 2: Dynamic Simulation Model for the Combined System." *Applied Thermal Engineering* 27(17–18):2902–10.

Wang, Fuqiao, Graeme Maidment, John Missenden, and Robert Tozer. 2007c. "The

Novel Use of Phase Change Materials in Refrigeration Plant. Part 3: PCM for Control and Energy Savings." *Applied Thermal Engineering* 27(17–18):2911–18.

Wu, XueHong et al. 2014. "The Optimization and Effect of Back Panel Structure on the Performance of Refrigerated Display Cabinet." *Food Control* 40(1):278–85.

Wu, XueHong, ZhiJuan Chang, QiuYang Ma, YanLi Lu, and XueMei Yin. 2015. "Optimization and Investigation of the Effect of Velocity Distribution of Air Curtains on the Performance of Food Refrigerated Display Cabinets." *Heat and Mass Transfer*.

Wu, Yezheng, Guozhen Xie, Zhongqi Chen, Lulin Niu, and Dawei Sun. 2004. "An Investigation on Flowing Patterns of the Airflow and Its Characteristics of Heat and Mass Transfer in an Island Open Display Cabinet with Goods." *Applied Thermal Engineering* 24(13):1945–57.

Xia, Bin and Da-Wen Sun. 2002. "Applications of Computational Fluid Dynamics (Cfd) in the Food Industry: A Review." *Computers and Electronics in Agriculture* 34(1–3):5–24. Retrieved March 9, 2016 (http://www.sciencedirect.com/science/article/pii/S0168169901001776).

Xiang, Weizhong. 2003. "Performance Improvement of Multi-Deck Display CabinetS and Reduction of Their Impact on the Store Environment." Brunel University London.

Yu, Ke zhi, Guo liang Ding, and Tian ji Chen. 2007. "Simulation of Air Curtains for Vertical Display Cases with a Two-Fluid Model." *Applied Thermal Engineering* 27(14–15):2583–91.

Yu, Ke zhi, Guo liang Ding, and Tian ji Chen. 2008. "Modified Two-Fluid Model for Air Curtains in Open Vertical Display Cabinets." *International Journal of Refrigeration* 31(3):472–82.

Yu, Ke zhi, Guo liang Ding, and Tian ji Chen. 2009a. "A Correlation Model of Thermal Entrainment Factor for Air Curtain in a Vertical Open Display Cabinet." *Applied Thermal Engineering* 29(14–15):2904–13.

Yu, Ke zhi, Guo liang Ding, and Tian ji Chen. 2009b. "Experimental Investigation on a Vertical Display Cabinet with Central Air Supply." *Energy Conversion and Management* 50(9):2257–65.

Yuan, Xu Dong and Wen Long Cheng. 2014. "Multi-Objective Optimization of Household Refrigerator with Novel Heat-Storage Condensers by Genetic Algorithm." *Energy Conversion and Management* 84:550–61.

Appendix A: Technical data of Euromax Cabinet

A complete Low Front Multideck range, the Euromax for multiplexing

- Temperature range M1 classification tested at ISO 3 standard
- Body lengths 1200, 1875 and 2400mm (lengths exclude end walls 25mm each)

Construction

- Supporting construction and exterior made from galvanised steel sheet.
- High quality stoved paint finish.
- Standard colour white with grey plinths.
- Large glass end panels ensure good product visibility from the side.
- High quality injected expanded polyurethane foam insulation is ozone layer friendly.
- Durable and hygienic ABS plastic basin.
- Adjustable legs.
- Height adjustable shelves can be straight or inclined.

Lighting

- Fluorescent tubes as standard in the front edge of the canopy.
- Lighting tubes are contained in protective plastic sleeves as standard. Long life (LL) fluorescent tubes in every model have treble the life expectancy of standard tubes.

Standard equipment

- Glazed end panels 25mm
- 450mm shelves with consoles

- Ticket strip
- Shelves with brackets
- Evaporator with fan
- Lighting in the front edge of the canopy
- Solar thermometer

Plug-in models

- 245 model - integral scroll compressor complete with control devices
- Refrigerant R404A 125/195 - 2 std Danfoss compressors
- Electrical defrost water disposal
- NRC-100 controller

Remote models

- Expansion valve for R404A
- wiring box
- defrost water outlet pipe

Optional accessories

- Mirrored end panel 25mm
- Acrylic divider panel - full height
- Price trims for shelves
- 80mm front grid on shelves
- Acrylic front riser on shelves

- Divider on shelf
- Base shelf divider
- Display rod for hanging products by hooks
- Straight mirror
- 3 stepped mirror
- Raised base shelf for fruit and veg, straight
- Raised base shelf for fruit and veg, 3 stepped
- Front risers for base shelf, 80mm and 120mm
- Under shelf lighting
- Condenser pressure control with signal light
- Control devices
- Multiplexing kit
- End bumper trim

Options for energy saving

The standard Plug-in models are equipped with automatic defrost water disposal. In order to minimise energy costs, instead of this the defrost water can be led direct to an external drain, if drains are located higher than the cabinet, a pump can be fitted.

Technical specifications at ambient temperature of +25°C and relative humidity of 60 %. Electrical supply 230V, single-phase, 50Hz.

Appendix B: NRC-100 CONTROL DEVICE

1.1 User interface

The user can control the status and programming of the controller using the display and four keys.

If Err6 is displayed, see 1.7 Display signals.

If the display is locked, see 1.13 Locking and unlocking the display.

1.2 Keys and menus

UP key – Scrolls through the menu items, increases the values and activates the manual defrost function

DOWN key – Scrolls through the menu items, decreases the values

FNC key – Exit function, accesses the menu

OK key – Accesses the menu, confirms the commands

1.3 Accessing and using menus

Resources are arranged in a menu that can be accessed by pressing a key:

1.4 Measuring menu (FNC key),

1.5 User menu (FNC key held down 5 seconds) and

1.6 Service menu (OK key held down 5 seconds). The service menu is password-protected. After pressing and holding the OK key for 5 seconds, four zeros (0000) appear. The password is 1953. Set the first number using the UP or DOWN keys. To move to the next number (left to right), press OK.

1.4 Measuring menu

To browse the menu parameters, press the UP or DOWN keys. To see the value of a parameter, press OK.

SEtt – Set point value

Nd – Next defrost time (hh.mm)

Pb 1.5 – Temperature: 1=Thermostat probe; 2=Evaporator probe; 3=Cabinet probe; 4.5=Condenser alarm probes

C on – The compressor that is on (0, 1, 2 or 12)

C1 t – Compressor 1 working hours * 10

C2 t – Compressor 2 working hours * 10

1.5 User menu ≡St1 (≡St2 if in use)

To access the contents of a folder, press the OK key. To browse other folders in the menu, press the UP or DOWN key.

Set point value group1 – folder (≡St1):

St1 – Set point value1

dIF1 – Differential. The compressor stops upon reaching the set point value and restarts at the temperature value equal to the set point plus the value of this difference. Must be a positive value.

dlt1 – Interval between defrost

dEt1 – Maximum duration of defrost

dSt1 – Defrost stop temperature

dt1 – Drying time starts when defrost stops.

This time allows the evaporator to eliminate water drops that might have formed due to defrost.

Appendix C: Instrumentation and Data Logging systems

This appendix provides the positions of the measurement points in the test rig, a display of the monitoring system and identification of the measurement points. Identification of the measurement points on the Data scan logger is presented in below.

Box NO1: Main data Logger		
Channel NO	**Sensor Symbol**	**Description**
1	TLRL	Top Left Rear Lower
2	TLRU	Top Left Rear Upper
3	TLFL	Top Left Front Lower
4	TLFU	Top Left Front Upper
5	TRRL	Top Right Rear Lower
6	TRRU	Top Right Rear Upper
7	TRFL	Top Right Front Lower
8	TRFU	Top Right Front Upper
9	MLRL	Middle Left Rear Lower
10	MLRU	Middle Left Rear Upper
11	MLFL	Middle Left Front Lower
12	MLFU	Middle Left Front Upper
13	MRRL	Middle Right Rear Lower
14	MRRU	Middle Right Rear Upper
15	MRFL	Middle Right Front Lower
16	MRFU	Middle Right Front Upper

Box NO2: data Logger		
Channel NO	**Sensor Symbol**	**Description**
1	BLRL	Bottom Left Rear Lower
2	BLRU	Bottom Left Rear Upper
3	BLFL	Bottom Left Front Lower
4	BLFU	Bottom Left Front Upper
5	BRRL	Bottom Right Rear Lower
6	BRRU	Bottom Right Rear Upper
7	BRFL	Bottom Right Front Lower
8	BRFU	Bottom Right Front Upper

Box NO3: data Logger		
Channel NO	**Sensor Symbol**	**Description**
1	CL	Ai Curtain Left temp.
2	CR	Ai Curtain Right temp.
3	OFF-L	Air evaporator outlet left temp.
4	OFF-R	Air evaporator outlet Right temp.
5	ON-L	Air evaporator inlet left temp.
6	ON-R	Air evaporator inlet Right temp.
7	T_1	Refrigerant temp. after Evaporator
8	T_1^*	Refrigerant temp. before Compressor
9	T_2	Refrigerant temp. after Compressor
10	T_3	Refrigerant temp. before Capillary
11	T_4	Refrigerant temp. after Capillary
12	T_5	Refrigerant temp. after condenser
13	-	-
14	-	-
15	TCH	Test chamber temp
16	RH	Test chamber relative humidity